THE ROLE OF KERATINOCYTE-SPECIFIC *SMAD2* LOSS IN SKIN SQUAMOUS CELL CARCINOMAS

by
Kristina E. Hoot

A DISSERTATION

Presented to the Department of Cell & Developmental Biology
and the Oregon Health & Science University
School of Medicine
in partial fulfillment of
the requirements for the degree of
Doctor of Philosophy
July 2008

School of Medicine

Oregon Health & Science University

CERTIFICATE OF APPROVAL

This is to certify that the Ph.D. dissertation of

Kristina Hoot

has been approved

_____

Mentor/Advisor

_____

Member

_____

Member

_____

Member

_____

Member

TABLE OF CONTENTS

LIST OF TABLES

LIST OF FIGURES

ACKNOWLEDGEMENTS

For mentorship, support, and their valuable time, energy, and advice

Dr. Xiao-Jing Wang, M.D., Ph.D.

Dr. De-Ann Pillers, M.D., Ph.D.

For creating the Smad2 floxed mouse and sharing it with us

Erwin Bottinger, Ph.D.

For providing the groundwork for this project

Dr. Allen Li, M.D., Ph.D.

Yasmin Siddiqui

For invaluable advice as to the direction of my work, my thesis advisory committee

Mihail Iordanov, Ph.D.

Peter Hurlin, Ph.D.

Charles Lopez, M.D., Ph.D.

Molly Kulesz-Martin

Grant and Institutional Support Sources

Pediatrics Traning Grant, NIH NICHD T32 HD46420

Smads in Cancer Grant, NIH NCI CA87849

OHSU Department of Dermatology Molecular Profiling Resource of human tissue samples, IRB#809

OHSU Cancer Institute, NCI CA069533

For making my day countless times, and helping me out when I needed it most

Sophia Bornstein

Dr. Shi-long Lu, M.D., Ph.D.

Dr. Kelli Salter, M.D., Ph.D.

Ruth White

The members of the Wang Lab for all their help:

Dr. Gangwen Han, M.D.

Jessyka Lighthall, M.D.

Dr. Stephen Malkoski, M.D., Ph.D.

Phil Owens

Donna Wang

Most importantly, for their love and support

John and Layla Hoot

Tom Hoot

Dena Khoury

Darren Young, M.D.

LIST OF ABBREVIATIONS

General Abbreviations

ALK	Activin-like Kinase
AK	Actinic Keratoses
BMP	Bone Morphogenic Proteins
BrdU	Bromodeoxyuridine
CBP	Creb-binding protein
Co-Smad	Common Smad
Cre*PR1	Cre* fused to truncated progesteron receptor
CrePR1	Cre fused to Truncated Progesterone Receptor
Ct	Cycle count
CtBP	C-terminal binding protein
DAB	diaminobenzidine
ΔBRII	Dominant negative TGFβRII
DMBA	dimethylbenz[α]anthracene
Ecad	ECadherin
EGFR	Epidermal Growth Factor Receptor
EMT	Epithelial-Mesenchymal Transition
eNOS	endothelial nitrogen oxide synthase
FBS	Fetal bovine serum
FGF	Fibroblast growth factor
GAPDH	Glyceraldehyde 3-phosphate dehydrogenase
GTPase	Guanosine Triphosphatases
h	hours
HDAC	Histone Deacetylase
Het	heterozygous
HGF	Hepatocyte growth factor
HIF	Hypoxia inducible factor
HK	Human Keratin
HMGA2	High mobility group A2
HNSCC	Head and Neck Squamous Cell Carcinoma
Id	Inhibitor of differentiation
IFN	Interfeuron
IGF	insulin-like growth factor
IL	Interleukin
IP	Immunoprecipitation
IP-10	inferon-induced protein-10
I-Smad	Inhibitory Smad
K1	Keratin 1
K13	Keratin 13
K14	Keratin 14
K5	Keratin 5
K6	Keratin 6
K8	Keratin 8

KGF	Keratinocyte growth factor
LOH	Loss of Heterozygosity
MAPK	Mitogen Activated Protein Kinase
MCP	Monocyte-chemotactic protein
MIP	Macrophage inflammatory protein
MMP	Matrix metalloproteinase
p	phosphorylated
Pap	Papilloma
PBS	Phosphate buffered saline
PDGF	Platelet derived growth factor
penn-strep	pennicillin and streptomycin antibiotics
PI3K	Phosphoinositide-3 Kinase
PR	Progesterone Receptor
PTEN	Phosphatase and Tensin Homolog
RNA Pol	RNA Polymerase
R-Smad	Receptor Smad
SBE	Smad Binding Element
SCC	Squamous Cell Carcinoma
SCF	Skp1-Cul1-F-box-protein
SEM	Standard Error of the Mean
sFlt	Soluble Flt
siRNA	Small interfering RNA
SPCC	Spindle Cell Carcinoma
TAM	Tumor associated macrophage
TBS	Tris buffered saline
TGFβ	Transforming Growth Factor Beta
TGFβRII	TGFβ Type II Receptor
TGIF	TGFB-induced factor
TNF	Tumor necrosis factor
TPA	12-O-tetradecanoyl-phorbol-13-acetate
TSP1	Thrombospondin 1
TSS	Transcriptional start site
TUNEL	Terminal deoxynucleotidyl Transferase Biotin-dUTP Nick End Labeling
UV	Ultraviolet
VEGF	Vascular endothelial growth factor
WT	wildtype
ΔPR	Truncated Progesterone Receptor

Materials and Method Abbreviations

ChIP	Chromatin Immunoprecipitation
ELISA	Enzyme-Linked Immunosorbent Assay
H&E	Hematoxylin and Eosin
IF	Immunofluorescence
IHC	Immunohistochemistry
MMC	Mitomycin C
PCR	Polymerase Chain Reaction
qRT-PCR	Quantitative Reverse Transcriptase Polymerase Chain Reaction

ABSTRACT

During my thesis work, I found that TGFβ signaling mediators, Smad2 and Smad4, but not Smad3, were frequently lost in human skin squamous cell carcinomas (SCCs). Previous studies reveal that *Smad4-/-* mouse epidermis develops spontaneous SCCs whereas *Smad3-/-* mice are resistant to carcinogen-induced skin cancer. To evaluate the significance of Smad2 loss in skin cancer, we generated mice with keratinocyte-specific *Smad2* deletion. These mice exhibited accelerated formation and malignant progression of chemically-induced skin tumors compared to wildtype mice. Consistent with the loss of Smad2 in poorly-differentiated human SCCs, *Smad2-/-* tumors were poorly differentiated and underwent epithelial-mesenchymal transition (EMT) prior to spontaneous Smad4 loss. Reduced E-cadherin and activation of its transcriptional repressor Snail were also found in *Smad2-/-* mouse epidermis, and occurred more frequently in Smad2 negative human SCCs than in Smad2 positive SCCs. Knocking down Snail abrogated Smad2 loss-associated EMT, suggesting that Snail upregulation is a major mediator for Smad2 loss-associated EMT. Further, Smad2 loss led to a significant increase in Smad4 binding to the Snail promoter, and knocking down either Smad3 or Smad4 in keratinocytes abrogated Smad2 loss-associated Snail overexpression. Additionally, *Smad2-/-* skin has increased HMGA2 bound to the Snail promoter and loses transcriptional co-repressor TGIF binding. My data suggest that enhanced Smad3/Smad4-mediated Snail transcription contributed to Smad2 loss-associated EMT during skin carcinogenesis.

Squamous cell carcinomas (SCCs) derived from keratinocyte-specific *Smad2* or *Smad4* knockout mice had three times the blood vessels of SCCs derived from wildtype mice. *Smad4*, but not *Smad2*, knockout tumors expressed increased vascular endothelial growth factor (VEGF), TGFβ1, and TGFβ-mediated proangiogenic components. In contrast, *Smad2*, but not *Smad4*, knockout tumors had increased hepatocyte growth factor (HGF). HGF and VEGF pathways converged downstream on pAKT. Pre-neoplastic skin lacking *Smad2* or *Smad4* had increased blood vessels and molecular alterations consistent with tumor angiogenesis. Consistently, Smad4 knockdown in human keratinocytes induced VEGF, which was abrogated by Smad3 co-knockdown. Smad2 knockdown in human keratinocytes induced HGF, which was abrogated by concomitant Smad3 or Smad4 co-knockdown. HGF promoter activity was increased by

Smad2 knockdown, which was abrogated by Smad3 or Smad4 co-knockdown. Comparative chromatin immunoprecipitation showed *Smad2*-null skin had increased transcriptional activators bound to the HGF promoter, whereas *Smad4*-null skin had increased transcriptional repressors bound. Co-immunoprecipitation of complexes involving Smad2-HDAC3 or Smad4-CBP/p300 to the HGF promoter indicated that Smad2 acts to repress, while Smad4 activates HGF expression. HGF expression in human skin SCCs correlated with Smad2-negative Smad4-positive tumors. Therefore, I conclude deletion of *Smad2* and *Smad4* created an angiogenic microenvironment through common and distinct mechanisms.

I. INTRODUCTION:

The role of TGFβ-signaling in skin carcinogenesis

DEVELOPMENT AND PROGRESSION OF HUMAN SKIN SQUAMOUS CELL CARCINOMAS

Skin cancer is the most common form of cancer in the United States, accounting for more cases than all other cancers combined (1). Squamous cell carcinoma (SCC) is the second most common form of skin cancer, with an annual rate of 250,000 cases (1). Risk factors for acquiring skin SCCs include ultraviolet (UV) exposure and immunosuppression (e.g. organ transplantation, advanced HIV, etc) (1). Sixty percent of skin SCCs arise from precursor lesions known as actinic keratoses (AK) (2). While in most cases, cure rates are high if caught early with the exception of aggressive skin cancer, which is life threatening and occurs frequently in immunocomprised patients.

Squamous cell carcinomas progress from the epithelium in a complex multi-step process referred to as "somatic evolution" termed for the Darwinian principle of genetic and epigenetic alterations leading to the cancer phenotype. Hanahan and Weinberg emphasized the final evolutionary outcomes by distilling the properties of transformed cells to six phenotypical hallmarks that are necessary for an invasive cancer (3). Gatenby et al. described the Darwinian dynamics as interactions of individual phenotypes with environmental selection forces that govern fitness and, therefore, proliferation. Thus, in the adaptive landscapes governing somatic evolution, microenvironmental barriers to proliferation are the selection forces controlling the proliferative capability of any new phenotype that is generated by genetic or epigenetic events. Thus, the six consistent phenotypical changes emphasized by Hanahan and Weinberg that emerge during carcinogenesis represent successful adaptations to these microenvironmental selection forces. Furthermore, these selection pressures are dynamic and change as a result of tumor population growth and evolution (4).

Normal epithelial cells are connected to each other via adherens junctions and integrins, which also connect the cells to the basement membrane, while they communicate through gap junctions. Though apoptosis and contact inhibition restrict growth, epithelial proliferation is governed by growth factors that diffuse from the blood vessels and mesenchymal cells across the basement membrane (Figure 1a). Thus, hyperproliferation occurs only in when mutations confer resistance to anoikis. Therefore, these changes, such as *Ras* mutation or E-cadherin loss, will be the first genetic and phenotypical events observed in carcinogenesis (4). As such, UV-induced mutations in *HRAS* and *KRAS* have been characterized in AK and SCC (2).

The adaptive landscape, after allowing proliferation away from the basement membrane, is dominated by "diffusion-reaction kinetics" (4). Growth factors must diffuse over increasingly large distances to reach the proliferating cells, which are now several cells from the basement membrane (Figure 1b). The reduced growth promoter concentration is a proliferation barrier that is overcome by paracrine/autocrine production of growth factors, increased numbers of membrane receptors, or upregulation of transduction pathways (Figure 1b). These represent functionally equivalent adaptive strategies, as they serve the same purpose, and at least one must occur in all cancers.

Due to the increased diffusion distance, regions of hypoxia and acidosis develop that are overcome by upregulation of glycolysis and resistance to acid-mediated toxicity leading to a transition from carcinoma in situ to invasive cancer (microinvasion) (Figure 1c). Once such adaptation is p53 mutation, seen in AK, carcinoma in situ, and invasive SCC with a rate of up to 45% (2). Here tumor growth is limited primarily by ischemia (4). Without angiogenesis, growth is limited to a few hundred micrometers. Clinically significant tumor formation requires the mesenchyma promote tumor growth via angiogenesis, production of growth factors, and production of matrix metalloproteinases (MMPs), which degrade the extracellular matrix. This landscape also promotes evolution of the invasive phenotype, wherein cells with increased motility migrate from proliferation-inhibited regions, characterized by substrate limitations and competition, with other cancer cells, into adjacent normal tissue lacking these constraints (4). Increased

motility results in rapid proliferation "rewarding" the invasive phenotype. The barriers to growth and strategies employed to overcome them are summarized in Figure 2.

Mouse models have been employed to study skin SCCs and their precursor lesions, papillomas. Currently, two main models exist: UVB-induced tumorigenesis and two-stage chemical carcinogenesis. In the former, mice are irradiated twice weekly for 25 weeks with a gradually increasing dose of UVB such that in week 1 they are exposed to 1KJ/cm^2/5 min and by the fourth week 6KJ/cm^2/30 min which is maintained in all subsequent weeks (5). In chemical carcinogenesis, the mouse is topically treated with a one-time, sub-carcinogenic dose of 20 μg of dimethylbenz[α]anthracene (DMBA), to induce *H-Ras* mutation. One week later, 5 μg of 12-O-tetradecanoyl-phorbol-13-acetate (TPA) is applied to skin twice a week for 20 weeks promoting subsequent mutations, including *p53* mutation (5). These two models recapitulate human tumor progression from normal epidermis through hyperplastic skin, papilloma, carcinoma in situ, to invasive SCC. Furthermore, due to the nature of mutation initiated in both models, rates of malignant conversion are similar between human AK to SCC and mouse papilloma to SCC (6).

RAS SIGNALING IN TUMORIGENESIS

Ras proteins transmit signals from a number of cell surface receptors. These include growth factor receptors, such as EGFR, and extracellular matrix receptors, such as integrins. These receptors convey signals to Ras via adaptors such as Grb2 and Gab1 as well as nucleotide exchange factors such as SOS. Ras exerts its effects via discrete downstream effector pathways that classically include Raf/Mek/Erk mitogen activated protein kinases (MAPKs), type I phosphatidylinositol-3 kinases (PI3Ks) and Ral guanine nucleotide exchange factors (RalGEFs) along with a number of additional pathways involving, Rin1, protein kinase C, and phospholipase C isoforms. The best-characterized mammalian pathway occurs through the MAP kinase pathway from Ras to MAPKKK (e.g. Raf), MAPKK (e.g. Mek1/2), then finally through MAP kinases (e.g. Erk1/2). The Ras/Erk MAPK cascade alters >140 target proteins and can affect a pleiotropic array of cellular functions, including proliferation, differentiation, survival, and migration(7).

Ras activation is amongst the most common mutations in human cancer, with an estimated frequency of up to 30%. Oncogenic *Ras* point mutations lead to constitutive GTP-binding and activation (7). Additional mechanisms of Ras activation occur in human tumors independent of activating point mutations, including *Ras* gene amplification and activation of wild-type Ras protein by overactive upstream activators, such as receptor tyrosine kinases. In a series of 416 human SCCs, at least one Ras isoform, with HRAS the most common, contained activating mutations in 22% of cancers (8), and in prior studies Ras mutation rates been reported to be as high as 46% of SCCs. Further, SCCs lacking any HRAS, KRAS or NRAS mutations display increased levels of active Ras-GTP in a majority of cases (7). Data generated in an array of murine genetic models, including classical DMBA/TPA multistage carcinogenesis in mouse skin, also indicate that Ras plays a pivotal role in initiating SCC development (2). Together these data point to Ras and its downstream effectors as critical regulators in epidermal neoplasia.

Ras mutation is tumorigenic primarily through its proliferative and anti-apoptotic roles. Mutation of upstream signaling molecules *Mek1* and *Mek2* in adult murine epidermal tissue led to epidermal apoptosis and tissue death associated with alterations in the pro-apoptotic protein, BAD. Diminished levels of the inhibitory phosphorylation of BAD, a known direct target of Erk MAPK pathway, were observed in the knockout epidermis (9). Furthermore, overexpression of oncogenic Ras or Raf alone in keratinocytes in vitro led to G1 arrest, despite of induction of cyclin D1 expression (10). This arrest was accompanied by suppressed Cdk4 protein levels and could be rescued by maintaining Cdk4 expression (10, 11). Unlike epidermal tissue expressing activated Ras alone, which became hyperplastic but not neoplastic in vivo, tissue also maintaining Cdk4 expression displayed accelerated proliferation and rapid global conversion to invasive neoplasia indistinguishable from SCC within weeks (10, 11). This process could be mimicked by other interventions that sustained Cdk4 expression, including NFkB blockade and activation of the JNK MAPK pathway (10, 11). Therefore, activated Ras initiates tumorigenesis through hyperproliferation with reduced apoptosis, but is insufficient to lead to invasive, metastatic SCCs without additional alterations.

TGFβ SIGNALING OVERVIEW

TGFβ signaling is involved in tissue homeostasis and cancer development (12). The TGFβ superfamily consists of three major subfamilies: TGFβ, activins/inhibins, and bone morphogenetic proteins (BMPs). These family members signal through two types of transmembrane serine/threonine kinase receptors, and Smad transcription factors were initially identified as their signaling mediators. Smads can be classified into three groups: R-(receptor-activated) Smads, co-(common) Smad and I-(inhibitory) Smads (13). R-Smads for BMP signaling include Smad1, Smad5, and Smad8. R-Smads for TGFβ/activin signaling include Smad2 and Smad3. When a TGFβ superfamily ligand binds its specific type II (RII) and type I (RI) receptor complex, the kinase domain of the type I receptor binds and phosphorylates R-Smads. Phosphorylated R-Smads can form heteromeric complexes with the co-Smad, Smad4, and translocate to the nucleus to regulate TGFβ responsive genes (Figure 3). Nuclear localization can be regulated by a number of phosphatases that dephosphorylate R-Smads which were recently identified (14). Following nuclear translocation, heteromeric Smad complexes regulate TGFβ-responsive genes via interaction with specific promoter sequences, termed Smad binding elements (SBEs). Specifically, Smad3 binds to the SBE of a target gene, and subsequently recruits Smad4 to the same SBE. Full-length Smad2 does not bind to DNA directly but complexes with Smad3 and Smad4 as either a co-activator or a co-repressor for Smad3 and Smad4 (13). While TGFβ auto-induces itself to form a positive feedback loop, it also upregulates I-Smads, Smad6 and Smad7, which inhibit phosphorylation of R-Smads and target TGFβ receptors for degradation by recruiting ubiquitin ligases, thus forming a negative feedback loop for the TGFβ signaling pathway (12, 15).

While only one TGFβRII has been identified in mammals, there are at least two different type one receptors (TGFβRIs). The classical TGFβRI, also known as activin receptor-like kinase (ALK)-5, is expressed on almost all cell types (16, 17). In contrast, endothelial cells preferentially express the other TGFβRI, ALK1. Activation of each TGFβRI utilizes different R-Smads and regulates expression of distinct sets of genes, leading to different cellular effects. When ALK5 is activated, it phosphorylates Smad2 and

Smad3 and turns on the expression of genes including collagen I and plasminogen activator inhibitor I (PAI-1). In contrast, ALK1 activation phosphorylates Smad-1, -5, and -8 to regulate expression of genes such as Id inhibitors of differentiation (Id-1, -2, -3) (18). Although Smads are critical for TGFβ signal transduction, compelling evidence has suggested that Smad-independent pathways may also mediate TGFβ signaling. For instance, TGFβ has been found to activate mitogen-activated protein kinases (MAPKs), phosphoinositide 3-kinase (PI3K), and Rho family guanosine triphosphatases (GTPases) to regulate cell growth and apoptosis (12).

TGFβ has dual effects on cell proliferation, differentiation, angiogenesis, and inflammation. For instance, TGFβ promotes proliferation of mesenchymal cells such as dermal fibroblasts, but it acts as a potent growth inhibitor of epithelial cells (e.g., keratinocytes), hematopoietic cells (e.g., lymphocytes), and neural cells by inducing antiproliferative gene responses during cell division (19, 20). In endothelia, ALK1-mediated TGFβ signaling leads to endothelial cell proliferation and migration that are essential for angiogenesis, whereas ALK5 activation opposes this effect, thereby preventing angiogenesis (16). TGFβ is well known as a strong chemoattractant for all leukocytes including granulocytes, lymphocytes, monocytes/macrophages, and mast cells. Thus, it is able to initiate inflammatory responses. However, TGFβ later deactivates leukocytes and contributes to the resolution of inflammation (21, 22). Due to the cell type and stage-specific roles of TGFβ, the role of TGFβ signaling in the maintenance of tissue homeostasis and in disease development is complex. Each of the R-Smads has been implicated by in vitro studies in mediating the multiple functions of TGFβ (23). However, increasing studies show that Smad-2, -3 and -4 are regulated differently and exhibit distinct physiological functions in vivo (13, 23). For instance, both *Smad2* and *Smad4* knockout mice are embryonic lethal due to failure in embryonic axis patterning and endoderm specification (24), and failure of proper endoderm and mesoderm formation (25), respectively. In contrast, *Smad3* knockout mice are viable but succumb to mucosal immunity defects after birth (26).

The diversity of TGFβ can be further modified at the transcriptional level through Smad-specific recruitment of transcriptional co-activators and co-repressors (Figure 3). After the Smad2/Smad3/Smad4 complex binds DNA, Smad2 can recruit transcriptional co-repressors such as c-Ski, TGIF, and CtBP (27). TGIF has been shown to bind HDACs 1-4 leading to gene silencing (27). There is evidence that Smads can recruit transcriptional activators, such as CBP/p300 inducing gene expression (27). TGIF binds to Smad2 and Smad3 in competititon with p300, so the relative levels of p300 and TGIF in a cell influence whether a Smad complex will bring one or the other to a target gene (27), and the same may be true of other transcriptional co-repressors. Increasing numbers of studies now show competition between Smad2 and Smad3 for transcriptional regulation – with each regulating gene expression in opposing directions (23, 28).

In many cancer types, TGFβ signaling has a tumor suppressive effect early in carcinogenesis primarily via growth inhibition, apoptosis, and maintenance of differentiation, but paradoxically it also promotes invasion and metastasis at later stages through increased angiogenesis, inflammation, and epithelial-mesenchymal transition (EMT) (13, 14, 29). We have shown that human skin SCCs exhibit increased levels of TGFβ1, but reduced levels of TGFβRII protein (30). Moreover, carcinoma in situ samples already exhibited these changes compared to normal epidermis (30). Increasing evidence suggests that the individual Smads mediate both tumor suppression and promotion functions of TGFβ. In epithelial cells, Smad-2, -3, and -4 are involved in growth inhibition (31, 32), a major tumor suppressive effect of TGFβ, and epithelial-mesenchymal transition (EMT) (12, 23), an early and major tumor promoting effect of TGFβ. However, genes associated with each of these biological processes are differentially regulated by individual Smads (13, 33). Thus, the net effects of individual Smads in cancer are complicated largely by the complex functions of TGFβ signaling. Therefore, in different contexts, each individual Smad has a distinct role in mediating TGFβ signaling during carcinogenesis.

EXPRESSION PATTERNS OF INDIVIDUAL SMADS IN SKIN CANCER

The majority of human epithelial cancers (>85%) including pancreatic, colon, breast, prostate, and lung, have aberrations in components of the TGFβ signaling pathway (34). For skin cancer, solar ultraviolet (UV) irradiation is the major etiological factor. To address the affect of UV irradiation on TGFβ signaling, Quan et al. examined Smad expression patterns in human sun-protected skin areas irradiated with an experimental ultraviolet B (UVB) source. Biopsies were taken after exposures ranging from 4 to 72 hours. While no change in the protein levels of Smad-2, -3, and -4 were detected, the irradiated skin exhibited an increase in Smad7 mRNA at 4 hours. However, Smad7 mRNA levels dropped below the initial basal level after 24 hours (35). Additionally, sun-exposed forearm and sun-protected upper inner-arm skin samples from human volunteers were compared and both Smad7 mRNA and protein expression were higher in sun-exposed epidermis than in sun-protected epidermis, similar to UVB-irradiated skin. Thus, Smad7 overexpression appears to be dependent on UV-irradiation. Interestingly, while Smad3 protein was present throughout the epidermis in sun-exposed and sun-protected skin, it was also detected in the dermis only in sun-exposed skin, suggesting that Smad3 mediates the TGFβ-induced fibrotic response in UV-irradiated skin. Although no significant differences in protein expression were observed in Smad2 or Smad4 between sun-exposed and sun-protected skin, phosphorylated Smad2 (pSmad2) protein was decreased in sun-exposed skin compared to sun-protected skin. This change could be a result of down-regulation of TGFβRII and up-regulation of Smad7 (35). In summary, UV-irradiated human skin has reduced TGFβ signaling evidenced by an increase in inhibitory Smad7, and down-regulation of TGFβRII and pSmad2. While acute UV irradiation alone is insufficient to alter the levels of Smad-2 and -4, our laboratory has recently reported that Smad2 was lost in almost all human skin SCCs examined (36).

Soon after Smads were first identified in mammals, our laboratory examined the status of individual Smads in normal mouse skin and experimentally-induced skin cancer at the genetic, mRNA and protein levels (36). Smad-1 and -5 were expressed in normal epidermis, while Smad6 and Smad7 were almost undetectable. In primary keratinocytes, Smad-2 and -4 underwent nuclear translocation in response

to exogenous TGFβ1, which correlated with reduced proliferation. This result suggests that Smad activation is required for TGFβ1-induced growth inhibition. During two-stage skin chemical carcinogenesis, mutations in *Smad-2*, and *-4* were not detected and transcripts for Smad-1 and -5 were retained. However, while Smad-1 and -5 proteins were retained in the majority of papillomas, they were significantly downregulated in SCCs and completely lost in spindle cell carcinomas (SPCCs) (13). One mechanism to explain Smad loss at the protein level is ubiquitin-mediated Smad degradation. For example, Smurf2 ubiquitin E3 ligase degrades Smad2 and $SCF^{\beta\text{-}TrCP1}$ and SCF^{Skp2} ubiquitin ligases lead to the degradation of Smad4 (13, 37). These E3 ligases can be either elevated in cancer cells or recruited by elevated Smad7 and Jab1 in cancer cells (36). In contrast to R-Smad loss in SCCs, Smad7 mRNA was upregulated in chemically induced papillomas and SCCs (38). Upregulation of Smad7 not only directly blocks R-Smad signaling, but could be responsible for reduced R-Smad proteins by recruiting Smurf2.

SPATIAL AND TEMPORAL EFFECTS OF TGFβ OVEREXPRESSION ON CARCINOGENESIS

TGFβ has been thought to inhibit proliferation and promote differentiation of keratinocytes. We have shown that in human skin cancers, TGFβ1 is overexpressed either suprabasally or throughout the tumor epithelia including basal proliferative cells (30). Whether or not the spatial patterns of TGFβ1 expression in tumor epithelia affect tumor prognosis is currently unknown. However, our studies using various transgenic mouse models have revealed functional differences, particularly in keratinocyte proliferation and inflammation, which may differentially affect tumor outcome. TGFβ was initially documented as a potent growth inhibitory cytokine of keratinocytes in vitro (39). Similarly, transgenic mice overexpressing a constitutively active form of TGFβ1 ($TGF\beta1^{act}$) in the differentiated keratinocytes of the epidermis driven by a human K1 promoter ($HK1.TGF\beta1^{act}$) showed significant growth arrest in the epidermis (40). Using a gene-switch transgenic mouse model we have also shown that acute induction of $TGF\beta1^{act}$ overexpression primarily in suprabasal layers of the epidermis reduces epidermal proliferation in quiescent skin and causes a resistance to phorbol 12-myristate 13-acetate (TPA)-induced epidermal

hyperproliferation (41). Sustained induction of suprabasal *TGFβ1*^{act} overexpression achieved by application of the transgene expression inducer to these mice daily for 7 days revealed no overt changes in the epidermis but significantly increased angiogenesis in the dermis (41). In contrast, constitutive overexpression of latent TGFβ1 (*TGFβ1*^{wt}) (42) or chronically induced overexpression of *TGFβ1*^{act} in the basal layer (43) under the control of a K5 promoter led to epidermal hyperproliferation accompanied with inflammation. Lastly, studies from R. Akhust laboratory have demonstrated that when *TGFβ1*^{act} transgene is constitutively overexpressed in the suprabasal layers of the epidermis, driven by a truncated human K10 promoter (44), or inducibly overexpressed by TPA under the control of a truncated K6 promoter (45), transgenic mice show an increased epidermal proliferative rate without histological changes. No obvious phenotypes in the dermis have been reported from these mice. These contradictory data have suggested that the effects of TGFβ1 overexpression on both the epidermis and the dermis may vary depending on expression level and spatial pattern (suprabasal or basal).

When subjected to skin chemical carcinogenesis protocol, transgenic mice overexpressing *TGFβ1*^{act} in the suprabasal layers of the epidermis show reduced papilloma formation, yet enhanced malignant conversion (46). This has led to a well-accepted concept that TGFβ inhibits benign tumor formation at early stages of skin carcinogenesis, but enhances malignant progression at later stages (46). In agreement with the tumor promotion role of TGFβ at later stages during skin carcinogenesis, we have demonstrated that directly inducing TGFβ1 overexpression in suprabasal layers of papilloma epithelia of gene-switch-TGFβ1 transgenic mice causes accelerated malignant transformation and rapid metastasis (30, 47). This is associated with an upregulation of matrix metalloproteinase (MMP) genes and increased angiogenesis, indicative of a paracrine effects of TGFβ1 on stromal cells such as fibroblasts and inflammatory cells (30, 47).

ROLE OF TGFβ–SIGNALING IN EMT AND METASTASIS

TGFβ-mediated EMT occurs through the direct and indirect repression of E-cadherin and upregulation of mesenchymal markers. E-cadherin is a component of adherens junctions and helps maintain epithelial cell apical-basal polarity. Loss of E-cadherin relieves anchorage-dependent growth restrictions and is critical for epithelial-to-mesenchymal transition. Transcriptional repressors of E-cadherin include Snail, Slug, and Twist, which have all been implicated as TGFβ target genes (32, 48-54). Further, another TGFβ target, HMGA2, has been shown to positively regulate Snail and Slug while negatively regulating E-cadherin (55). Additionally, loss of TGFβ-signaling upregulates mesenchymal marker expression including αSMA, vimentin, and tenascin C contributing to a mesenchymal phenotype (50, 51). However, which Smads regulate the expression of each of these TGFβ targets, has yet to determined.

To assess the effect of combined TGFβ1 overexpression and loss of TGFβRII in skin cancer, we generated transgenic mice that allowed inducible expression of TGFβ1 in keratinocytes expressing a dominant negative TGFβRII (*ΔβRII*) in the epidermis (30, 56). Induction of TGFβ1 transgene expression alone in late stage chemically-induced papillomas failed to inhibit tumor growth, but increased metastasis and epithelial-to-mesenchymal transition (EMT), i.e., formation of spindle cell carcinomas. Although *ΔβRII* expression in tumor epithelia was able to abrogate TGFβ1-mediated EMT, a metastasis-associated oncogenic event, it promoted tumor metastasis in cooperation with TGFβ1. *TGFβ1/ΔβRII*-transgenic tumors progressed to metastasis without losing membrane-associated E-cadherin/catenin complexes, and at a rate higher than those observed in non-transgenic, TGFβ1 transgenic, or *ΔβRII* transgenic mice. Abrogation of Smad activation by *ΔβRII* correlated with the blockade of EMT. However, *ΔβRII* did not alter TGFβ1-mediated expression of RhoA/Rac, Erk or JNK, which contributed to increased metastasis (30). Our study provides evidence that TGFβ1 induces EMT and invasion via distinct mechanisms. TGFβ1-mediated EMT requires functional TGFβRII, whereas TGFβ1-mediated tumor invasion cooperates with reduced TGFβRII signaling in tumor epithelia. The present study has raised a very interesting

conclusion that TGFβ1-mediated EMT in tumor epithelia is dispensable for tumor invasion and metastasis, which can be largely contributed to by the effects of TGFβ1 on the stroma, where TGFβ responsiveness remains intact. Thus, TGFβ1-mediated tumor invasion and EMT can be uncoupled.

ROLE OF TGFβ IN INFLAMMATION AND CARCINOGENESIS

Inflammation has been associated with cancer development, and many inflammatory cytokines and chemokines stimulate cell proliferation and angiogenesis, which facilitate tumor growth (57, 58). With respect to skin cancer, paradoxical effects of inflammation on cancer development have also been reported. Psoriatic patients with chronic skin inflammation do not show an increased risk of developing skin cancer on psoriatic plaques (59). However, in a human papilloma virus oncogene-induced skin carcinogenesis model, mice devoid of pro-inflammatory CD4+ T cells exhibited a lower incidence of tumors and delayed neoplastic progression, providing an unexpected role of CD4+ T cells in immune enhancement of skin carcinogenesis (60). In order to assess the role of TGFβ1 in skin inflammation and carcinogenesis, we generated transgenic mice expressing wild-type TGFβ1 in basal keratinocytes and hair follicles (*K5.TGFβ1*^{wt}). Transgenic mice developed a severe inflammatory skin disorder (42). Interestingly, histological examination of *K5.TGFβ1*^{wt} transgenic skin demonstrated inflammatory cell infiltration and angiogenesis as early as day 17 after birth, when the *K5.TGFβ1*^{wt} mice were macroscopically indistinguishable from non-transgenic littermates (30, 61), suggesting that epidermal hyperplasia may be a secondary effect of inflammation and angiogenesis. Molecular analysis revealed that the skin inflammatory phenotype was associated with an upregulation in a variety of genes encoding inflammatory cytokines [*e.g.*, IL-1, IL-2, TNFα, and interferon (IFN)-γ], chemokines [*e.g.*, MIP-2 (murine counterpart of IL-8), monocyte-chemotactic protein (MCP)-1, and interferon-induced protein-10 (IP-10)], growth regulators [*e.g.*, insulin-like growth factor (IGF)-1, amphiregulin, and KGF], matrix metalloproteinases (MMPs) (*e.g.*, MMP-2, -3, and –9), angiogenic factors (*e.g.*, VEGF) and their receptors (*e.g.*, Flt-1 and Flk-1) (42). These molecules participate in epidermal proliferation, inflammatory cell infiltration, angiogenesis, and basement membrane degradation, all of which play a part in skin carcinogenesis.

TGFβ IN ANGIOGENESIS AND CARCINOGENESIS

While the molecular alterations within the tumor epithelia are critical for tumor development and progression, interaction with the underlying stroma also plays a critical role (4, 62). Tumor growth rate and metastasis are often dependent on tumor angiogenesis (63). TGFβ has a direct effect on endothelial cell growth and migration (63). The Alk1 endothelial type I TGFβ receptor (TGFβRI) promotes cell growth and migration through Smad1/5/8 signaling, whereas the Alk5 TGFβRI inhibits vessel growth through Smad2/3 signaling (62). Several other diffusible factors that are regulated by TGFβ, are potent initiators of angiogenesis (62), including vascular endothelial growth factor (VEGF) (reviewed in (64)), and hepatocyte growth factor (HGF) (62). VEGF is the most potent widely targeted stimulator of angiogenesis (65). VEGF receptor binding stimulates endothelial cell survival, proliferation, migration, and permeability (66). VEGF transcription can be stimulated by hypoxia inducible factor HIF1α and Smad3 binding to its promoter (64). HGF has been shown to be an independent, potent angiogenic factor through stimulation of endothelial cell growth, migration, scatter, and elongation (67). Previous studies have shown TGFβ can either stimulate (47, 67, 68) or inhibit (69, 70) HGF transcription in a tissue and context specific manner. The role of individual Smads in regulating HGF transcription has not been established.

DISTINCT ROLES OF SMADS IN MOUSE SKIN CARCINOGENESIS

To further dissect Smad deregulation during carcinogenesis, *Smad-2, -3, -4,* and *-7* were genetically modified in the murine epidermis, and altering each Smad resulted in a different cancer phenotype. Thus, each Smad likely has a unique role in carcinogenesis. The distinct attributes of these phenotypes will be discussed below.

Smad2

The loss of Smad2 in human cancers suggests that Smad2 plays a tumor suppressive role. To further assess the in vivo role of Smad2 in skin carcinogenesis, Tannehill-Gregg et al. used heterozygous germline

Smad2 (*Smad2+/-*) mice to perform a skin carcinogenesis experiment (38). *Smad2+/-* mice exhibited accelerated skin tumor formation. In addition, while wild-type mice developed papillomas, well-, and moderately-differentiated SCCs, *Smad2+/-* mice developed only moderately-differentiated SCCs with locally invasive and spindle-cell keratinocytes (31). These studies suggest that wild-type Smad2 acts as a tumor suppressor and maintains keratinocyte differentiation. In contrast to the above studies, a study from Oft et al. suggests that Smad2 activation promotes metastasis and EMT (31). These authors reported that co-transfection of an SCC cell line with activated *Smad2* and *H-ras*, but not with *H-ras* alone, resulted in spindle morphology and EMT. As a result, these spindle-cells produced more invasive and metastatic tumors than the parental cell line when injected into nude mice. In contrast, spindle-cell lines expressing dominantly negative *Smad2* were unable to form tumors (38). Since SCC and SPCC cell lines have lost response to TGFβ-induced growth arrest, introducing activated *Smad2* would preferentially restore TGFβ-mediated tumor promotion effect. Thus, the above study suggests that Smad2 is required to mediate the effect of TGFβ on EMT and metastasis. Considering that loss of *Smad2* also caused an EMT phenotype in vivo (71), it remains to be determined whether Smad2 can affect EMT via both TGFβ-dependent and independent pathways. It is also possible that the effect of Smad2 on EMT is dose-dependent, i.e., a normal level of Smad2 may repress EMT, whereas Smad2 overexpression may promote EMT.

Smad3

In contrast to *Smad2* and *Smad4*, *Smad3* mutation is infrequent in human cancer (72-74). Among three germline *Smad3* knockout mouse models, only one developed cancer (75). In a xenograft experiment (75), *Smad3-/-* keratinocytes transduced with *v-ras*^{Ha} demonstrated a ten-fold reduction in TGFβ-induced growth inhibition compared to *Smad3+/+* controls. Correspondingly, changes in mRNA expression of TGFβ target genes involved in cell cycle arrest were found in *Smad3-/-* compared to *Smad3+/+* keratinocytes after *v-ras*^{Ha} transduction, including increased c-myc and reduced p15^{Ink4b}. This data suggests that in vitro, Smad3 is important for the growth-inhibitory role of TGFβ (75). Additionally, *v-ras*^{Ha}-transduced *Smad3-/-* or *Smad3+/+* primary keratinocytes were grafted onto nude mice. Although no difference in papilloma formation was noted between *Smad3-/-* and *Smad3+/+* grafts, *Smad3-/-* grafts, but

not *Smad3+/+* grafts, progressed to malignant SCCs (38). This experiment suggests that Smad3 does not alter proliferation but prevents malignant conversion of papillomas formed by engraftment onto nude mice. In contrast to this study, Tannehill-Gregg et al. showed that rather than the accelerated tumor formation and progression seen with *Smad2+/-* mice, germline *Smad3+/-* mice (the same line used to derive *Smad3-/-* cells in the above graft experiment) developed significantly fewer tumors compared to wildtype or *Smad2+/-* mice, when they were exposed to skin chemical carcinogenesis (38, 75). Notably, both *Smad2+/-* and *Smad3+/-* mice used in this study, and the *Smad3-/-* keratinocytes used in the above graft experiment are derived from the same genetic background (61). Thus, it is unlikely that genetic modifiers could explain the above opposite observations. Furthermore, using the same *Smad3* knockout mouse line, we have found that *Smad3-/-* and *Smad3+/-* mice are resistant to two-stage skin chemical carcinogenesis, with reduced papilloma formation and resistance to SCC formation, compared to wild-type mice (42). In the above chemical carcinogenesis studies, *Smad3* is knocked-out in both the epithelia and the stroma, and this could explain, at least in part, the difference between these two studies and the above graft study in which *Smad3* is only ablated in keratinocytes. Indeed, we found a dramatic reduction in inflammation in *Smad3* knockout tumors compared to wild-type tumors, with particular loss of tumor-associated macrophages (TAMs) (42). It is well known that TPA treatment induces skin inflammation, and this stromal effect is critical for cancer development. TGFβ1 is a major cytokine induced by TPA. We have shown that TGFβ1 overexpression in keratinocytes has a profound effect on inducing skin inflammation (61, 75). Therefore, our study suggests that Smad3 is required for TGFβ1-mediated inflammation. Additionally, *Smad3* knockout skin demonstrated reduced epidermal hyperplasia, reduced proliferation in papillomas, and increased apoptosis in skin and papillomas compared to wild-type mice. TPA-induction increases TGFβ1 levels in keratinocytes, which normally leads to the upregulation of tumor promoting factors including TGF-α and AP-1 family members such as c-fos, c-jun, junB, and junD. However, Smad3 knockout TPA-treated skin, papillomas, and tumors demonstrated decreased induction of these molecules, indicating that Smad3 is required for this aspect of TPA-related tumor promotion. These results may also explain why grafted *v-ras^{Ha}/Smad3-/-* keratinocytes did not show resistance to malignant progression, as

overexpression of *v-ras*^{Ha} in the in vitro co-transfection study may be able to bypass the TGFα overexpression necessary for TPA-induced tumor progression (76).

Smad4

Somatic inactivation of Smad4 has been documented in multiple tumor types including pancreatic, colon, breast, and prostate cancer (77, 78). Additionally, deletion of *Smad4* in multiple murine tissues results in spontaneous cancers (77, 78). Our own studies and others have shown that epidermal-specific *Smad4* deletion blocks the growth inhibitory effect of TGFβ, resulting in hyperproliferation, with down-regulation of p21 and p27, and upregulation of c-Myc and cyclin D1 (77, 78). Further, all *Smad4-/-* mice developed spontaneous skin tumors including primarily SCCs, as well as sebaceous adenomas, basal cell carcinomas, and tricoepitheliomas (77, 78). *Smad4-/-* SCCs demonstrated inactivated Pten and activated Akt, representing activation of a key cell survival pathway (78). Mice with epidermal-specific deletion of both *Smad4* and *Pten* resulted in accelerated tumor formation, suggesting there is crosstalk between TGFβ signaling and Pten signaling in epidermal proliferation and survival (76). However, no spindle cell carcinomas resulting from EMT were observed. Interestingly, increased nuclear Smad3 levels were observed in Smad4 knockout SCCs (unpublished data). This result suggests that Smad4 loss abrogates TGFβ-mediated EMT but not TGFβ-mediated invasion, the latter of which may be mediated by Smad3.

Smad7

As mentioned previously, Smad7 is expressed at very low levels in normal epithelia, but is overexpressed in certain cancers (79). To further investigate the role of Smad7 in the skin, we generated keratinocyte-specific *Smad7* transgenic mice. *Smad7* transgenic mice displayed severe epithelial hyperplasia, potentially due to inhibition of TGFβ-induced growth inhibition and apoptosis. Further characterization of *Smad7* transgenic epithelia revealed down-regulation of TGFβ, BMP, and Activin receptors, and decreased levels of activated Smad 2 and 3 proteins, which is consistent with the reported role of Smad7 in inhibiting TGFβ superfamily signaling (80). A report from Liu et al. demonstrated that overexpression of *Smad7* in *v-ras*^{Ha}-transduced keratinocytes resulted in a marked increase in cell

proliferation, reduced *v-ras*^{Ha}-induced senescence, and upregulation of EGF-like growth factor superfamily members (81). To further investigate the role of Smad7 in a xenograft model, primary keratinocytes were co-infected with *Smad7* and *v-ras*^{Ha}, mixed with dermal fibroblasts, and grafted onto nude mice. *V-ras*^{Ha}*/Smad7*, but not *v-ras*^{Ha} grafts progressed to SCCs. Characterization of *v-ras*^{Ha}*/Smad7* SCCs revealed increased proliferation and invasive growth, upregulation of keratin 8, and lack of nuclear Smad-2, -3, or -5. Recently, a surprising finding from our laboratory shows that Smad7 binds a major mediator of Wnt signaling, β-catenin, and induces β-catenin degradation by recruiting the Smurf2 ubiquitin ligase to the Smad7/β-catenin complex (82). Since reduced Wnt signaling results in spontaneous skin cancer in mice (83), it would be interesting to examine whether Smad7-mediated β-catenin degradation contributes to the oncogenic role of Smad7 in skin cancer. On the other hand, enhanced Wnt signaling contributes to many types of cancer and also results in spontaneous skin cancer formation in mice (12). To this end, Smad7-mediated β-catenin degradation may also have a tumor suppressive role. Further, Smad7 overexpression in transgenic skin abrogated TGFβ-induced inflammation (our unpublished data), which may also contribute to tumor suppression. Therefore, Smad7 may play a dual role in carcinogenesis and future studies directly examining the role of Smad7 in cancer are warranted.

In the current study, we assessed the role and molecular mechanisms of keratinocyte-specific Smad2 ablation in skin chemical carcinogenesis. Further, we determined how loss of Smad2 or Smad4 in skin leads to similar and distinct molecular alterations promoting increased angiogenesis, contributing to a tumor-promoting microenvironment.

FIGURES

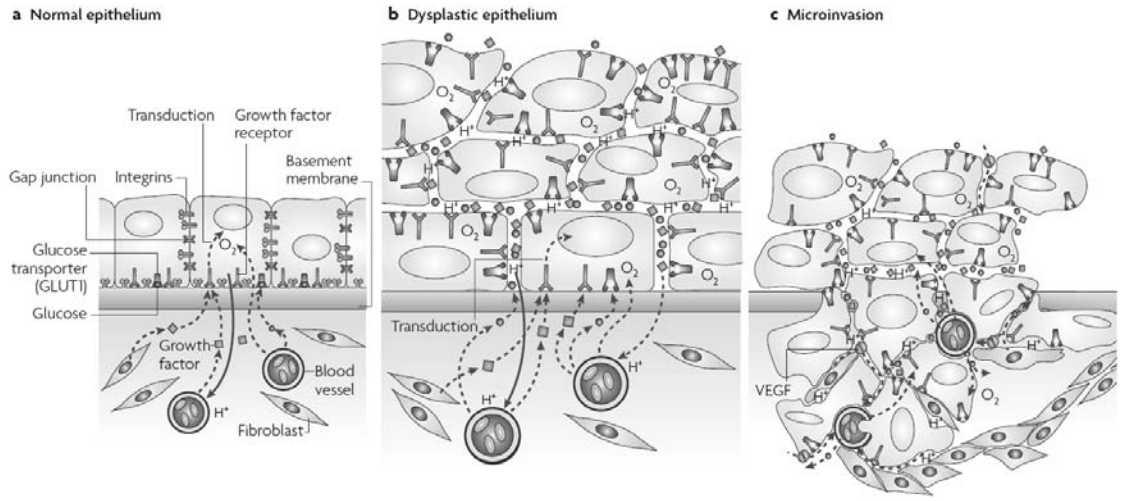

Figure 1. Cartoons of the three distinctive adaptive landscapes during evolution of invasive cancer. A: Normal simple epithelia with a single layer of epithelial cells connected to each other and the basement membrane by integrins and communicating through gap junctions. Apoptosis and contact inhibition restrict growth. B: Initial carcinogenic mutations allow proliferation away from the basement membrane. Diffusion-limited growth as growth factors and substrate must diffuse over increasingly large distances to reach the proliferating cells that proliferate away from the basement membrane. Adaptations arise including paracrine or autocrine production of growth factors, increased numbers of membrane receptors (as shown) or upregulation of transduction pathways. C: The adaptive landscape following of invasive carcinoma (microinvasion). Tumor growth is limited primarily by insufficient blood flow. Tumor cells adapt to co-opt normal mesenchymal cells leading to constitutive upregulation of vascular endothelial growth factor (VEGF, shown). Further, increased motility is rewarded with access to growth promoters and substrate without competition of other tumor cells resulting in rapid proliferation, which promotes evolution of the invasive phenotype. Note that the adaptive landscapes in A and B are avascular so that the delivery of substrate and growth factors from the blood supply requires diffusion-reaction kinetics. The adaptive landscape in C involves direct interaction of tumor cells with blood vessels and other elements of the mesenchyma. Figure and legend adopted from Gatenby RA, Gillies RJ. (2008) A microenvironmental model of carcinogenesis. *Nat Rev Cancer*, **8**, 56-61.

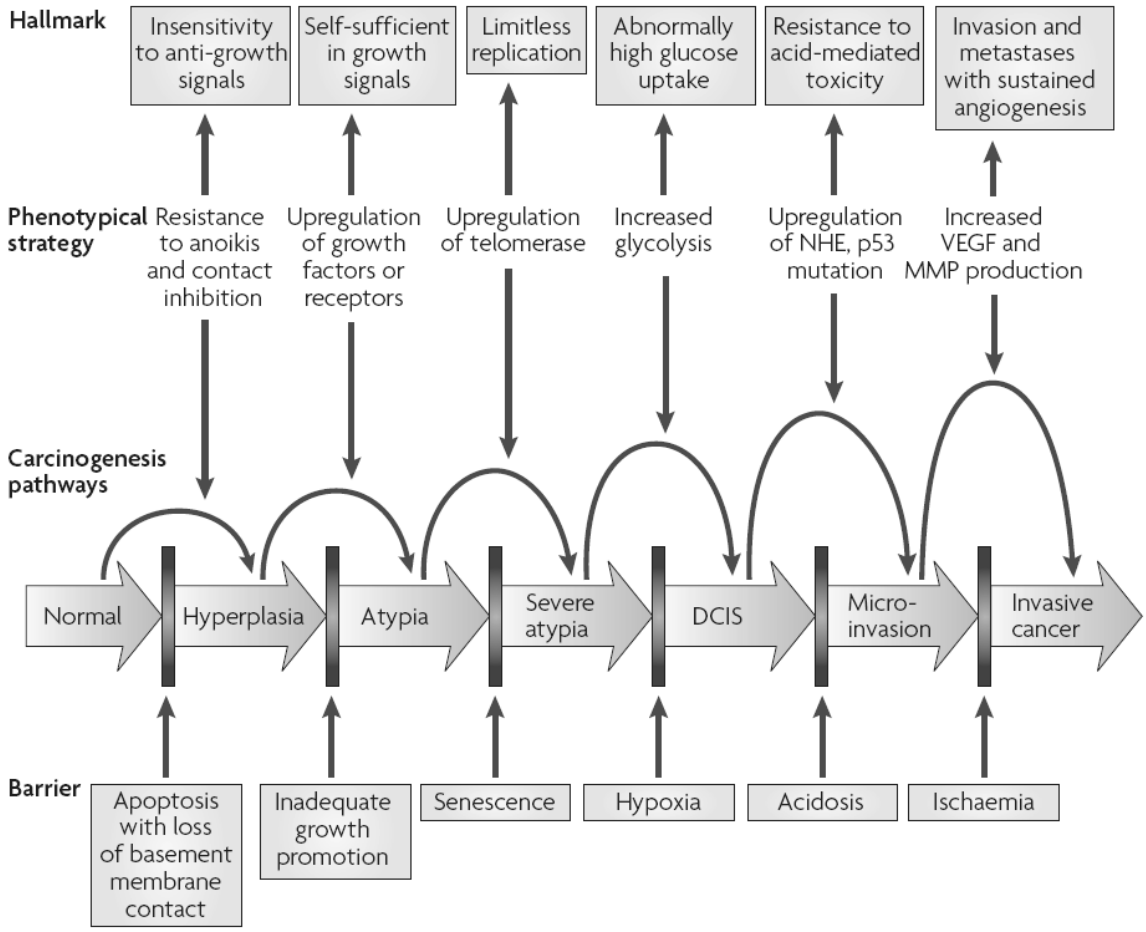

Figure 2. Proposed barriers to carcinogenesis based on the adaptive landscapes in Figure 1.

The phenotypical strategy to each barrier is shown along with general population hallmarks. The height of the curved arrows reflects growing cell populations. All cancers must overcome all of the barriers, but this can be accomplished using different strategies. Furthermore, alterations in a single multifunctional protein such as Ras, TGFβ, or hypoxia-inducible factor 1α may initially serve to overcome one barrier but then accelerate the subsequent pace of somatic evolution by lowering other barriers. The specific sequence of barriers is based on changes in the adaptive landscapes of premalignant lesions shown in Figure 1a. This should not be regarded as invariant, as the adaptive landscapes shown in Figure 1b may generate escape of more than one barrier simultaneously. DCIS, ductal carcinoma in situ; MMP, matrix metalloproteinase; NHE, Na^+/H^+ exchangers; VEGF, vascular endothelial growth factor. Figure and legend adopted from Gatenby RA, Gillies RJ. (2008) A microenvironmental model of carcinogenesis. *Nat Rev Cancer*, **8**, 56-61.

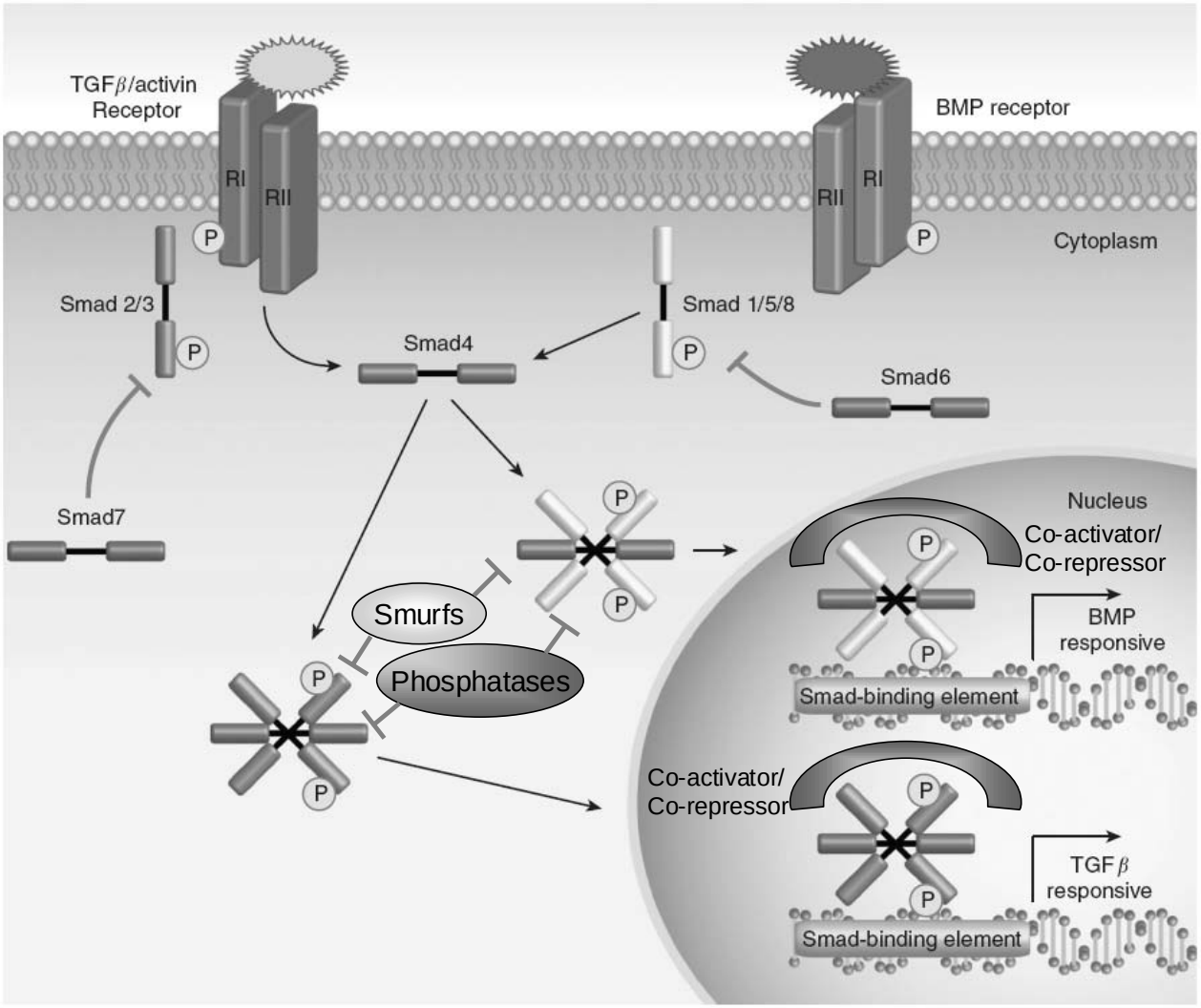

Figure 3. TGFβ- and BMP-signaling schematic.

TGFβ/Activin ligand binding to heteromers of TGFβ type I and type II receptors (TGFβRI and TGFβRII) induces TGFβRI to phosphorylate Smad2 and Smad3. Phosphorylated Smad2 and Smad3 bind a co-Smad, Smad4, and the heteromeric Smad complexes translocate into the nucleus to regulate transcription of TGFβ target genes. Smad3 binds to the Smad binding element (SBE) of a target gene, and subsequently recruits Smad4 to the same SBE. Smad2 does not bind to DNA directly but complexes with Smad3 and Smad4 as either a co-activator or a co-repressor for Smad3 and Smad4. Further, once bound to DNA, the Smad

complex binds other co-activators and co-repressors influencing transcriptional activation. Smad7 blocks Smad2/3 association with the phosphorylated receptor and prevents its activation. BMP ligand binding to heteromers of BMPRI and BMPRII causes phosphorylation of Smad1 and Smad5. Phosphorylated Smad1 or Smad5 then bind Smad4 and translocate into the nucleus to effect gene transcription. SMURF E3 ligases and phosphatases further regulate Smads.

II. CHAPTER 1:

Keratinocyte-Specific Smad2 ablation results in increased epithelial-mesenchymal transition during skin cancer formation and progression

MATERIALS AND METHODS

Human skin SCC collection and sample preparation

Human skin SCC and normal skin samples were from a human SCC tissue array (US Biomax) and collected from surgically resected specimens between the years 2000 and 2005 from consenting patients at the Departments of Dermatology and Otolaryngology, Oregon Health and Science University, under an Institutional Review Board-approved protocol. The tissue array contained 75 SCCs and 4 normal skin samples graded by two pathologists from the vendor. We confirmed the grading (well- vs. poorly-differentiated SCCs) for samples from both the tissue array and the ones collected by ourselves by reviewing hematoxylin and eosin (H&E) stained sections. Tissues used for IHC included 83 SCC cases and 10 normal skin samples. Tissues used for qRT-PCR assays included 33 poorly-differentiated skin SCCs and 6 normal skin samples. Among these samples, 21 samples, which contain adjacent non-neoplastic skin in paraffin sections, were manually dissected, and tissues sections of non-neoplastic skin and SCCs were collected separately. DNA from these tissue sections was extracted using the WaxFree^{TM} DNA Paraffin Sample DNA extraction kit (TrimGen Inc.). Subsequently this DNA was used for LOH PCR using primers for microsatellite repeat regions (84) (D18S555, FP 5'-FAM- GTGCGATGGCAAAATAGATG-3', RP 5'-ATTTTCTAGGAAAGAGCTAGC-3'; D18S1137, FP 5'-FAM-TGACTATTTGCACATCTGGC-3', RP 5'- GGACTTGCACGCTAATGAC-3'; D18S460, FP 5'-FAM-CTGAAGGGTCCTTGCC-3', RP 5'-GCCAGCCTTGGCAGTC-3'). PCR products were column purified (Promega) and analyzed using fragment length polymorphism analysis (ABI). LOH was determined using the following formula:

Peak height of allele 1 of tumor/Peak height of allele 2 of tumor vs. Peak height of allele 1 of adjacent skin/Peak height of Allele 2 of adjacent skin $\geq$1.5

Tissue histology, tumor classification, and IHC

Dissected skin and tumor samples were fixed in 10% neutral-buffered formalin at 4^{o}C overnight, embedded in paraffin, sectioned to 6 μm thickness and stained with H&E. Tumor types were determined by H&E analysis performed on papillomas at different time points using the criteria described previously (84). Generally, papillomas appeared as exophytic, pedunculated proliferations consisting of multiple fingerlike hyperkeratotic epidermal projections having an intact basement membrane creating a distinct border from the underlying dermis. Squamous cell carcinomas (SCCs) were characterized by invasive tumor cell proliferation into the dermis in a lobular pattern and numerous mitotic figures within tumor lobules. SCCs were further classified into well-, moderately- and poorly-differentiated groups based on disturbed cell polarity (mainly in basal cells), basal cell hyperplasia, disturbed maturational sequence, increased number of mitoses, mitoses in suprabasal layers, abnormal mitoses, nuclear hyperchromatism, prominent nucleoli, and increased nuclear/cytoplasmic ratio (56).

IHC was performed on paraffin sections. Sections were deparaffinized and rehydrated in Xylene for 30 minutes followed by 100% EtOH, 70% EtOH, and 50% EtOH for 5 minutes each. Slides were then boiled in 10mM Citric Acid in 0.1M Sodium Citrate for antigen retrieval. Intrinsic peroxidase activity was blocked by placing slides in 3% H_2O_2 for 10 minutes. Sections were blocked in PBS with 5% serum of host animal for secondary antibody for 1hr at room temperature. Primary antibodies were applied overnight at 4^{o}C. We used primary antibodies against human and mouse Smad2 (1:200, Zymed), Smad3 (1:100, Santa Cruz Biotechnologies) and Smad4 (1:100, Santa Cruz Biotechnologies). Biotinylated secondary antibodies (Vector Laboratories) were diluted 1:400 and preincubated in 10% Normal Mouse Serum for 1 hour before application. Secondary antibodies were applied for 10 minutes at room temperature. Avidin conjugated chromingen (M.O.M. kit, Vector Laboratories) was applied for 15 minutes at room temperature. DAB chromingen substrate (Dako Chemicals) was applied for 30 seconds to 5 minutes. Sections were counterstained with Hematoxylin. Protein levels detected by

immunohistochemistry were visually evaluated. A double-blind evaluation was performed by two investigators using the methods as we have previously described (85-87).

Generation of inducible and keratinocyte-specific Smad2 and Smad4 knockout mice

The inducible and keratinocyte-specific Cre line, *K5.Cre*PR1*, the *Smad2* floxed line (*Smad2*$^{f/f}$), and *Smad4* floxed line (*Smad4*$^{f/f}$) were generated in a by our colloborators in a *C57BL/6* background as previously reported (85-87). *K5.Cre*PR1* mice were crossed with *Smad2*$^{f/f}$ or *Smad4*$^{f/f}$ mice to generate wildtype, *K5.Smad2*$^{f/wt}$, *K5.Smad2*$^{f/f}$ or *K5.Smad4*$^{f/f}$ genotypes. For genotyping, DNA was obtained from tail clippings of 3 week old pups. PCR amplification of the floxed region and the Cre recombinase was performed using the following primers (86, 87): Cre*1: (5'-TACAGCTCCTGGGCAACGTG-3') and Cre*2 (5'- CACAGCATTGGAGTCAGAAG –3'). Smad2Flox1 (5′-TTCCATCATCCTTCATGCAAT-3′) and Smad2Flox2 (5′-CTTGTGGCAAATGCCCTTAT-3′), resulting in a 451-bp PCR product for floxed allele and 271-bp for wild-type alleles. Smad4Flox1 (5'-AAGAGCCACAGGTCAAGCAG-3') and Smad4Flox2 (5'-GGGCAGCGTAGCATATAAGA-3'), resulting in a 450-bp PCR product for the floxed allele and 390-bp product for the wild-type allele. Cre-mediated *Smad2* or *Smad4* deletion was achieved with topically treated with RU486 (20μg in 100μL ethanol) once a day for 3-5 days at time points specified in the Results section. *Smad2* or *Smad4* gene deletion was detected by PCR on DNA extracted from RU486-treated skin, using deletion-specific primers (61).

Skin chemical carcinogenesis protocol

Two weeks after the final RU486 treatment, the two-stage chemical carcinogenesis protocol (42) was applied. Briefly, the back of the mouse skin was shaved and topically treated with a one time dose of 20 μg of DMBA (Sigma, dissolved in 50 μl acetone). One week later, 5 μg of TPA (Sigma, dissolved in 50 μl acetone) was applied to skin twice a week for 20 weeks. In total, 20 *Smad2+/+*, 19 *Smad2-/-* and 12 *Smad2+/-* mice with equal distribution of genders in each group were used in the carcinogenesis study.

Double-stain immunofluorescence

Double-stain immunofluorescence on paraffin-embedded tissue sections was performed as we have previously described (77). After deparaffinization, antigen retrieval was performed by microwaving slides in 10 mM sodium citrate solution for 10 minutes. Each section was incubated overnight at 4°C with a primary antibody diluted in phosphate-buffered saline (PBS) containing 12% bovine serum albumin (BSA) and in most cases together with a guinea-pig antiserum against mouse K14, the latter of which highlights the epithelial compartment of the skin (5). The sections were then washed with PBS and incubated with fluorescence dye-conjugated secondary antibodies, an Alexa Fluo 488-conjugated (green) secondary antibody against the species of the primary antibody (1:100-1:400, Molecular Probes) and Alexa Fluo 594-conjugated (red) anti-guinea pig secondary antibody (1:100, Molecular Probes). The primary antibodies included keratin 1(K1) (1:500, Covance), keratin 8 (K8) (1:100, Fitzgerald), vimentin (1:200, Sigma), E-cadherin (1:100, BD Bioscience), keratin 14 (K14) (1:400, Fitzgerald), and Snail (1:200, Abcam). The fluorescence dye-conjugated secondary antibodies were diluted in 12% BSA-PBS and applied to the tissue sections at room temperature for 30 minutes. Slides were mounted with DAPI Slow-Fade (Molecular Probes).

RNA extraction and quantitative RT-PCR (qRT-PCR)

Total RNA was isolated from human and mouse skin and tumors using RNAzol B (Tel-Test), and a standard trizol-chloroform extraction (43), and further purified using a QIAGEN® RNeasy Mini kit (Qiagen). The qRT-PCR was performed using 50ng of RNA per well and the One-Step Brilliant II QRT-PCR system (Stratagene). Transcripts of human and mouse Smad2, Smad4, K8, Snail1, Snail2, Snail3, Twist, Vimentin, Tenascin C, and E-cadherin were examined using corresponding Taqman® Assays-on-Demand™ probes (Applied Biosystems). A K14 or GAPDH RNA probe was used as an internal control. Three to nine samples from each genotype of mice were used for qRT-PCR. For Smad2 gene expression assays, the expression levels from all *K5.Smad2*$^{+/+}$ samples were set as "1" arbitrary unit, which was used as a baseline to compare expression levels of the same gene in samples with different Smad2 genotypes. In

analyzing the relative expression levels of other genes, the average expression level from *K5.Smad2*$^{+/+}$ samples (unless otherwise specified) of each particular gene being analyzed was set as "1" arbitrary unit.

Comparative Chromatin Immunoprecipitation

Backskin from 4 mice of each genotype (wildtype, *K5.Smad2-/-*, and *K5.Smad4-/-*) were combined in 5mL of 1% formalin and homogenized on ice. An additional 5mL of 1% formalin were then added to each tube and allowed to incubate at room temperature for 30 minutes. One milliliter of 10X Glycine Stop Solution (Active Motif) was added and sample incubated at room temperature for 5 minutes. Samples were then centrifuged at 2500rpm for 10 minutes at 4^{o}C. The resulting pellet was then used following the manufacturer's protocol for ChIP using Enzymatic Digestion (Active Motif). Antibodies to Smad2 (3μg, Zymed), Smad3 (3 μg, Upstate), Smad4 (3 μg, Upstate), HMGA2 (3 μg, Santa Cruz Biotechnologies), TGIF (3 μg, Santa Cruz Biotechnologies), and Rabbit IgG (3 μg, Santa Cruz Biotechnologies) were used to immunoprecipitate the sheared chromatin complexes. DNA obtained from eluted beads was used for comparative PCR using Power SYBR Green Master Mix (Applied Biosystems). Primers encompassing the SBE sites of the Snail promoter (Table 1) were used for PCR. Positive binding was defined as antibody binding >10-fold of the IgG-negative control. ΔCt values were obtained by normalizing IP Ct values to Input values for each group. ΔΔCt values were obtained by comparing the ΔCt values of *Smad2-/-* skin to WT skin. Values are expressed as fold-change based on ΔΔCt values.

Cell Culture

HaCaT cells were cultured in high-glucose DMEM with 10% FBS and penn-strep antibiotics. Twenty-four hours prior to transfection or TGFβ treatment, cells were switched to low-glucose DMEM with 0.2% FBS and penn-strep antibiotics. Cells were transfected using XtremeGene siRNA Transfection Reagent (Roche) in 6-well plates or chamber slides, at a final concentration of 50pmol siRNA/uL in Optimem media. Four hours post-transfection, media was switched to high-glucose DMEM. Cells were harvested for RNA using Qiashredder and RNeasy kits (Qiagen). Chamber slides were fixed for 40

minutes at room temperature in 2% paraformaldehyde and stained with antibodies specified in the Results section using the methods as described above. siRNA sequence information in Table 2.

Protein Extraction, Western Blot, and ELISA

Protein was extracted from cells harvested in Complete Lysis Buffer M (Roche). Total protein was determined using detergent compatible to Bradford Assay reagents (BioRad). ELISA kit for TGFβ1 (R&D Systems) was used to determine the concentration of TGFβ1, as per the manufacturer's instructions.

For Western blot, equal amounts of protein were separated on a 10% SDS-PAGE resolving gel with a 4% SDS-PAGE stacking gel. Protein was transferred to a nitrocellulose membrane and blocked using 5% non-fat milk in 0.1% Tween in TBS for 1 h at room temperature. Blots were double stained with 700nm and 800nm donkey IRDye-labeled secondary antibodies (Rockland, 1:5,000) against target and loading control primary antibodies. Target primary antibodies included rabbit anti-human-Smad2 antibody (Zymed,1:1,000), rabbit anti-human-Smad3 (Santa Cruz Biotechnologies, 1:1,000), mouse monoclonal anti-human-Smad4 (Santa Cruz Biotechnologies, 1:1,000), rabbit anti-human Snail (Zymed, 1:1,000), rabbit anti-mouse Akt (Cell Signaling, 1:500), rabbit anti-mouse Erk1/2 (Cell Signaling, 1:500), rabbit anti-mouse Jnk (Cell Signaling, 1:250), rabbit anti-mouse p38 (Cell Signaling, 1:500), rabbit anti-mouse pAkt (Cell Signaling, 1:500), rabbit anti-mouse pErk1/2 (Cell Signaling, 1:250), rabbit anti-mouse pJnk (Cell Signaling, 1:100), and rabbit anti-mouse p-p38 (Cell Signaling, 1:250). Loading control primary antibodies included rabbit anti-human GAPDH (Santa Cruz Biotechnologies, 1:5,000), mouse anti-human Actin (Santa Cruz Biotechnologies, 1:2,500), or mouse anti-mouse tubulin (Sigma, 1:3000). Gels were scanned and analyzed using LiCor Odyssey scanner (LI-COR Biotechnology).

Matrigel Assay

HaCaT cells were siRNA treated as described above. At 24h post-transfection, cells were either TGFβ treated as described above, or placed in low glucose DMEM. 24h post-TGFβ treatment, cells were trypsinized and placed on matrigel membranes in triplicate. The following day, cells invading the matrix

were fixed and stained using HEMA3 stain set (Protocol), visualized via microscopy, and manually quantified.

Statistics

Significant differences between the values obtained in each assay on samples from various genotypes were determined using the Student's t-test and expressed as mean ± standard error of the mean, with the exception of evaluation of human SCCs and tumor malignancy where a Chi-Squared (χ^2) test was used.

RESULTS

Smad2 and Smad4 were frequently lost in human skin SCCs

We examined Smad2 expression patterns by immunohistochemistry (IHC) in 83 human skin SCCs. Smad3, a Smad2 signaling partner, and co-Smad, Smad4, were also examined. Staining of Smad2, Smad3 and Smad4 was predominantly localized to the epidermis in normal skin (Figure 4). Smad2 and Smad4 each were lost in 58/83 (70%) of skin SCC samples (Figure 4, Table 3). In contrast, Smad3 loss was only seen in 4/83 (5%) cases (Figure 4, Table 3). Additionally, Smad2 loss occurred in 100% of poorly differentiated SCCs (53/53 samples), whereas only 17% (5/30 samples) of well differentiated tumors showed Smad2 loss. To a lesser degree, Smad4 loss also correlated with de-differentiation, with 83% (44/53) of poorly differentiated and 47% (14/30) of well differentiated SCCs having Smad4 loss.

To determine whether loss of Smad2 and Smad4 proteins in human skin cancer occurs at the pre-translational level, we examined mRNA levels of Smad2 and Smad4 from 33 cases of poorly differentiated human SCCs collected from consented patients at the OHSU Dermatology and Otolaryngology clinics. Six normal skin samples were used as controls. In comparison with control skin, 31/33 (94%) of human skin SCC samples showed at least a 50% reduction of Smad2 mRNA, and 28/33 (85%) of these samples showed at least a 50% reduction of Smad4 mRNA (Figure 5A). Such high rates of Smad2 and Smad4 loss at the mRNA level prompted us to examine if they are lost at the genetic level. Among samples with >50% mRNA reduction of Smad2 and Smad4, 21 samples contained adjacent non-neoplastic skin in their paraffin sections. We dissected the adjacent non-neoplastic skin in each section as a control for each tumor sample and performed a loss of heterozygosity (LOH) analysis for *Smad2* and *Smad4* (Figure 5B and Figure 6). We found that 14 samples (67%) exhibited LOH at the *Smad2* locus, and 12 samples (57%) exhibited LOH at the *Smad4* locus. A total of 17 samples (81%) had LOH at either the *Smad2* or *Smad4* locus.

Keratinocyte-specific Smad2 deletion resulted in increased susceptibility to skin carcinogenesis

Our previous study has revealed that Smad4 loss in keratinocytes results in spontaneous skin SCCs (88). To determine if the high incidence of Smad2 loss, with a rate similar to Smad4 loss, in human

skin SCCs also plays a causal role in skin carcinogenesis, we generated keratinocyte-specific *Smad2* knockout mice (Figure 7). Mice with RU486-controlled Cre recombinase targeted by a Keratin 5 promoter (*K5.Cre*PR1*) were generated as previously reported (87). We mated *K5.Cre*PR1* mice with *Smad2* floxed mice ($Smad2^{f/f}$) (61). *Smad2* deletion in keratinocytes was achieved by topical application of RU486. After *Smad2* was deleted in keratinocytes, mice were monitored for eighteen months. Unlike *Smad4-/-* epidermis, *Smad2-/-* epidermis did not exhibit increased proliferation (Figure 8) or develop spontaneous tumors, suggesting that Smad2 loss is insufficient to initiate tumor formation.

To further assess whether Smad2 loss alters susceptibility to skin carcinogenesis, we applied a two-stage chemical carcinogenesis protocol, which gives discrete stages of benign papillomas and malignant SCCs in normal mice (89). Littermates from *K5.Cre*PR1* and $Smad2^{f/f}$ breeding were divided by their genotypes (*K5.Cre*PR1/*$Smad2^{f/f}$ for *K5.Smad2-/-*; *K5.Cre*PR1/*$Smad2^{f/wt}$ for *K5.Smad2+/-*; *K5.Cre*PR1*, $Smad2^{f/f}$, and $Smad2^{f/wt}$ for *Smad2+/+*) and treated with 20 μg RU486 daily for 5 days at 6 weeks of age to induce *Smad2* gene deletion in keratinocytes. Two weeks after RU486 treatment, when keratinocytes in the entire epidermis were expected to be replaced with *Smad2-/-* or *Smad2+/-* epidermal stem cells in *K5.Cre*PR1/*$Smad2^{f/f}$ or *K5.Cre*PR1/*$Smad2^{f/wt}$ mice, respectively, we topically applied a subcarcinogenic dose of dimethylbenz[α]anthracene (DMBA, 20 μg/mouse). One week later we began to topically apply 12-O-tetradecanoyl-phorbol-13-acetate (TPA, 5 μg/mouse) twice a week for 20 weeks. *K5.Smad2-/-* and *K5.Smad2+/-* mice developed tumors faster and had 2-3 fold more tumors per mouse than *Smad2+/+* mice ($p<0.001$, Figure 9A). Malignant conversion was also accelerated in *K5.Smad2-/-* and *K5.Smad2+/-* mice ($p<0.05$ compared with *Smad2+/+* mice). The earliest SCC formation was 16 weeks, 28 weeks, and 33 weeks for *K5.Smad2-/-*, *K5.Smad2+/-* and *K5.Smad2+/+* mice, respectively. Notably, at each time point, more *K5.Smad2-/-* and *K5.Smad2+/-* mice developed SCCs than *Smad2+/+* mice (Figure 9B). These results indicate *Smad2* deficient epidermis is more susceptible to skin tumor formation and malignant conversion.

Because *K5.Smad2+/-* also exhibited accelerated tumor formation and malignant progression similar to *K5.Smad2-/-* mice, we examined endogenous Smad2 levels in *K5.Smad2+/-* tumors. Smad2 protein was still detectable in all *K5.Smad2+/-* papillomas, but was lost in 60% cases of *K5.Smad2+/-* SCCs (Figure 10). At this stage, ~45% SCC cases from *Smad2+/+* mice also lost Smad2 protein as determined by Smad2 antibody staining (Figure 10, $p>0.05$). These data suggest haploinsufficiency of *Smad2+/-* keratinocytes at early stages of skin carcinogenesis, and spontaneous Smad2 protein loss from the remaining allele in SCCs caused them to progress to malignancy similar to *Smad2-/-* SCCs.

K5.Smad2-/- *tumors were poorly differentiated and exhibited an increase in EMT*

To determine whether accelerated skin carcinogenesis in *K5.Smad2-/-* mice was a result of abrogating TGFβ-induced growth inhibition and/or apoptosis, we evaluated cell proliferation via BrdU incorporation and apoptosis via the TUNEL assay. The apoptosis rate in *K5.Smad2-/-* non-lesional and tumor tissues did not differ from those in *K5.Smad2+/+* controls (unpublished data from our lab). Although non-lesional *K5.Smad2-/-* skin did not show increased proliferation, TPA-treated *K5.Smad2-/-* skin exhibited increased proliferation and epidermal hyperplasia (Figure 8). However, proliferation rates became comparable in tumors between *K5.Smad2-/-* and wildtype mice (our lab's previous, unpublished data). Histological analyses revealed that *K5.Smad2-/-* tumors were generally poorly differentiated. The earliest *K5.Smad2-/-* papillomas lacked stratified epithelial structure (Figure 9C) and keratin K1, an early differentiation marker (Figure 9C), but expressed keratin K8 (Figure 9C), a marker of simple epithelia that is not expressed in stratified epithelia but is usually expressed in late-stage SCCs (90). In contrast, papillomas in wildtype mice lacked K8 expression but retained uniform K1 expression (Figure 9C). At the SCC stage, *K5.Smad2-/-* SCCs were poorly differentiated and often showed clusters of cells that underwent EMT (Figure 9C), whereas most SCCs from wildtype mice were well differentiated (Figure 9C). While only 1 out of 20 wildtype mice developed an EMT-type of spindle cell carcinoma (SPCC) 50 weeks after TPA promotion, *K5.Smad2+/-* and *K5.Smad2-/-* mice developed more SPCCs at earlier time points (3 out of 12 *K5.Smad2+/-* and 5 out of 19 *K5.Smad2-/-* starting at 27-35wks).

K5.Smad2-/- *tumors exhibited pathological alterations associated with EMT*

The poorly differentiated nature of *Smad2-/-* tumors prompted us to examine the status of E-cadherin, an adhesion molecule critical for maintaining epithelial structure. While E-cadherin was lost in only patchy areas of late stage *Smad2+/+* papillomas, *Smad2-/-* papillomas exhibited nearly complete loss of E-cadherin (Figure 11). In contrast, early stage *Smad4-/-* spontaneous SCCs retained membrane-associated E-cadherin in most tumor cells (Figure 4). We then examined expression patterns of Snail, a known transcriptional repressor of E-cadherin (91, 92). Snail antibody staining, which recognizes all Snail isoforms, revealed a patchy, cytoplasmic staining pattern in wildtype papillomas and early stage *Smad4-/-* spontaneous SCCs (Figure 11). In contrast, *Smad2-/-* tumors exhibited strong Snail staining primarily in the nucleus (Figure 11). Both chemically-induced wildtype SCCs and *Smad4-/-* spontaneous SCCs showed reduced E-cadherin and increased Snail nuclear staining in late stages, ~10-20 weeks after SCC formation. *K5.Smad2-/-* tumors also showed an increase in mesenchymal markers, vimentin and αSMA, (Figure 12A), which are associated with motility and invasiveness (93). These markers were restricted to the stroma of *K5.Smad2+/+* papillomas and spontaneous *Smad4-/-* SCCs, but were detected in both tumor epithelia and stroma of *K5.Smad2-/-* papillomas. Additionally, vimentin and αSMA were present in the hyperplastic epidermis adjacent to papillomas of *K5.Smad2-/-* mice (Figure 12B), suggesting that EMT is a relatively early event in *K5.Smad2-/-* carcinogenesis. We then examined if the EMT phenotype occurs in *K5.Smad2-/-* without exposure to a carcinogen. Seventy two hours after *Smad2* was deleted in neonatal skin, a marked loss of E-cadherin and an associated upregulation of nuclear Snail expression were seen in *Smad2-/-* epidermis and hair follicles, when compared to RU486 treated wildtype and *K5.Smad4-/-* skin (Figure 11B). However, vimentin and αSMA were not detected in *K5.Smad2-/-* epidermis. These results suggest that EMT is an early effect of Smad2 loss and additional insults during carcinogenesis further enhanced Smad2 loss-associated EMT phenotype.

K5.Smad2-/- *tumors exhibited mRNA alterations of TGFβ target genes associated with EMT*

To assess if Smad2 loss-associated EMT was associated with increased TGFβ1 ligand, which plays an important role in EMT (56), we examined TGFβ1 levels in wildtype and *Smad2-/-* skin and

tumors. We found neither elevated TGFβ1 nor alterations of Smad3 and Smad4 in *K5.Smad2-/-* skin and papillomas in comparison with wildtype controls. Elevated TGFβ1 protein was found in wildtype and *K5.Smad2-/-* SCCs at comparable levels (Supplemental Figure 6). Consistent with this data, western analyses showed that *K5.Smad2-/-* tumors did not have increased levels of pJNK, pERK, pMAPK (Figure 13), the major non-Smad pathways of TGFβ-induced EMT that require a higher level of TGFβ1 than that found in wildtype tumors (36). Consistent with our previous observation that ~30-40% of chemically-induced SCC cases exhibited reduction in Smad3 and Smad4 at late stages (32, 52), both wildtype and *K5.Smad2-/-* SCCs showed reduced Smad3 and Smad4 in ~40% cases. SCCs which retained Smad3, showed similar patterns between wildtype and *K5.Smad2-/-* mice (Figure 14). *K5.Smad2-/-* SCCs which retained Smad4 showed more nuclear staining than *K5.Smad2+/+* SCCs (Figure 14). To further determine whether changes in EMT-associated proteins are the result of transcriptional deregulation of these genes by Smad2 loss, we examined mRNA levels of these molecules in *K5.Smad2-/-* and *K5.Smad2+/+* papillomas, at the stage prior to the pathological appearance of EMT cells in *K5.Smad2-/-* tumors. Transcripts of K8, Snail, Slug, vimentin, and Tenascin C were all significantly increased in *K5.Smad2-/-* papillomas in comparison with wildtype papillomas (Figure 15A). In contrast, transcripts of E-cadherin were reduced in *Smad2-/-* papillomas in comparison with wildtype controls (Figure 15B). Further, increased transcripts of Snail and Slug, and decreased E-cadherin transcripts were also detected in day 3 *K5.Smad2-/-* skin in comparison with wildtype skin (Figure 15C, D). These data suggest that upregulation of Snail/Slug and the subsequent of E-cadherin reduction represent an early effect of Smad2 loss in keratinocytes. To further assess if Smad2 regulates Snail and Slug differently from Smad3 and Smad4 in keratinocytes, we examined transcript levels of Snail and Slug in cultured human HaCaT keratinocytes after knocking down Smad-2, -3 or -4. After 48 to 72 h of transfection of HaCaT cells with siRNAs for Smad-2, -3, or -4, the respective mRNA levels were reduced by at least 70% (Figure 16). In mock-transfected cells, increased Snail mRNA was detected after 1 h of TGFβ1 treatment, and remained increased for 48 h (Figure 16J), with a 9-fold increase at 2 h (Figure 15E). After Smad2 was knocked down for 72hrs, Snail transcript was increased by 13-fold, and further increased by 24-fold after 2 h TGFβ1 treatment (Figure 5E). In contrast, knockdown of Smad3 did not affect baseline Snail expression but significantly suppressed TGFβ1-induced Snail

expression (Figure 15E). Knocking down Smad4 abrogated both baseline and TGFβ1-induced Snail expression (Figure 15E). Slug transcript was also induced by TGFβ1 treatment, with a 2-fold increase 2 h after TGFβ1 treatment (Figure 15F). However, none of the individual Smads affected Slug expression levels, with or without TGFβ1 treatment (Figure 15F). These data suggest that expression of Snail, but not Slug, is regulated by Smads. Thus, in vivo Slug overexpression in *K5.Smad2-/-* keratinocytes could be a secondary event.

Next, we assessed if Smad2 loss correlated to Snail overexpression in human skin SCCs. Overall, Snail overexpression and E-cadherin loss occurred at high frequencies in human skin SCCs. However, consistent with the association of Smad2 loss with poorly- differentiated SCCs (Table 3), Smad2 negative SCCs exhibited a higher incidence of Snail overexpression than Smad2 positive SCCs (90% vs. 73%, $p<0.05$, Figure 17, Table 4). Similarly, the rate of E-cadherin loss occurred in 79% of Smad2 negative SCCs vs. 60% in Smad2 positive SCCs ($p<0.05$, Figure 17, Table 4).

Elevated Snail was sufficient to mediate Smad2 loss-associated EMT

To determine whether increased Snail expression was functionally responsible for Smad2 loss-associated EMT, we knocked down Snail together with Smad2 in HaCaT cells (Figure 18). In control keratinocytes, Snail staining was cytoplasmic in most cells with sporadic nuclear staining cells, and E-cadherin stained the cell membrane. After 72 h of Snail knockdown, Snail expression was reduced by 80% (Figure 16). Additionally, E-cadherin staining in Snail-siRNA treated cells retained a similar pattern to control cells. After 72 h of Smad2 knockdown, HaCaT cells appeared more spindle-like, which correlated with increased Snail nuclear staining and loss of E-cadherin (Figure 18). However, knocking down both Smad2 and Snail restored membrane-associated E-cadherin staining and epithelial morphology, suggesting that Snail is the major target of Smad2 loss and mediates Smad2 loss-associated EMT.

Enhanced Smad4 binding to the Snail promoter in Smad2-deficient keratinocytes

To further analyze if Snail overexpression induced by Smad2 loss was the result of enhanced transcriptional activity of Smad3 and/or Smad4, we performed *in vivo* chromatin immunoprecipitation (ChIP) for Smad binding to the Snail promoter in neonatal wildtype and *Smad2-/-* mouse skin. Within the TGFβ-regulatory region of the mouse Snail promoter, as identified by previous studies (94), there are two Smad binding elements (SBEs) at 438bp and 1077bp upstream of the Snail transcriptional start site (TSS). We found that in wildtype skin, Smad-2, -3, and -4 bound to both sites (Figure 19A, B) but not to intronic regions of the gene. Comparative PCR on the precipitated chromatin revealed that in *Smad2-/-* skin, Smad3 binding to both SBEs was at a capacity similar to that in wildtype skin (Figure 19A, B), suggesting that Smad2 does not affect the affinity of Smad3 binding to the Snail promoter. However, Smad4 binding to the Snail promoter increased by 8- and 29-fold on the -438bp and the -1077bp sites, respectively, in *K5.Smad2-/-* skin compared to that in wildtype skin (Figure 19A, B). Therefore, these data suggest that normally, Smad2 either competes with, or impedes Smad4 binding to the SBE at the Smad3 binding site on the Snail promoter. To further assess if Smad2 loss-associated increase in Smad4 binding to the Snail promoter contributes to Snail overexpression, we knocked down Smad4 together with knockdown of Smad2. Knocking down Smad4 abrogated Smad2 loss-associated Snail overexpression (Figure 19C), suggesting that increased Smad4 binding contributed to transcriptional regulation of Snail in *K5.Smad2-/-* keratinocytes. Knockdown of Smad3 also abrogated Smad2 loss-associated Snail overexpression, suggesting that Smad3 binding in a complex with Smad4 is required for increased Snail transcription in Smad2-deficient keratinocytes.

Enhanced HMGA2 and reduced TGIF binding to the Snail promoter in Smad2-deficient keratinocytes

Previous studies have demonstrated TGFβ induces Snail both directly and indirectly through upregulation of HMGA2 (55). While we found Snail to be upregulated loss of Smad2, we could not discern whether the enhanced Smad4 binding to the Snail promoter in Smad2-deficient skin and keratinocytes was a result of relief of repression or enhanced differential recruitment of co-activators, like HMGA2, or both. Therefore, we performed comparative ChIP for Snail transcriptional activator, HMGA2

(55) and Smad interacting co-repressor, TGIF (27). We identified an HMGA2 binding site –134bp upstream of the mouse Snail transcriptional start site. Binding of HMGA2 was 65-fold stronger in *K5.Smad2-/-* skin than in wildtype skin, while Smad3 and Smad4 binding to this region was increased, though not statistically significantly (Figure 20A). Therefore, when Smad2 is lost, HMGA2 binds with more affinity contributing to Smad3/4-mediated expression of Snail. Further, when we evaluated transcriptional co-repressors at the SBE –437bp upstream of the TSS, we found TGIF was essentially unbound in *K5.Smad2-/-* skin compared to wildtype (Figure 20B), but bound nearly 8-fold stronger in *K5.Smad4-/-* skin (Figure 20B), which lacks Snail expression (Figure 11) and has increased Smad2 bound to the promoter (Figure 20B). This data indicates Smad2-loss mediated expression of Snail is due to both relief of repression and Smad3/4/HMGA2-mediated activation of Snail.

Smad2 knockdown does not increase migration

In order to evaluate the effect of Smad2 loss on migration, we performed in vitro migration assays using a Matrigel system (BD Bioscience). HaCaT cells were treated with siRNAs to Smad2, Smad3, Smad4, and Snail and in various combinations. Cells were then treated with and without TGFβ and assayed for migration through the Matrigel matrix membrane. Consistent with the lack of increased metastasis in vivo, our Smad2 siRNA treated HaCaT cells showed a reduction in migration when compared to mock treated cells (Figure 21A). We considered this may be due to a lack of Ras-activation, as is common in skin SCCs, and induced in our chemical carcinogenesis protocol. In order to assess whether Ras activation combined with Smad loss had an effect we utilized two Ras-transduced HaCaT cell lines, the HaCaT-II4 cells which form papillomas in xenograft models, and the HaCaT-RT3 cells, which form highly metastatic SCCs in xenograft models. Again, we saw Smad2 siRNA treated cells had reduced migration through the matrix (Figure 21B and 21C) indicating that although Smad2 loss promotes EMT, it prevents metastasis, further elucidating the dual role of TGFβ in carcinogenesis.

DISCUSSION

Smad2 and Smad4, but not Smad3, are frequently lost in human skin SCCs

In the current study, we found that proteins of Smad2 or Smad4, but not Smad3, were frequently lost in human skin SCCs. The rates of loss of Smad2 and Smad4 transcripts reached ~90% in samples with protein loss of Smad2 and Smad4, suggesting that loss of Smad2 and Smad4 in human skin SCCs is preferentially at the pre-translational level. Among them, we identified LOH of *Smad2* and *Smad4* in 67% and 57% cases, respectively. In cases with LOH of *Smad2* or *Smad4*, single-copy genetic loss may contribute to at least 50% loss of their transcripts and protein in each case, as mice with heterozygous deletion of *Smad2* or *Smad4* exhibited ~50% loss of transcripts and protein of these two molecules [(95-98), and the current study]. Additionally, transcriptional and post-translational modifications could contribute to further loss of the remaining Smad2 and Smad4 transcripts and protein. Several Smad ubiquitin-E3 ligases, which contribute to Smad protein degradation, have been identified, some of which have been shown to be overexpressed in cancer (99). Thus, multiple mechanisms from the genetic to the post-translational level could explain loss of Smad2 and Smad4 proteins, which are among the most frequent molecular alterations in skin cancer. Indeed, Smad2 and Smad4 loss occur more frequently than the currently known common molecular alterations in human skin SCCs, e.g., oncogene ras activation or loss of the p53 tumor suppressor (100). Notably, the incidences of Smad2 and Smad4 loss in skin SCCs found in this study are much higher than in head and neck SCCs (38, 61, 77, 78). These differences may reflect cancer etiology, which is largely attributed to UV irradiation in skin cancer and to tobacco carcinogen exposure in head and neck cancer.

Smad2 has a tumor suppressive effect on the skin

Consistent with the data from human skin SCCs, studies from animal models suggest that Smad2 and Smad4, but not Smad3, have tumor suppressive functions in the skin [(56), and our current study]. However, unlike keratinocyte-specific *Smad4* knockout mice which developed spontaneous skin SCCs, *K5.Smad2-/-* mice developed skin tumors neither spontaneously nor with TPA treatment alone (without DMBA initiation), even though *K5.Smad2-/-* epidermis exhibited an increase in proliferation in response to

TPA application. Thus, the increased proliferative potential of *K5.Smad2-/-* epidermis is insufficient as an initiator for skin carcinogenesis. This result is consistent with Smad2 expression patterns in human skin SCCs, in which Smad2 loss occurs only in SCCs but not in early stage actinic keratosis (101). Conversely, in the presence of a DMBA-induced H-ras mutation, a genetic alteration mimicking early stage human skin cancer (38), *K5.Smad2-/-* mice still did not develop skin tumors without TPA promotion. Thus, Smad2 loss alone is also insufficient to promote initiated cells for cancer development. However, with both DMBA initiation and TPA promotion, *K5.Smad2-/-* mice were more susceptible to skin tumor formation and malignant conversion than wildtype mice. Although the current study limits the assessment of the true malignant conversion rate for each papilloma due to the necessity of euthanizing SCC-bearing mice with multiple papillomas, more *K5.Smad2-/-* mice developed SCCs at the same time points when compared to wildtype mice. Additionally, *K5.Smad2-/-* papillomas already harbored molecular changes seen in wildtype SCCs but not in papillomas, suggesting that the malignant progression program was in place prior to the pathological progression in *K5.Smad2-/-* tumors. Thus, Smad2 loss appears to cooperate with other molecular alterations elicited by the chemical carcinogenesis protocol to promote skin carcinogenesis. Interestingly, *K5.Smad2+/-* mice displayed tumor kinetics similar to *K5.Smad2-/-* mice. This observation is also consistent with a previous report that germline *Smad2* heterozygous mice exhibited accelerated tumor formation and malignant progression in a skin chemical carcinogenesis experiment (93). These studies suggest a haploid insufficiency for *Smad2* in tumor suppression.

Smad2 loss triggers molecular and pathological alterations associated with EMT

Our current study reveals that in human skin cancer, Smad2 loss was associated with de-differentiation, loss of E-cadherin and Snail activation. Correlated with this observation, the accompanying animal study reveals that loss of Smad2 triggers pathological and molecular alterations associated with de-differentiation and EMT, started in non-lesional *Smad2-/-* epidermis. Among EMT associated genes, Snail exhibited the most dramatic upregulation in *Smad2-/-* skin and tumors in vivo and in Smad2 siRNA transfected keratinocytes in vitro, and knocking down Snail is sufficient to reverse Smad2 loss-associated

EMT phenotype. Therefore, Snail overexpression appears to be a major target and mediator of Smad2 loss-induced EMT.

The effect of Smad2 loss on EMT is somewhat surprising given that TGFβ signaling is well documented to promote EMT via both Smad and non-Smad pathways (56, 102). Unlike keratinocytes with knockdown of TGFβRII, which overexpress TGFβ1 (13), Smad2 loss did not cause increased TGFβ1. However, our data revealed a significant increase in promoter binding of Smad4 and HMGA2 to the Snail promoter in *Smad2-/-* keratinocytes. It is possible that normally Smad2 either competes with or impedes the ability of Smad4 to bind Smad3 on the SBEs of the Snail promoter, therefore Smad2 loss confers more binding of Smad4 with Smad3. Although Smad2 has been shown to activate Snail, it is likely that Smad2 has a much weaker effect than Smad4, given the fact that Smad2, but not Smad4, normally recruits transcriptional co-repressors to SBEs (32), as was seen with loss of TGIF binding to Snail promoter in *K5.Smad2-/-* skin, but increased in *K5.Smad4-/-* skin corresponding to levels of Smad2 binding to the Snail promoter. Based on this, once Smad2 is lost, the co-repressors would not be recruited to the SBEs, and Smad3 together with Smad4 and HMGA2 would drive a higher level of Snail transcription. Supporting this explanation, knocking down either Smad3 or Smad4 abrogated Smad2 loss-associated Snail overexpression, and a previous study showed that the combination of Smad3 and Smad4 had the highest transcriptional activity on the Snail promoter (31). Our data also complements data showing TGFβ-induced EMT occurs partially through transcriptional upregulation of HMGA2 and its cooperative effects on TGFβ-induced Snail (55). Our data also helps to explain the difference between our current finding and a previous finding showing that a dominant negative form of either Smad2 or Smad3 blocked TGFβ1-induced EMT in skin SCC cells (103). In that study, either increased Smad4 binding to the Snail promoter or the loss of co-repressors should not occur due to the presence of wildtype Smad2. Since *Smad4-/-* skin and early stage SCCs did not undergo EMT or exhibit the associated molecular alterations even in the presence of Smad2 and Smad3, Smad4 appears to be indispensable for EMT at least at early stages of skin carcinogenesis. Similar to our current finding, a previous study shows that pancreatic ductal adenocarcinomas derived from *Smad4* null cells are more well-differentiated and have less EMT in

comparison with tumors with intact Smad4 (87). Consistently, Ju *et al*. (104, 105) reported that in hepatocyte-specific *Smad2* knockout mice, hepatocytes underwent de-differentiation and EMT, whereas *Smad3-/-* hepatocytes did not. Since Smad4 was not lost in *Smad2-/-* skin and in early stage tumor cells, enhanced Smad4 binding to the Snail promoter is likely the major contributor to increased Snail expression, at least at early stages of skin carcinogenesis in *Smad2-/-* mice. When Smad4 is lost at late stages, multiple genetic/epigenetic alterations accumulated in tumor epithelia could be sufficient to sustain EMT and invasion. To this end, other pathways commonly activated in late stage skin carcinogenesis, e.g., AKT and NFκB, have been shown to activate Snail expression and EMT (77, 78).

It is worthwhile to mention that accelerated EMT phenotype does not always contribute to malignant progression. For instance, *Smad4-/-* keratinocytes did not exhibit EMT but proceeded to spontaneous SCCs (106-110). Conversely, accelerated EMT in *Smad2-/-* keratinocytes was insufficient to cause spontaneous skin cancer formation. Thus, EMT would promote tumor invasion in vivo only when coupled with other oncogenic events. Further, all of the EMT-associated genes upregulated in *K5.Smad2-/-* tumors also have additional functions for promoting cancer invasion. For instance, Snail and Slug regulate cell survival and apoptosis (111), and Snail overexpression in the epidermis causes keratinocyte hyperproliferation (112). Tenascin C has been implicated in angiogenesis (113). All these functions could contribute to accelerated tumor formation and progression *K5.Smad2-/-* mice. Additionally, we saw decreased ability to degrade matrix in our in vitro system, even with Ras-transduced Smad2 knockdown cells. Therefore, we again see an example of the uncoupling of EMT and metastasis.

In summary, we report that Smad2 and Smad4 are frequently lost in human skin SCCs. The LOH of *Smad2* and *Smad4* in human skin SCCs, and the haploid insufficiency of *Smad2* and *Smad4* in mouse skin carcinogenesis [the current study, and (114)] suggest that in human skin cancer, even if cancer lesions lose one allele of the *Smad2* or *Smad4*, or reduce their proteins to less than 50%, these lesions may have lost the tumor suppressive effect of Smad2 or Smad4. On the other hand, our study also shows that Smad2 loss-associated increase in Smad4 binding to the Snail promoter beyond a physiological level facilitates

Snail activation and EMT. It remains to be determined if this mechanism applies to other Smad target genes associated with EMT or with other TGFβ-mediated tumor promotion activities in *Smad2-/-* cells. Thus, our study prompts future research into how loss of both Smad2 and Smad4 affects skin carcinogenesis in vivo. It also remains to be determined how Smad2 loss after tumor formation, as seen in human cancers, affects tumor differentiation and malignant progression.

TABLES

Table 1. Snail ChIP primers.

Primer Name	Tm	%GC	Sequence	Ampllicon Length (bp)	SBE Flanked
Snail1 ChIP 2F	60	60	GGACTCAGGGAGACTCATGG	197	-1076
Snail1 ChIP 2R	60.87	60	GGGTCTACGGAAACCTCTGG		
Snail1 ChIP 3F	59.99	55	CGGTGCTTCTTCACTTCCTC	200	-437
Snail1 ChIP 3R	60.21	60	ACTACCCAGGGATGCCCTAC		

Table 2. siRNA Sequence Information.

siRNA	Sequence	Vendor
Smad2	UUCUCAAGCUCAUCUAACCGUCCUG	Invitrogen
Smad3	CCUGCUGGAUUGAGCUACACCUGAA	Invitrogen
Smad4	GGUGAUGUUUGGGUCAGGUGCCUUA	Invitrogen
Snail	GAGUAAUGGCUGUCACUUGUU	Dharmacon
	GCGAGCUGCAGGACUCUAAUU	
	AAUCGGAAGCCUAACUACAUU	
	GUGACUAACUAUGCAAUAAUU	

Table 3. Proteins of Smad2 and Smad4, but not Smad3, were lost in human skin SCCs.

	Smad2 Loss	Smad3 Loss	Smad4 loss
Total	**58/83**	**4/83**	**58/83**
Loss/Well Differentiated	**5/30**†	**1/30**	**14/30**
Loss/Poorly Differentiated	**53/53***‡	**3/53**	**44/53***

The number of SCC cases with individual Smad protein loss/total number of SCC cases in a tissue array was presented under each column. Both Smad2 and Smad4 loss occurred at higher rates in poorly differentiated SCCs vs. in well differentiated SCCs (*$p<0.001$). However, Smad2 loss was more closely correlated with poorly differentiated SCCs than Smad4 loss ($^{\dagger}p=0.025$; $^{\ddagger}p=0.005$, compared to cases with Smad2 loss to cases with Smad4 loss).

Table 4. Rates of Snail activation and E-cadherin loss in Smad2-negative and –positive skin SCC cases in humans.

	Snail-Positive	E-cadherin-Negative
Smad2-	47/52* (90%)	41/52* (79%)
Smad2+	17/23 (73%)	14/23 (60%)

*$p<0.05$, compared to Smad2 positive cases.

FIGURES

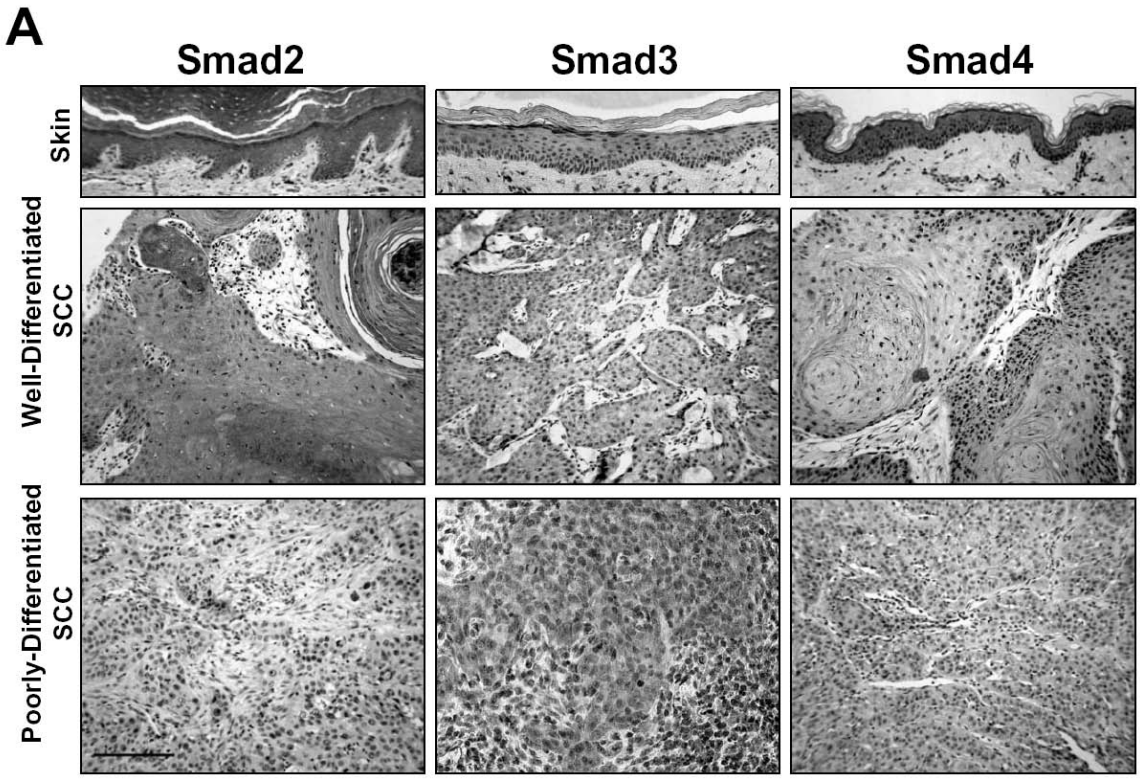

Figure 4. Loss of Smad2 and Smad4, but not Smad3 protein in human skin SCCs.

Loss of Smad2 and Smad4, but not Smad3 protein in human skin SCCs. Immunohistochemistry (IHC) staining in 83 human skin SCCs were performed. Staining of Smad2, Smad3 and Smad4 was predominantly localized to the epidermis in normal skin. IHC for Smad2 was preserved in well differentiated tumors, but lost in poorly differentiated SCCs. The intensity of Smad4 staining was reduced in well-differentiated SCCs, and completely lost in poorly differentiated SCCs. In contrast, Smad3 was largely retained. Scale bar represents 100μm.

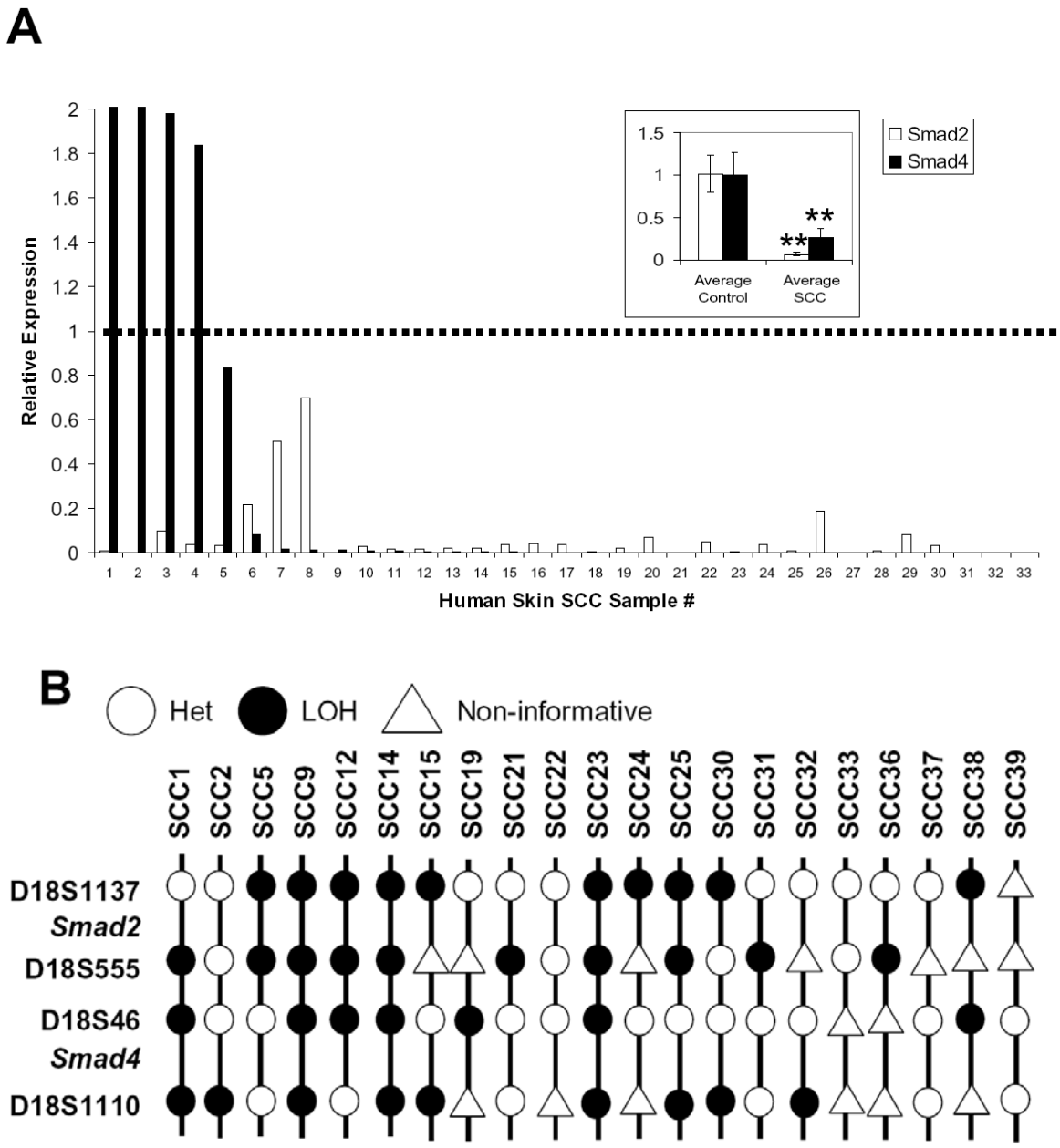

Figure 5. Reduced mRNA and LOH of *Smad2* and *Smad4* in human skin SCCs.

A: qRT-PCR of 33 human skin SCCs showed loss of Smad2 (31/33 samples) and Smad4 (28/33 samples) expression compared to normal skin controls. **: $p<0.001$. B: LOH of *Smad2* and *Smad4* in human SCCs. Microsatellite markers D18S1137 and D18S555 were used to assess *Smad2* LOH, and D18S46 and

D18S1110 were used to assess *Smad4* LOH. Het: heterzygosity. Non-informative: adjacent tissue exhibited homozygosity.

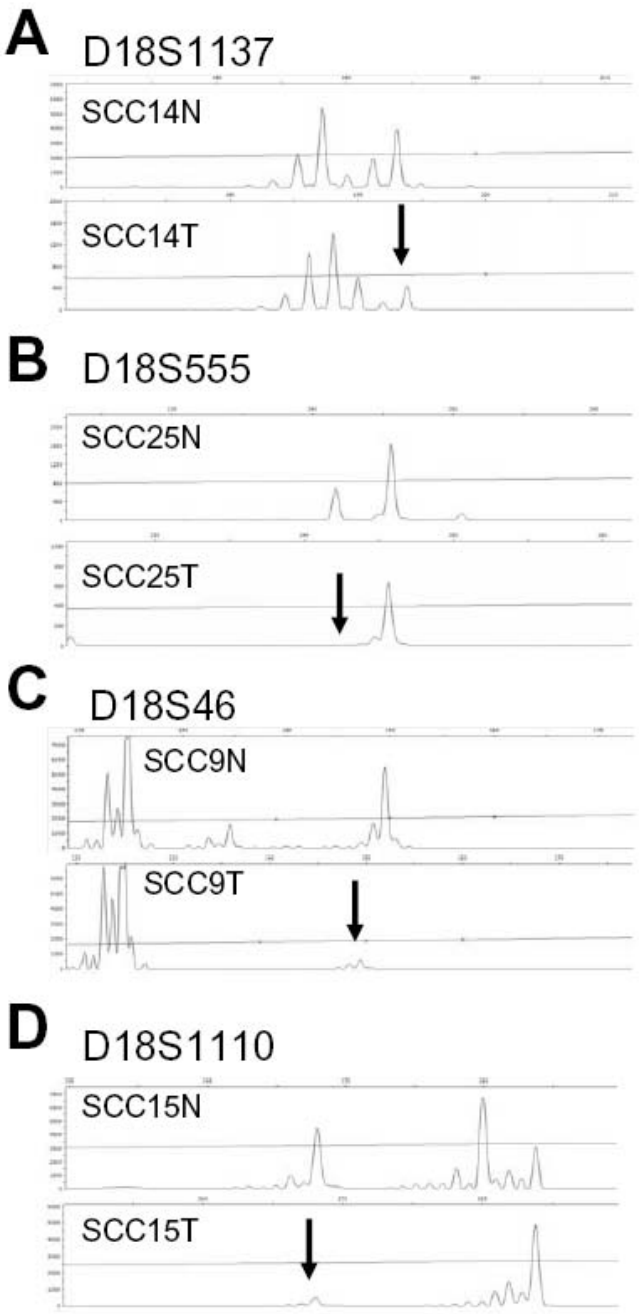

Figure 6. Examples of loss of heterozygosity peaks used for analysis at markers.

Sample profiles for cases exhibiting LOH at microsatellite markers used for *Smad2* A: D18S1137 and B: D18S555 and for *Smad4* C: D18S46 and D: D18S1110. N: denotes normal adjacent dissected tissue, T: denotes dissected tumor tissue. Arrow denotes allele peak lost for LOH.

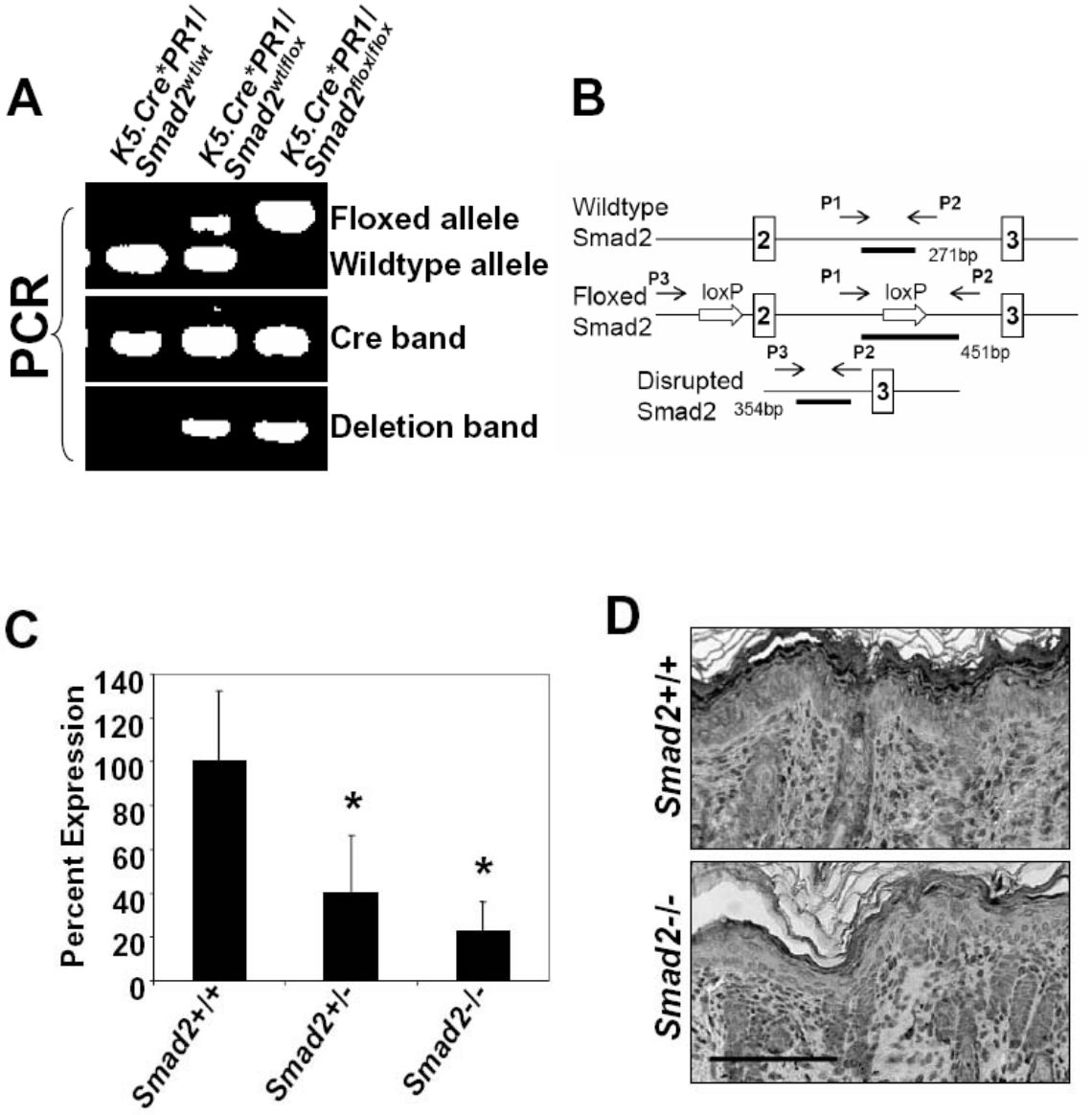

Figure 7. Generation of keratinocyte-specific *Smad2* knockout mice.

Monogenic mice (*K5.Cre*PR1* or *Smad2*$^{f/f}$) treated with RU486 were used as wildtype controls. Heterozygous and homozygous bigenic mice (*K5.Cre*PR1/Smad2*$^{f/wt}$ and *K5.Cre*PR1/Smad2*$^{f/f}$, respectively) were used to generate heterozygous and homozygous *Smad2* deletion in keratinocytes (designated as *K5.Smad2+/-* and *K5.Smad2-/-*). A: PCR confirmation of *Smad2* genotype. All mice have

the Cre band, but control mice lack a *Smad2* floxed allele, heterozygotes contain one *Smad2* floxed allele, and knockouts lack a wildtype allele. B: Schematic representation of expected bands. C: qRT-PCR of Smad2 mRNA normalized to GAPDH. *K5.Smad2+/-* and *K5.Smad2-/-* displayed a significant reduction in Smad2 expression. Residual Smad2 expression in knockouts is due to non-keratinocyte populations in the stroma of the sample. n=3 mice per genotype. D: Newborn pups were treated daily with RU486 (20μg in 100μl ethanol) for 3 days and sacrificed on the third day. IHC of Smad2 protein in RU486 treated neonatal back skin. Note Smad2 loss in knockout epidermis, but Smad2 staining remained in the stroma. Scale bar represents 100μm. *: $p < 0.05$. Portions of this figure provided by Allen Li.

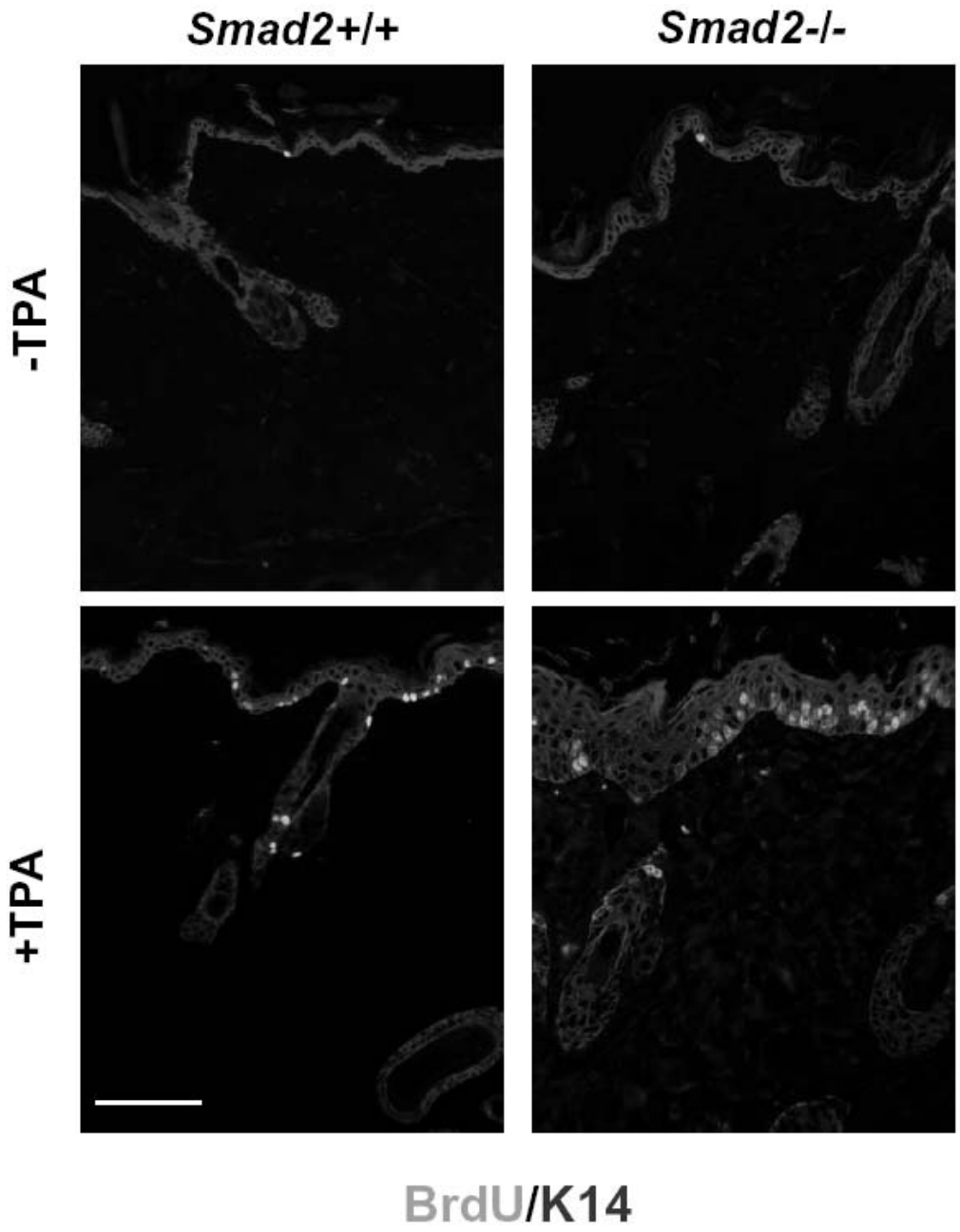

Figure 8. Increased proliferation in TPA-treated *K5.Smad2-/-* skin.

Increased proliferation in TPA-treated *K5.Smad2-/-* skin. Six-week-old monogenic and bigenic mice were treated with RU486 (20μg in 100μl ethanol for 5 days) to induce *Smad2* deletion in bigenic mice. Two weeks later, mice were treated with TPA (5μg per mouse), and sacrificed forty-eight hours later. Two

hours prior to sacrifice, mice were injected with BrdU. Ten-week-old RU486 treated mice, not treated with TPA were used as control (top panel). BrdU (green) staining in TPA treated skin showed increased proliferation amongst *K5.Smad2-/-* mice compared to *K5.Smad2+/+* mice. Keratinocytes are highlighted with K14 (red). No difference in proliferation was noted among non-TPA treated skin. Scale bar represents 100μm. Portions of this figure provided by Allen Li.

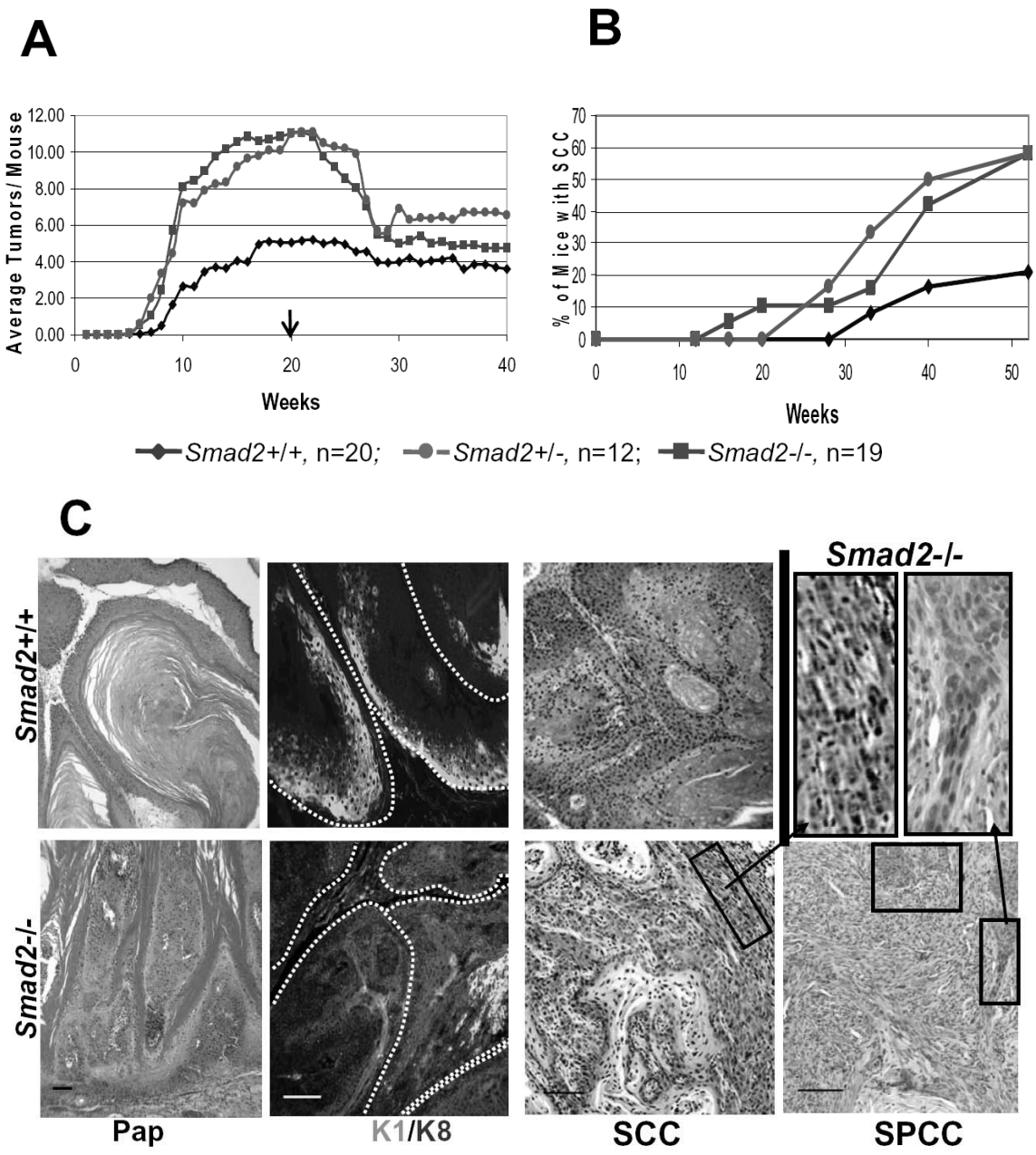

Figure 9. Accelerated tumor formation and malignant conversion of skin carcinogenesis in *K5.Smad2* knockout mice.

Accelerated tumor formation and malignant conversion of skin carcinogenesis in *K5.Smad2* knockout mice. A: Kinetics of tumor formation. Arrow indicates TPA withdrawal. $p<0.001$ between *K5.Smad2-/-* or *K5.Smad2+/-* and *Smad2+/+*. The seemingly more rapid tumor regression after TPA withdrawal in

Smad2+/- and *Smad2*-/- groups is due to necessity of euthanizing mice with a higher tumor burden. B: Kinetics of malignant conversion. *Smad2*+/- and *Smad2*-/- mice had higher rates of malignant conversion ($p<0.05$ compared with *Smad2*+/+ mice). The total number of mice of each genotype was used as a denominator for all time points through the entire course of tumor kinetics in A and B. C: Tumor pathology and keratin markers. H&E staining of *K5.Smad2*-/- tumors showed less differentiation compared to *K5.Smad2*+/+ tumors. Immunofluorescence staining revealed that at the same histological stage, *Smad2*+/+ papillomas expressed keratin K1 (green) in suprabasal layers, whereas *K5.Smad2*-/- papillomas expressed keratin K8 (red) and almost lost K1 in suprabasal layers. The dotted lines delineate the basement membrane. At SCC stages, *K5.Smad2*-/- tumors developed SPCCs when *K5.Smad2*+/+ tumors were well-differentiated SCCs. Insets are enlarged to illustrate areas of local transition from a *K5.Smad2*-/- SCC to SPCC. Scale bars in bottom panels represent 100μm for both upper and bottom panels in the same column in C except for the enlarged insets.

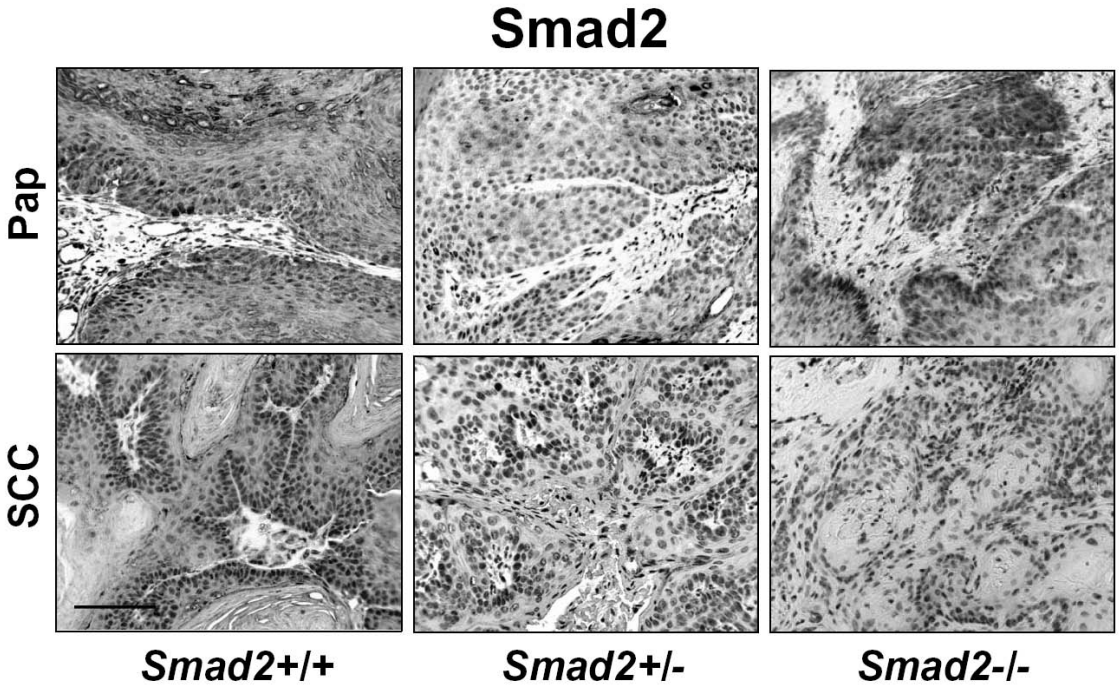

Figure 10. Immunohistochemistry of Smad2 in mouse tumors.

Smad2 expression was retained in wildtype and to a lesser degree in heterozygotes, at the papilloma stage indicating haploid insufficiency. At later stages, Smad2 was lost with equal frequency in wildtype and heterozygotes. Scale bar represents 100μm.

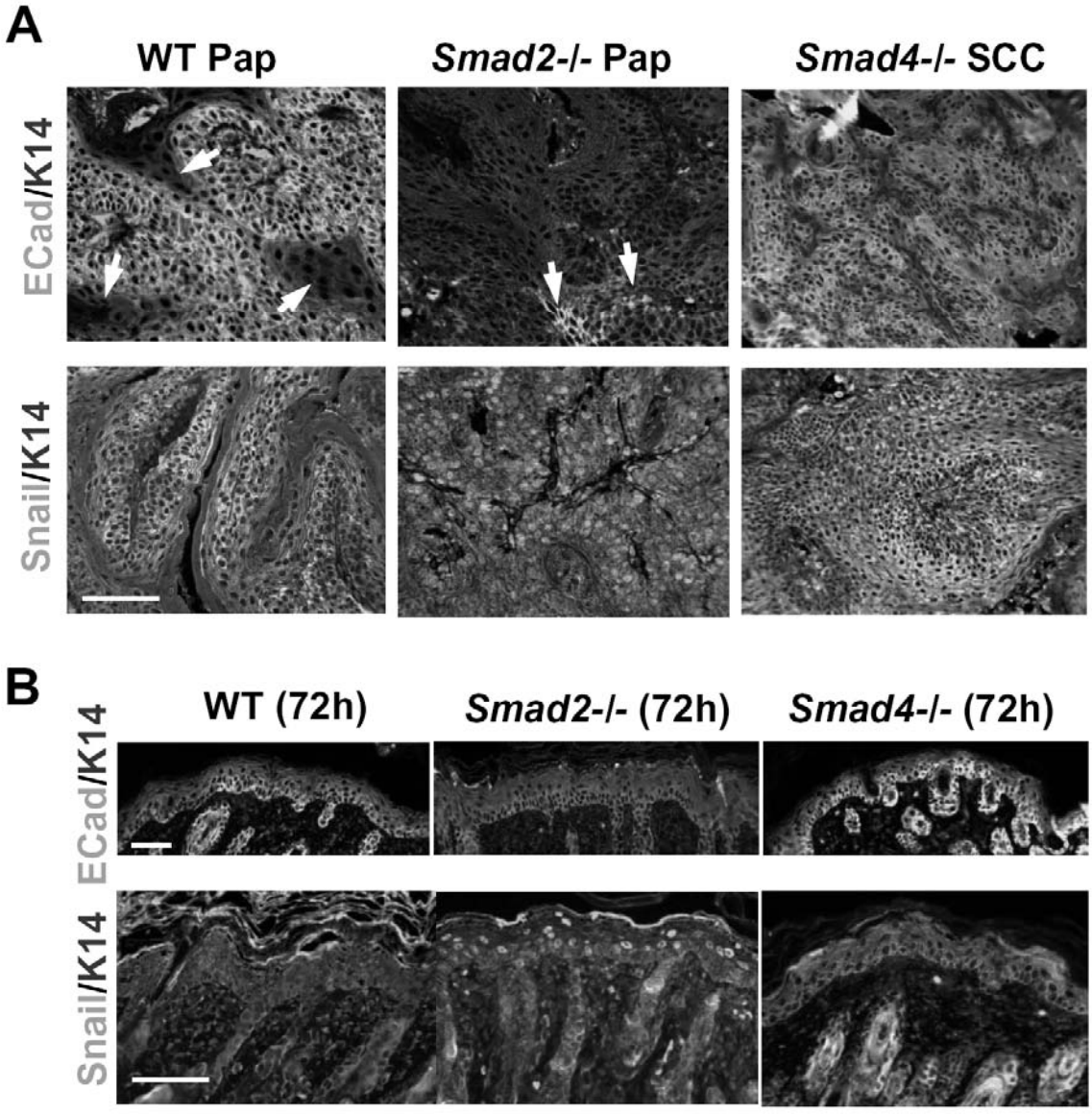

Figure 11. Snail activation and E-cadherin (ECad) loss in *K5.Smad2-/-* tissues.

A K14 antibody was used for counterstain (red). A: *K5.Smad2-/-* papillomas undergo EMT. When most of cells in *Smad2+/+* papillomas or spontaneous *Smad4-/-* SCCs still retained E-cadherin staining (green), *K5.Smad2-/-* papillomas show significant loss of E-cadherin (green). Arrowheads in *K5.Smad2+/+* image indicate patchy areas of E-cadherin loss, whereas arrowheads in *K5.Smad2-/-* tumors show patchy retention of E-cadherin (top panel). At this stage, Snail staining (green) was primarily cytoplasmic in *Smad2+/+* papillomas and spontaneous *Smad4-/-* SCCs, but *K5.Smad2-/-* tumors displayed nuclear Snail staining

(bottom panel). Scale bar represents 100μm for all panels (A). B: *K5.Smad2-/-* pup skin 72 h after *Smad2* deletion demonstrated significant reduction of E-cadherin (green, upper panel) with a concomitant increase in nuclear Snail (green, bottom panel). *K5.Smad4-/-* pup skin 72 h after *Smad4* deletion showed no change in E-cadherin and Snail expression patterns from wildtype skin. Scale bar represents 100μm for all panels in each row in B.

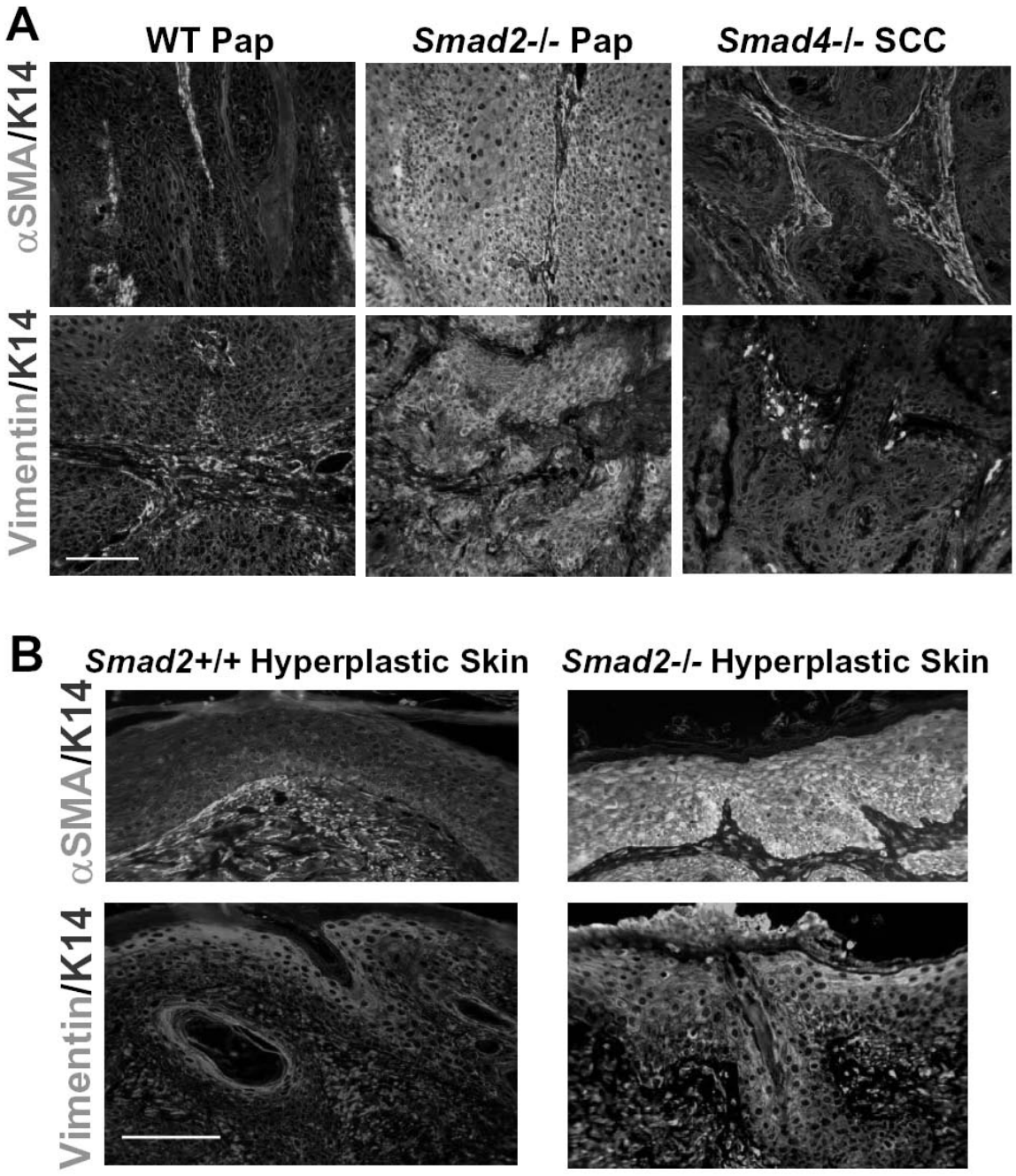

Figure 12. Epithelial expression of mesenchymal markers in *K5.Smad2-/-* tissues.

A: *K5.Smad2-/-* papillomas (pap) showed increased presence of mesenchymal marker αSMA in green (top panel) and vimentin in green (bottom panel). Keratinocytes are highlighted with K14 (red). Wildtype

papillomas and *K5.Smad4-/-* spontaneous SCCs showed exclusive stromal staining for αSMA and vimentin. B: Mesenchymal marker staining in the hyperplastic skin of *K5.Smad2-/-* animals adjacent to SCC formation. αSMA (green, top panel) and vimentin (green, bottom panel) were stained in *K5.Smad2-/-* epidermis, but were stained exclusively in the stroma of *K5.Smad2+/+* skin. Keratinocytes are highlighted with K14 (red). Scale bar represents 100μm.

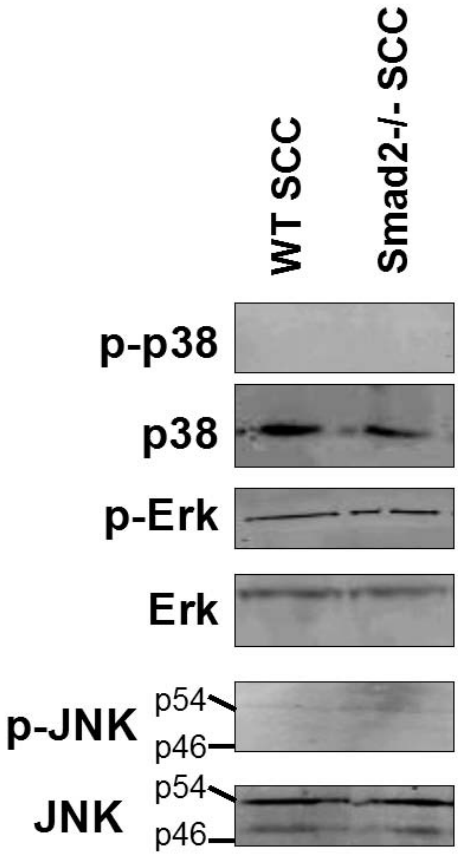

Figure 13. MAPK signaling unchanged in *K5.Smad2-/-* tumors.

Representative western blot analysis of *Smad2-/-* SCCs revealed activated MAPK levels to be similar to that of wildtype SCCs. n=5 tumors per genotype.

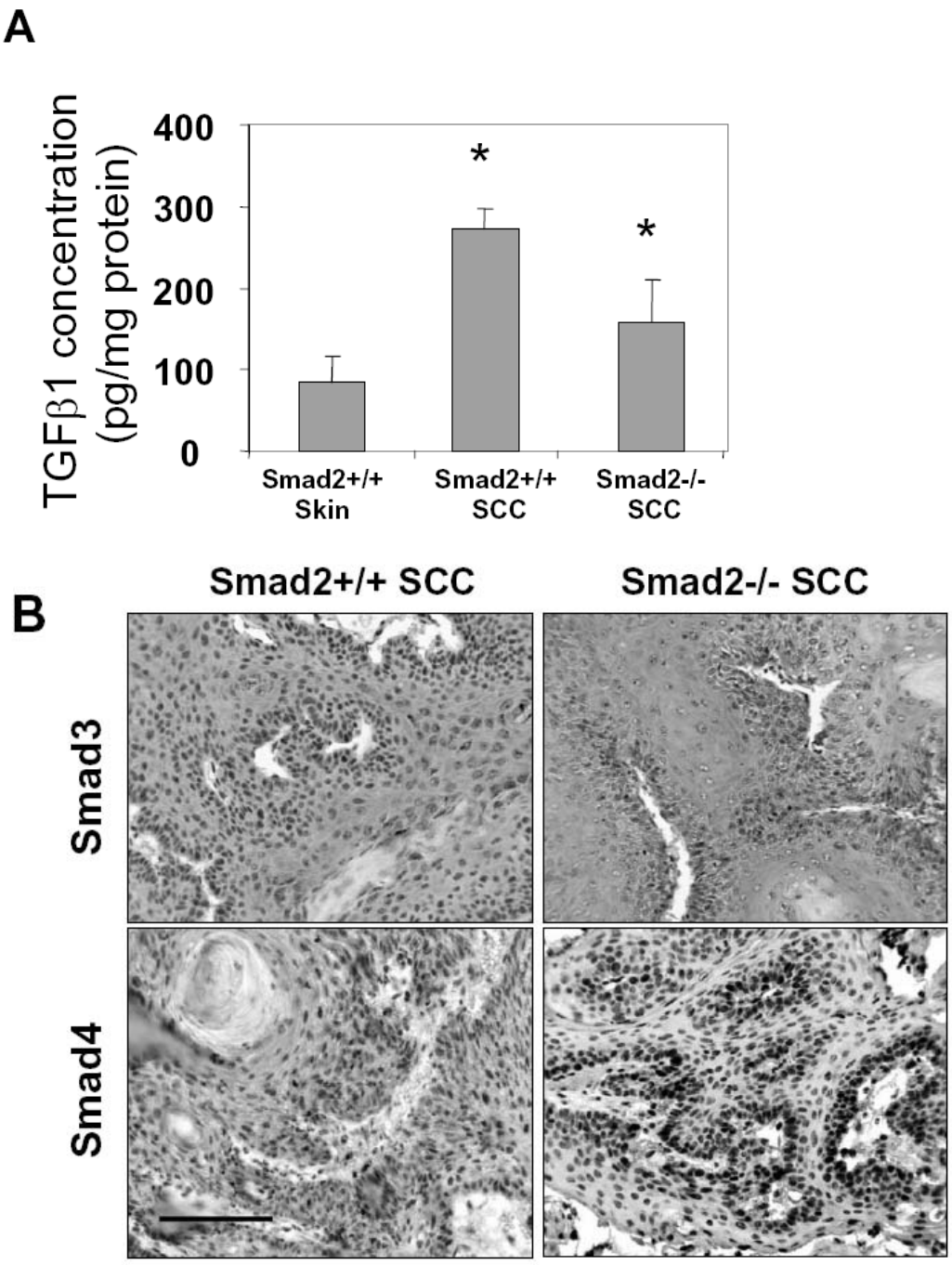

Figure 14. TGFβ1 protein levels and Smad expression patters in *K5.Smad2*+/+ and *K5.Smad2*-/- SCCs.

Protein extraction was performed by homogenizing tissue in Complete Lysis Buffer M (Roche). Total protein was determined using detergent compatible to Bradford Assay reagents (BioRad). ELISA kit for

TGFβ1 (R&D Systems) was used to determine the concentration of TGFβ1, as per the manufacturer's instructions. A: TGFβ1 level was comparable between *K5.Smad2+/+* and *K5.Smad2-/-* SCCs. *$p<0.05$ compared to K5.Smad2+/+ skin. n=5 samples per group. B: Smad3 and Smad4 staining (brown) showed patterns in *K5.Smad2-/-* SCCs similar to *K5.Smad2+/+* SCCs. Hematoxylin was used as counterstain. Scale bar represents 100μm.

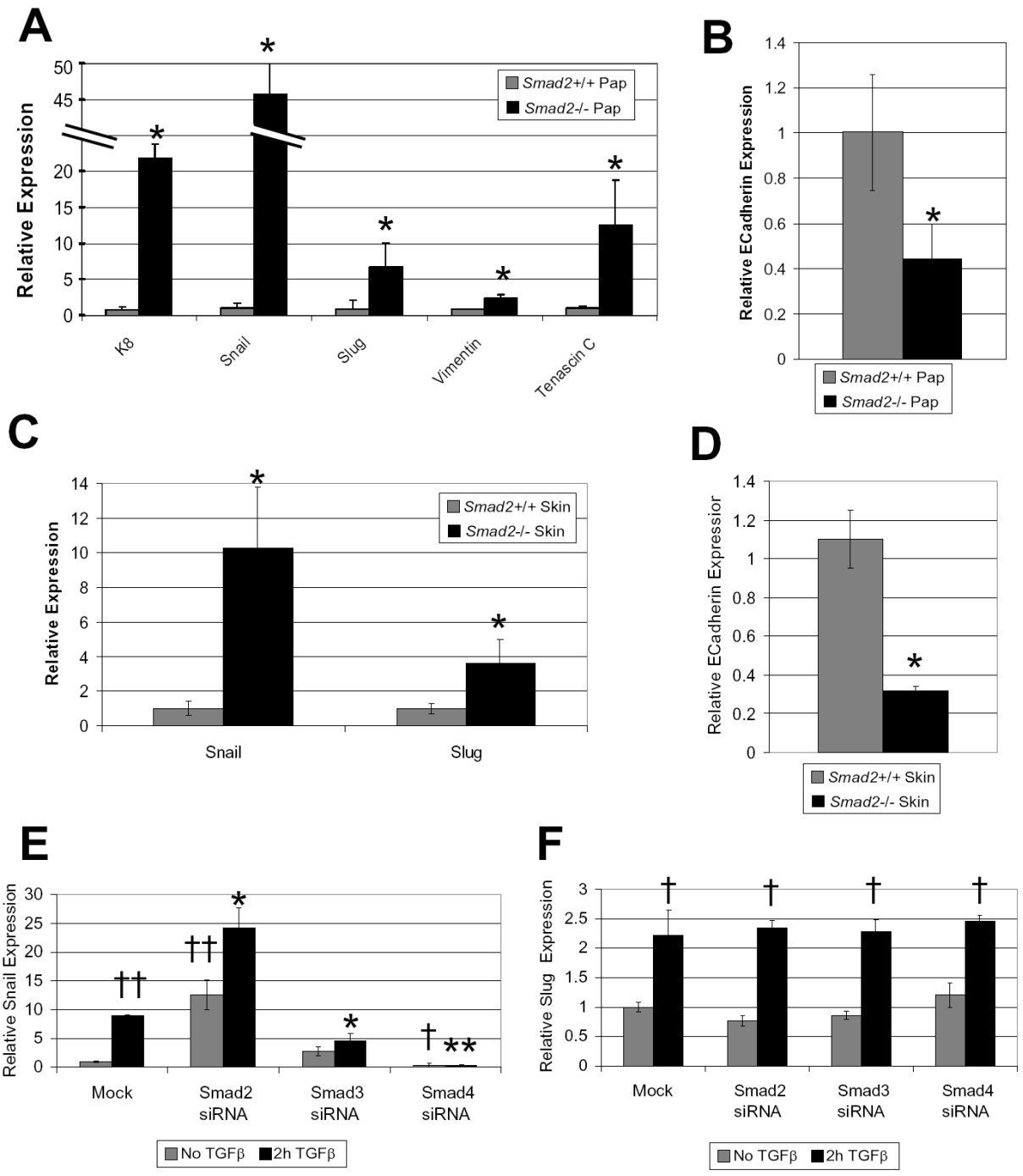
A
Relative Expression
50
45
20
15
10
5
0
*
*
*
*
*
Smad2+/+ Pap
Smad2-/- Pap
K8
Snail
Slug
Vimentin
Tenascin C
B
Relative ECadherin Expression
1.4
1.2
1
0.8
0.6
0.4
0.2
0
*
Smad2+/+ Pap
Smad2-/- Pap
C
Relative Expression
14
12
10
8
6
4
2
0
*
*
Smad2+/+ Skin
Smad2-/- Skin
Snail
Slug
D
Relative ECadherin Expression
1.4
1.2
1
0.8
0.6
0.4
0.2
0
*
Smad2+/+ Skin
Smad2-/- Skin
E
Relative Snail Expression
30
25
20
15
10
5
0
††
††
*
*
†
**
Mock
Smad2 siRNA
Smad3 siRNA
Smad4 siRNA
No TGFβ
2h TGFβ
F
Relative Slug Expression
3
2.5
2
1.5
1
0.5
0
†
†
†
†
Mock
Smad2 siRNA
Smad3 siRNA
Smad4 siRNA
No TGFβ
2h TGFβ

Figure 15. Altered gene expression associated with de-differentiation and EMT in *K5.Smad2-/-* papillomas and epidermis.

A: Increased mRNA transcript of K8 and EMT-associated molecules in *K5.Smad2-/-* papillomas. n=5 samples per genotype. B: Reduced E-cadherin transcript in *K5.Smad2-/-* papillomas. All changes in *Smad2-/-* papillomas are statistically significant, in comparison with *Smad2+/+* papillomas ($p<0.05$). n=5 samples per genotype. C: Increased Snail and Slug mRNA in *K5.Smad2-/-* epidermis. n=6 samples per genotype. D: Reduced E-cadherin transcript in *K5.Smad2-/-* epidermis. n=6 samples per genotype. * in C and D: $p<0.01$ compared to wildtype skin. E: Snail mRNA levels after knocking down individual Smads in HaCaT cells. F: Snail transcript levels after knocking down individual Smads in HaCaT cells. * in E: $p<0.05$ compared to mock transfection treatment, with TGFβ1. ** $p<0.001$ compared to mock transfection with TGFβ1 treatment. †† in E: $p<0.001$ compared to mock transfection without TGFβ1. † in E and F: $p<0.05$ compared to mock transfection without TGFβ1.

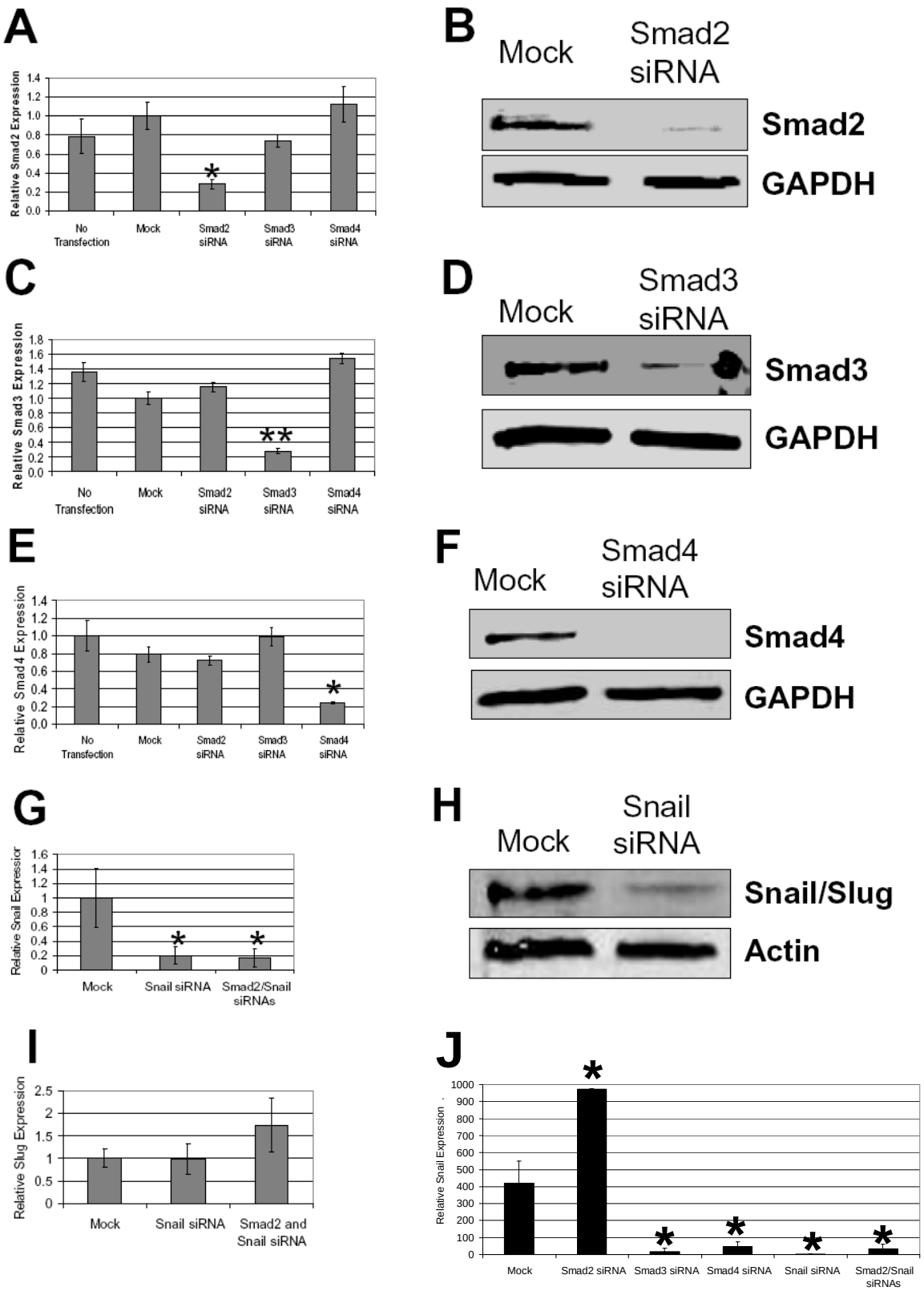
A
Relative Smad2 Expression
1.4
1.2
1.0
0.8
0.6
0.4
0.2
0.0
*
No Transfection
Mock
Smad2 siRNA
Smad3 siRNA
Smad4 siRNA
B
Mock
Smad2 siRNA
Smad2
GAPDH
C
Relative Smad3 Expression
1.8
1.6
1.4
1.2
1.0
0.8
0.6
0.4
0.2
0.0
**
No Transfection
Mock
Smad2 siRNA
Smad3 siRNA
Smad4 siRNA
D
Mock
Smad3 siRNA
Smad3
GAPDH
E
Relative Smad4 Expression
1.4
1.2
1.0
0.8
0.6
0.4
0.2
0.0
*
No Transfection
Mock
Smad2 siRNA
Smad3 siRNA
Smad4 siRNA
F
Mock
Smad4 siRNA
Smad4
GAPDH
G
Relative Snail Expressior
1.6
1.4
1.2
1
0.8
0.6
0.4
0.2
0
*
*
Mock
Snail siRNA
Smad2/Snail siRNAs
H
Mock
Snail siRNA
Snail/Slug
Actin
I
Relative Slug Expression
2.5
2
1.5
1
0.5
0
Mock
Snail siRNA
Smad2 and Snail siRNA
J
Relative Snail Expression
1000
900
800
700
600
500
400
300
200
100
0
*
*
*
*
Mock
Smad2 siRNA
Smad3 siRNA
Smad4 siRNA
Snail siRNA
Smad2/Snail siRNAs

Figure 16. Knockdown of Smads or Snail by siRNA.

Knockdown of Smads or Snail by siRNA. RNA extraction followed by qRT-PCR was performed as described previously . Protein was extracted from cells harvested in Complete Lysis Buffer M (Roche). Equal amounts of protein were separated on a 10% SDS-PAGE resolving gel with a 4% SDS-PAGE stacking gel. Protein was transferred to a nitrocellulose membrane and blocked using 5% non-fat milk in 0.1% Tween in TBS for 1 h at room temperature. Blots were double stained with 700nm and 800nm donkey IRDye-labeled secondary antibodies (Rockland, 1:5,000) against target and loading control primary antibodies. Target primary antibodies included rabbit anti-human-Smad2 antibody (Zymed,1:1,000), rabbit anti-human-Smad3 (Santa Cruz Biotechnologies, 1:1,000), mouse monoclonal anti-human-Smad4 (Santa Cruz Biotechnologies, 1:1,000), and rabbit anti-human Snail (Zymed, 1:1,000). Loading control primary antibodies included rabbit anti-human GAPDH (Santa Cruz Biotechnologies, 1:5,000) or mouse anti-human Actin (Santa Cruz Biotechnologies, 1:2,500). Gels were scanned and analyzed using LiCor Odyssey scanner (LiCor Biotechnology). Smad2 siRNA specifically knocked down Smad2 expression at the mRNA (A) and protein (B) levels. Smad3 siRNA specifically knocked down Smad3 expression at the mRNA (C) and protein (D) levels. Smad4 siRNA specifically knocked down Smad4 expression at the mRNA (E) and protein (F) levels. G: Snail siRNA significantly reduced Snail mRNA expression after 72 h of knockdown. H: Western analysis for Snail protein demonstrated ~80% reduction in signal in Snail siRNA transfected cells shown in G. However, the cross-reaction of the Snail antibody with Slug could also account for remaining signal. I: Snail siRNA transfected cells in G did not show alterations in Slug mRNA expression after 72 h of knockdown. J: Snail expression remains elevated in Smad2 siRNA treated cells 48hrs after TGFβ treatment. *$p<0.05$ compared to mock transfection. **$p<0.001$ compared to mock transfection.

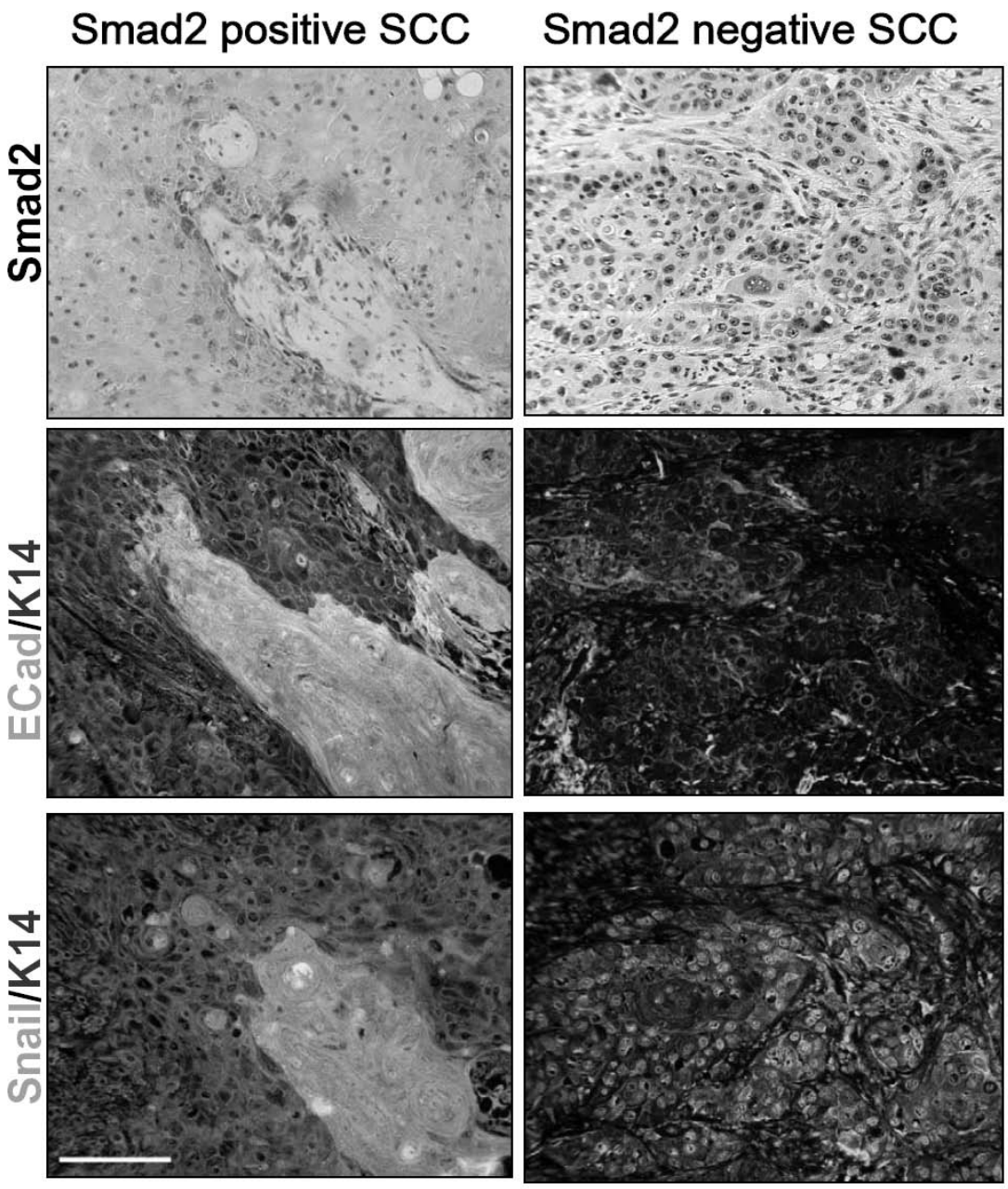

Figure 17. Human skin SCCs with Smad2 loss correlated with E-cadherin (ECad) loss and nuclear Snail.

Skin SCCs were stained for Smad2 IHC (brown, top panel), immunofluorescence for E-cadherin (green, middle panel) and Snail (green, lower panel). A K14 antibody was used for immunofluorescent counterstain (red). An example of a pair of SCCs from serial sections showed that a Smad2 positive SCC

retained membrane-associated E-cadherin with a few Snail nuclear staining cells. In contrast, SCC with Smad2 loss lost membrane-associated E-cadherin but uniformly expressed Snail in the nucleus. Scale bar represents 100μm for all panels.

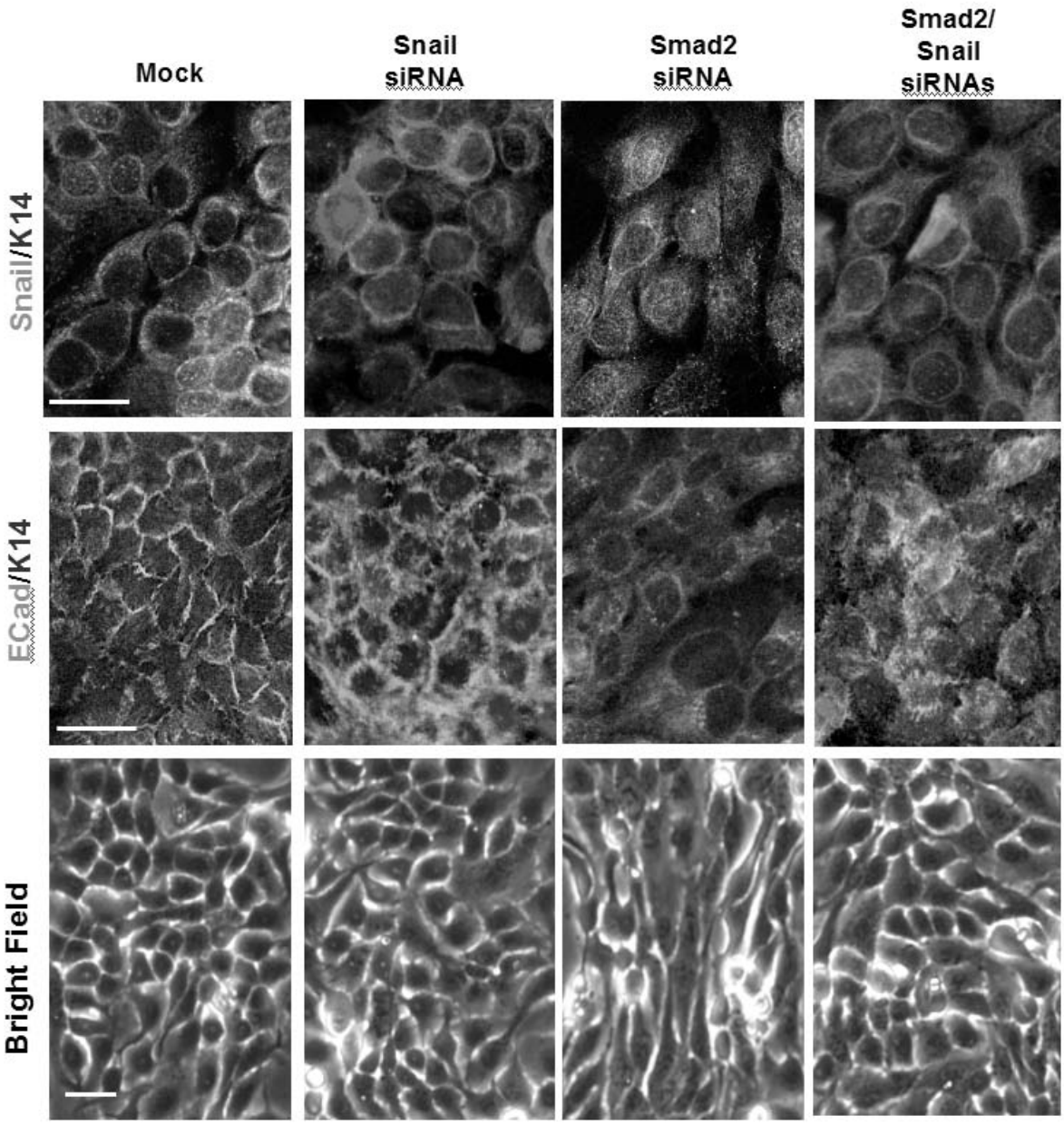

Figure 18. Snail contributed to Smad2 loss-associated EMT.

Smad2 knockdown caused an increase in Snail nuclear staining (green) compared to mock transfection and loss of E-cadherin (ECad, green) membrane staining with more spindle-like morphology in HaCaT keratinocytes. A K14 antibody was used for counterstain (red). Remaining Snail staining in Snail siRNA transfected cells could be due to antibody cross reaction with Slug. E-cadherin staining had a pattern similar to mock control. Smad2 and Snail concomitant knockdown resulted in reduced Snail staining in comparison with Smad2 siRNA transfected cells and restoration of membrane E-cadherin staining. Bright

field photos show epithelial morphology of the mock-transfected or Snail siRNA transfected cells. Epithelial morphology was lost in Smad2 siRNA-transfected cells, but was restored by co-transfection with Snail siRNA. Scale bar represents 20μm for all panels.

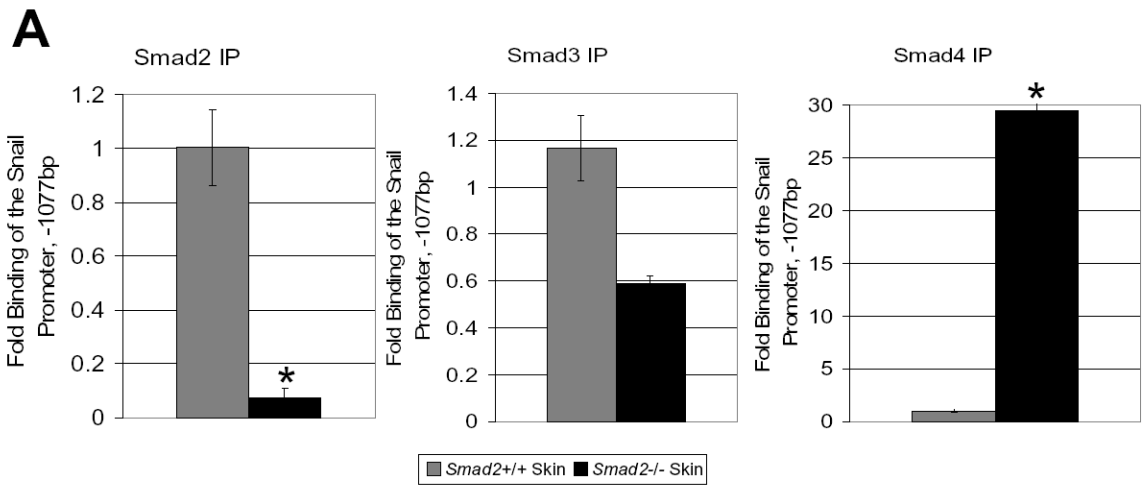
A
Smad2 IP
Smad3 IP
Smad4 IP
Fold Binding of the Snail Promoter, -1077bp
1.2
1
0.8
0.6
0.4
0.2
0
1.4
1.2
1
0.8
0.6
0.4
0.2
0
30
25
20
15
10
5
0
*
*
*
Smad2+/+ Skin
Smad2-/- Skin

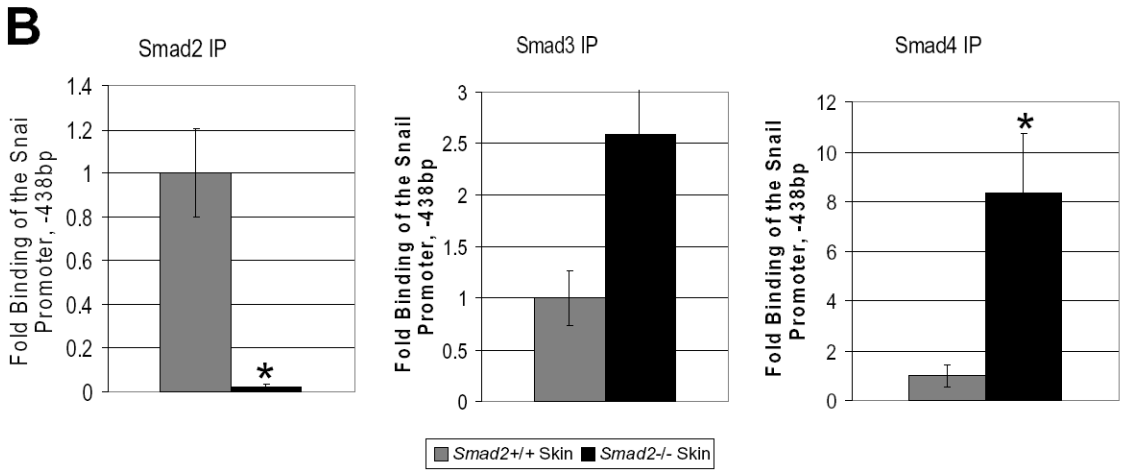
B
Smad2 IP
Smad3 IP
Smad4 IP
Fold Binding of the Snai Promoter, -438bp
Fold Binding of the Snail Promoter, -438bp
1.4
1.2
1
0.8
0.6
0.4
0.2
0
3
2.5
2
1.5
1
0.5
0
12
10
8
6
4
2
0
*
*
*
Smad2+/+ Skin
Smad2-/- Skin

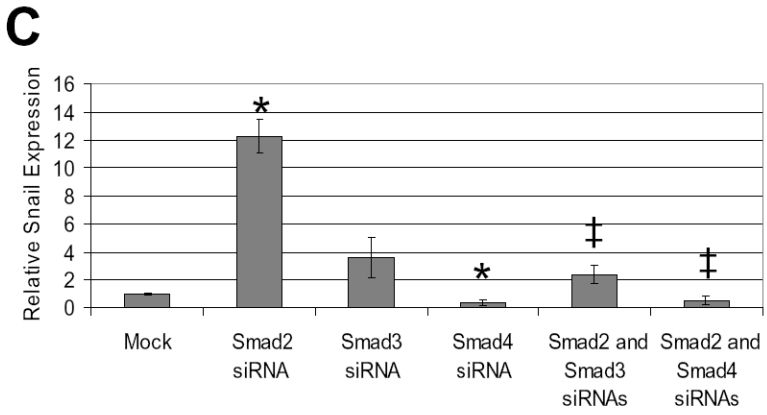
C
Relative Snail Expression
16
14
12
10
8
6
4
2
0
*
*
‡
‡
Mock
Smad2 siRNA
Smad3 siRNA
Smad4 siRNA
Smad2 and Smad3 siRNAs
Smad2 and Smad4 siRNAs

Figure 19. Increased Smad3/Smad4-mediated Snail transcription contributes to Smad2 loss-associated Snail overexpression.

A and B: Comparative PCR from ChIP showed an increase in Smad4 binding to the Snail promoter in *Smad2-/-* skin compared to wildtype skin. Residue Smad2 binding in *Smad2-/-* skin was from non-keratinocyte population of the whole skin. Smad3 binding to the Snail promoter was not significantly changed in *Smad2-/-* skin in comparison with wildtype skin. Smad4 binding to the Snail promoter was significantly increased in *Smad2-/-* skin. *$p<0.05$. C: Dual knockdown of Smad2 and Smad3 or Smad2 and Smad4 abrogated Smad2 loss-associated Snail overexpression. Smad2 knockdown (48 h) caused a significant increase in Snail transcript. Knockdown of Smad4 alone caused a reduction in Snail transcript. Concomitant knockdown of Smad2 and Smad3 or of Smad2 and Smad4 reduced Snail mRNA back to mock transfection levels. * $p<0.05$ compared to mock transfection. ‡ $p<0.05$ compared to Smad2 siRNA treatment.

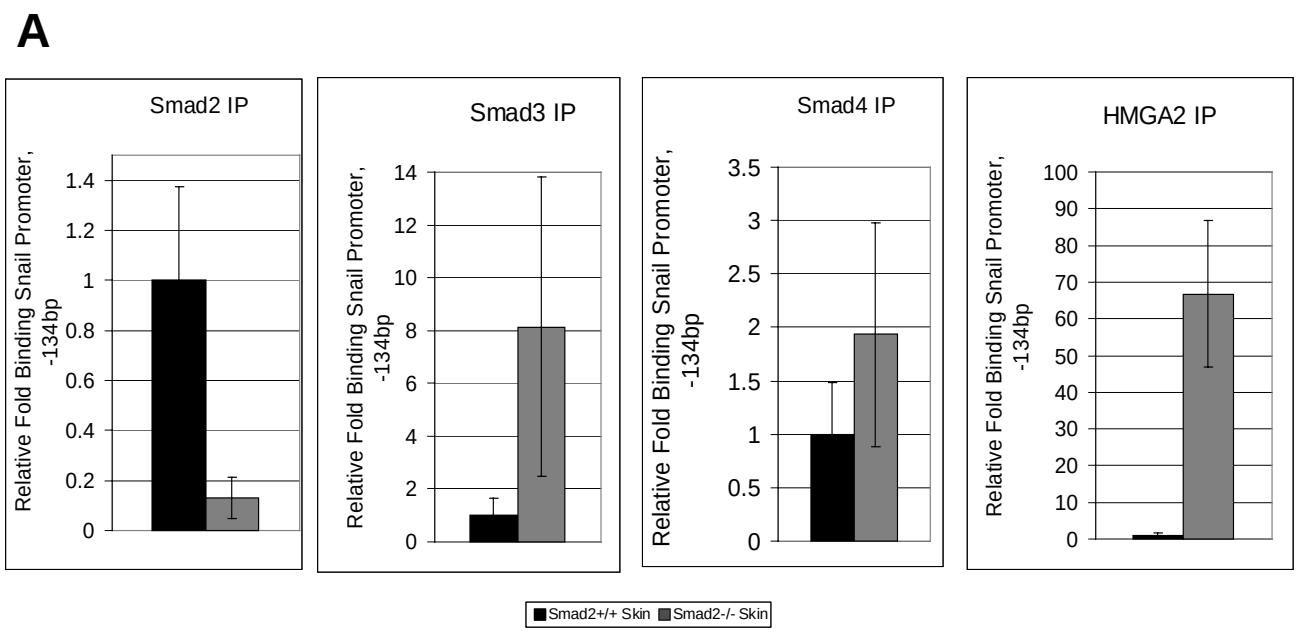

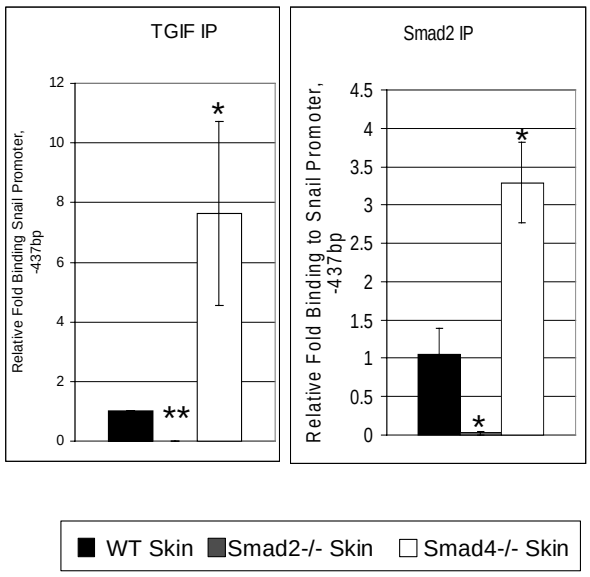

Figure 20. Increased HMGA2 and reduced TGIF bound in *K5.Smad2-/-* skin.

A: Increased HMGA2 binding to Snail promoter, -134bp upstream of the TSS in *K5.Smad2-/-* skin. Smad2 binding is reduced and Smad3 and Smad4 are increased, though not significantly in *K5.Smad2-/-* skin. B: TGIF binding to the SBE –437bp upstream of the Snail TSS is nearly absent entirely in *K5.Smad2-/-* skin,

while it is increased in *K5.Smad4-/-* skin. Increased TGIF binding corresponds to increased Smad2 binding, right.

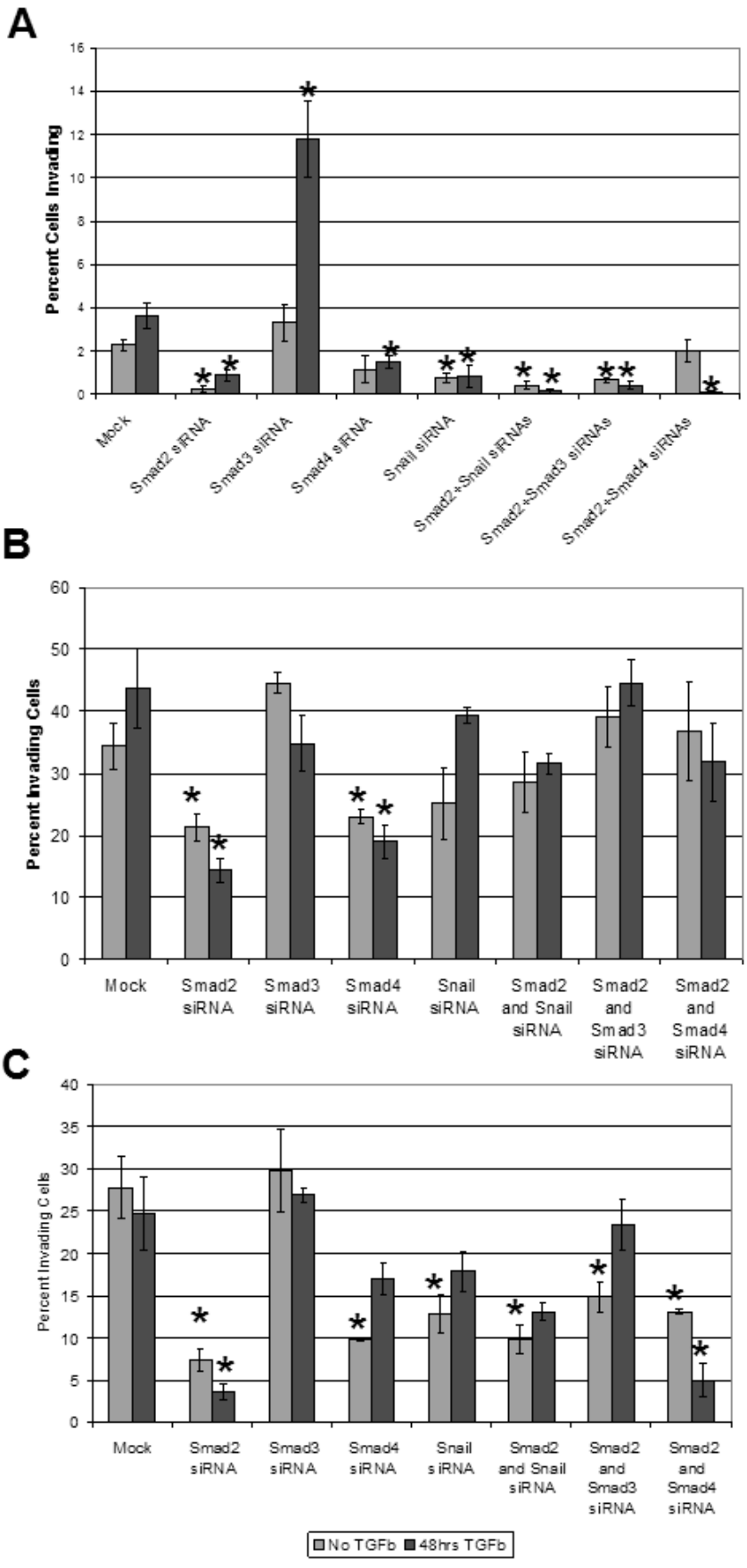
A
Percent Cells Invading
16
14
12
10
8
6
4
2
0
Mock
Smad2 siRNA
Smad3 siRNA
Smad4 siRNA
Snail siRNA
Smad2+Snail siRNAs
Smad2+Smad3 siRNAs
Smad2+Smad4 siRNAs
B
Percent Invading Cells
60
50
40
30
20
10
0
Mock
Smad2 siRNA
Smad3 siRNA
Smad4 siRNA
Snail siRNA
Smad2 and Snail siRNA
Smad2 and Smad3 siRNA
Smad2 and Smad4 siRNA
C
Percent Invading Cells
40
35
30
25
20
15
10
5
0
Mock
Smad2 siRNA
Smad3 siRNA
Smad4 siRNA
Snail siRNA
Smad2 and Snail siRNA
Smad2 and Smad3 siRNA
Smad2 and Smad4 siRNA
No TGFb
48hrs TGFb

Figure 21. Smad2 knockdown does not increase cell migration through a 3D matrix.

A: siRNA treated HaCaT cells plated on a Matrigel matrix for 24h without TGFβ (blue) or with 48h of TGFβ treatment (red). Smad2 knockdown resulted in less migratory cells. However, few cells migrated at all, even in mock treated groups. Treatment with Smad3 siRNA and TGFb led to increased migration. n=3 samples per group. B: Papilloma forming Ras-transduced HaCaT cells (HaCaT-II4) subjected to the same treatment as in A had more overall migration. However, siRNA treatment with Smad2 or Smad4 resulted in decreased migration. n=3 samples per group. C: SCC forming Ras-transduced HaCaT cells (HaCaT-RT3) subjected to the same treamtent as in A had an intermediate amount of overall migration. Smad2 siRNA treatment resulted in reduced migration. n=3 samples per group. *$p<0.05$ compared to mock treatment with same TGFβ condition.

III. CHAPTER 2:

Common and distinct pathways activated in Smad2- and Smad4-loss mediated angiogenesis

MATERIALS AND METHODS

Generation of inducible and keratinocyte-specific Smad2 and Smad4 knockout mice

The inducible and keratinocyte-specific *Cre* line, *K5.Cre*PR1*, the *Smad2* floxed line (*Smad2*$^{f/f}$), and *Smad4* floxed line (*Smad4*$^{f/f}$) were generated in *C57BL/6* background as previously reported (86-88). *K5.Cre*PR1* mice were crossed with *Smad2*$^{f/f}$ or *Smad4*$^{f/f}$ mice to generate wildtype, *K5.Smad2*$^{f/f}$ or *K5.Smad4*$^{f/f}$ genotypes. Genotyping PCR using tail DNA was performed using primers specific for the floxed region and the *Cre* recombinase as previously reported (86-88). Cre-mediated *Smad2* or *Smad4* deletion in keratinocytes was achieved with topical application of RU486 (20μg in 100μL ethanol) once a day for 3-5 days at time points specified in the Results section. *Smad2* or *Smad4* gene deletion was detected by PCR on DNA extracted from RU486-treated skin, using deletion-specific primers described above.

RNA extraction and quantitative RT-PCR (qRT-PCR)

Total RNA was isolated from mouse skin and tumors using RNAzol B (Tel-Test), as described above, and further purified using a QIAGEN® RNeasy Mini kit (Qiagen). The qRT-PCR was performed as described above. Transcripts of VEGF, cMET, and eNOS were examined using corresponding Taqman® Assays-on-Demand™ probes (Applied Biosystems). HGF levels were determined using Power SYBR Green Master Mix (Applied Biosystems) and custom primers (for mouse: 1F-GAACTGCAAGCATGATGTGG, 1R-GATGCTGGAAATAGGGCAGAA; for human: 1F-AAAGGACTTCCATTCACTTGC, 1R-CGCTCTCCCTTACTCAAGCTA). A GAPDH RNA probe was used as an internal control. Three to nine samples from each genotype of mice were used for qRT-PCR. In

analyzing the relative expression levels of individual genes, the average expression level from wildtype samples (unless otherwise specified) of each particular gene being analyzed was set as "1" arbitrary unit.

Tissue histology, tumor classification, and IHC

Dissected skin and tumor samples were fixed in 10% neutral-buffered formalin at 4^{o}C overnight, embedded in paraffin, sectioned to 6 µm thickness. IHC was performed on paraffin sections, as described above, using primary antibodies against HGF (1:10, R&D Systems), p-cMET (1:50, Cell Signaling), and eNOS (1:50, Abcam). Sections were counterstained with Hematoxylin. A double-blind evaluation for IHC was performed by two investigators using the methods as we have previously described (56).

Double-stain immunofluorescence

Each section was incubated overnight at 4°C with a primary antibody together with either a guinea-pig antiserum against mouse K14 (1:400, Fitzgerald), which highlights the epithelial compartment of the skin (114), or CD31 (1:100, BD Biosciences) which highlights endothelium. The primary antibodies included Alk1 (1:50, R&D Systems), phosphorylated-Smads1/5/8 (pS1/5/8) (1:50, Cell Signaling), pAKT (1:100, Cell Signaling), and p-cMET (1:50, Cell Signaling). Frozen sections were fixed for 2 minutes in methanol. An Alexa-Fluor 488-conjugated (green) secondary antibody against the species of the primary antibody (1:200, Molecular Probes, Eugene, OR) and Alexa Fluor 594-conjugated (red) anti-guinea pig secondary antibody (1:200, Molecular Probes) for K14 counterstain or Alexa Fluor 594-conjugated (red) anti-rat secondary antibody (1:200, Molecular Probes) for CD31 were used to visualize the staining. Sections were visualized under a Nikon Eclipse E600W fluorescence microscope (Melville, NY). Images were acquired using MetaMorph® (Universal Imaging Corporation^{TM}) and processed using Adobe Photoshop 6.0. Quantitation of angiogenesis was done using MetaMorph® software and expressed as percent of stroma occupied by vessels ± SEM and number of vessels per mm^2 stromal area ± SEM.

Superarray

RNA was amplified and labeled using Affymetrix protocols http://www.affymetrix.com/support/technical/manual/expression_manual.affx) with the help of the OHSU Affymetrix Microarray Core and hybridized against the Oligo GEArray® Mouse Cancer Pathway Microarray (Superarray), following the manufacturer's instructions. Briefly, membranes were incubated with 10 μg biotinylated RNA in triplicate, in a Multi-Chamber HybPlate (Superarray) at 60 degrees overnight. Membranes were washed, blocked with GEAblocking Solution Q (Superarray) for 40 minutes, and incubated with a Streptavidin Alexa Fluor 680-conjugated antibody (Molecular Probes) at 1:7500 for 10 minutes. Membranes were washed and scanned with the Odyssey Infrared Imaging System (LI-COR Biosciences).

Comparative Chromatin Immunoprecipitation

At least four mouse backskins from each group of wildtype, *K5.Smad2-/-*, and *K5.Smad4-/-* mice were homogenized on ice in 5 ml of 1% formalin, and incubated at room temperature for 30 minutes after adding an additional 5 ml of 1% formalin to each tube. Each sample was then diluted in 1 ml of 10X Glycine Stop Solution (Active Motif), incubated at room temperature for 5 minutes, and then centrifuged at 2,500 rpm for 10 minutes at 4^{o}C. The resulting pellet was used for ChIP Enzymatic Digestion following the manufacturer's protocol (Active Motif). Antibodies, 3μg each, to Smad2 (Zymed), Smad3 (Upstate), Smad4 (Upstate), RNA Pol II (Upstate), CBP/p300 (Upstate), TGIF (Santa Cruz Biotechnologies), CtBP (gift from Qinghong Zhang) and HDAC3 (Abcam) were used to immunoprecipitate the sheared chromatin complexes. Rabbit IgG (3μg, Santa Cruz Biotechnologies) or Mouse IgG (3μg, Upstate) was used as a negative control for antibody specificity. DNA obtained from eluted beads was used for comparative PCR using Power SYBR Green Master Mix (Applied Biosystems). Primers encompassing the SBE sites of the HGF promoter (FP: AGTCCAACGGGTCTCAAGTG, RP: CCAAACCACTGCAAAAGGAT) were used for PCR. Positive binding was defined as antibody binding >10-fold of the IgG-negative control. ΔCt values were obtained by normalizing IP Ct values to Input values for each group. ΔΔCt values were

obtained by comparing the ΔCt values of *K5.Smad2-/-* and *K5.Smad4-/-* skin to WT skin. Values are expressed as fold-change based on ΔΔCt values.

HaCaT keratinocyte culture and siRNA knockdown

HaCaT keratinocytes were cultured in high-glucose DMEM with 10% FBS and penn-strep antibiotics. Twenty-four h prior to siRNA transfection, cells were switched to low-glucose DMEM with 0.2% FBS and penn-strep antibiotics. Cells were transfected with siRNAs for human Smad2, Smad3 or Smad4 (see Table 2 for sequences) using XtremeGene siRNA Transfection Reagent (Roche) in 6-well plates at a final concentration of 50pmol siRNA/μl in Optimem media (Gibco). Four hours post-transfection, media was switched to high-glucose DMEM. Cells were harvested at 72 hours after siRNA transfection for RNA extraction using Qiashredder and RNeasy kits (Qiagen).

Luciferase Constructs

Normal *C57BL/6* mouse genomic DNA was used to amplify the HGF promoter region using the following set of primers: FP- CTCCCTCCCTGAAGACTGTG, RP- CTCAGCCCAATCGCTAAGTC using the Easy-A cloning kit (Promega). The gel extracted promoter was ligated to the pGEM T-Easy vector (Promega) as per the manufacturer's instructions. The vector was sequence verified. Using XhoI and HindIII-labeled forward and reverse primers from above, we amplified the promoter. Using XhoI and HindIII (New England Biosystems) we restriction enzyme digested the insert and pGL4.26 Luciferase Vector (Promega). We gel extracted the digested insert and pGL4.26 backbone and ligated them together.

HGF-pGL4.26, pGL4.74 (Promega), and siRNAs were transfected into 50% confluent HaCaT cells in a 24-well plate using XtremeGene siRNA Transfection Reagent (Roche). Cells were harvested for luciferase using the Dual Luciferase Assay reagents (Promega) as per the manufacturer's instructions. Luciferase reporter assay was done using the 96-well plate GLO-MAX dual-injector luminometer (Promega).

Protein Extraction and ELISA

Protein extraction was performed by homogenizing tissue in Complete Lysis Buffer M (Roche). Total protein was determined using detergent compatable Bradford Assay reagents (BioRad). Quantikine ELISA kit for VEGF (R&D Systems) was used to determine the concentration of VEGF, as per the manufacturer's instructions.

Statistics

Significant differences between the values obtained in each assay on samples from various genotypes were determined using the Student's t-test and expressed as mean ± standard error of the mean, with the exception of evaluation of human SCCs where a Chi-Squared (χ^2) test was used.

RESULTS

K5.Smad2-/- *and* K5.Smad4-/- *SCCs had more blood vessels than tumors derived from wildtype mice*

We have previously reported keratinocyte-specific deletion of *Smad4* leads to spontaneous skin tumor formation (77). Additionally, our lab has reported keratinocyte-specific deletion of *Smad2* leads to increased susceptibility to skin chemical carcinogenesis (115). We analyzed squamous cell carcinomas from 19 *K5.Smad2-/-* mice, 26 *K5.Smad4-/-* mice, and 24 wildtype mice. We found that *K5.Smad2-/-* and *K5.Smad4-/-* tumors contained approximately three times the number of blood vessels as their stage-matched wildtype counterparts (580±90/mm^2 stroma and 604±114/mm^2 stroma vs. 223±31/mm^2 stroma, respectively) (Figures 22A and B). Similarly, *K5.Smad2-/-* and *K5.Smad4-/-* SCC stromal area was approximately three times more occupied by blood vessels (25.9±4.4% and 24.8±3.0% vs. 7.7±2.9%, respectively) (Figures 22A and 22C).

K5.Smad4-/- *SCCs, but not* K5.Smad2-/- *SCCs, had increased VEGF and TGFβ-mediated angiogenesis*

We evaluated the tumor groups for the presence of the potent angiogenic mediator VEGF. *K5.Smad4-/-* tumors showed approximately four times more VEGF protein by ELISA when compared to wildtype SCCs (Figure 23A), whereas *K5.Smad2-/-* SCCs had reduced VEGF protein. Consistently, *K5.Smad4-/-* SCCs also had a dramatic increase in VEGFa transcript by qRT (Figure 23B). *K5.Smad2-/-* tumors showed reduced VEGF transcript compared to wildtype tumors (Figure 23B). VEGFb and VEGFc isoforms were unchanged or undetectable in the tumors (data not shown).

TGFβ is a known positive mediator of angiogenesis via endothelial TGFβR Alk1 (63). We evaluated *K5.Smad2-/-* and *K5.Smad4-/-* SCCs for increased endothelial TGFβ signaling. *K5.Smad4-/-* SCCs have increased TGFβ1 ligand, whereas *K5.Smad2-/-* SCCs do not, when compared to wildtype SCCs (Figure 24). Consistently, *K5.Smad4-/-*, but not *K5.Smad2-/-* or wildtype SCCs, had increased Alk1 and subsequently increased endothelial pSmad1/5/8 (Figure 23C). These data suggest *K5.Smad2-/-* SCCs initiate angiogenesis through a non-Alk1 mechanism.

K5.Smad2-/- *SCCs, but not* K5.Smad4-/- *SCCs had increased HGF*

Since *K5.Smad2-/-* SCCs had increased angiogenesis, independent of VEGF-mediated or TGFβ-mediated angiogenesis, we evaluated alternate angiogenic pathways. Notably, *K5.Smad2-/-* SCCs showed increased epithelial hepatocyte growth factor (HGF) protein expression, not seen in the *K5.Smad4-/-* SCCs (Figure 25A). Consistently, *K5.Smad2-/-* SCCs showed increased HGF mRNA levels, while *K5.Smad4-/-* SCCs had decreased HGF expression compared to WT SCCs (Figure 25B). No alterations were detected in TSP1, Flt, sFLT, TIMPs, MMPs, MAPKs, FGFs, PDGFs, or TNFa (Figure 26 and Table 5).

Angiogenic Pathways Converge in K5.Smad2-/- *and* K5.Smad4-/- *SCCs*

To determine whether increased HGF ligand in *K5.Smad2-/-* SCCs induced downstream alterations in signaling components, we evalued the expression of HGF receptor, cMET. Immunohistochemical staining of the active, phosphorylated cMET receptor showed that *K5.Smad2-/-* had increased endothelial expression compared to wildtype SCCs (Figure 25A). Interestingly although *K5.Smad4-/-* SCCs did not exhibit increased HGF, they exhibited increased endothelial p-cMET, albeit to a lesser extent than *K5.Smad2-/-* SCCs (Figure 25A). Furthermore, qRT-PCR indicated that the receptor transcript was also upregulated in both groups (Figure 25C). This result is particularly interesting as it indicates loss of Smad2 or Smad4 may lead to angiogenesis through a convergence of pathways on cMET. To further confirm activation of downstream angiogenic mediators, we looked at endothelial pAKT staining, activated by both VEGF and HGF (116). Both *K5.Smad2-/-* and *K5.Smad4-/-* SCC vessels show increased pAKT staining compared to wildtype SCC vessels (Figure 25A). Finally, we looked at endothelial nitrogen oxide sythetase, an angiogenic target of VEGF and HGF through pAKT (117, 118), and found it was increased in both *K5.Smad2-/-* and *K5.Smad4-/-* SCCs at both the protein and RNA level (Figures 25A and 25D). These results indicate that unique upstream alterations in the *K5.Smad2-/-* and *K5.Smad4-/-* SCCs lead to a common angiogenic cascade.

Increased Angiogenesis and Molecular Alterations Similar to K5.Smad2-/- *and* K5.Smad4-/- *SCCs also occurred in non-neoplastic skins*

In order to assess whether the changes we observed in the SCCs were due genetic loss of *Smad2* and *Smad4* or whether they were due to secondary effects of carcinogenesis, we evaluated the number and density of vessels in neonatal pups. *K5.Smad2-/-* and *K5.Smad4-/-* neonatal mice exhibited increased number of vessels compared to wildtype neonates (442.0±32.8/mm^2 stroma and 438.8±27.8/mm^2 stroma versus 336.7±16.7/mm^2 stroma, respectively) (Figures 27A and 27B). Furthermore, *K5.Smad2-/-* and *K5.Smad4-/-* neonatal skin contained approximately four times the stromal area covered in vessels compared to wildtype neonates (8.4±2.1% and 10.6±1.6% versus 2.7±0.7%, respectively) (Figures 27A and 27C). These results indicate *Smad2* and *Smad4* loss in the skin are sufficient to create increased angiogenesis in the underlying stroma, without the secondary effects of carcinogenesis.

Based on our findings in *K5.Smad4-/-* tumors, we evaluated neonatal skin for VEGF and TGFβ levels. We found that VEGF levels were approximately twice as high in *K5.Smad4-/-* skin compared to WT skin (Figure 28A). Thus, upregulation of VEGF is an early event related to Smad4 loss, prior to carcinogenesis. Additionally, we found that *K5.Smad2-/-* skin has reduced VEGF compared to WT skin (Figure 28A), and is therefore not responsible for the increased angiogenesis in *K5.Smad2-/-* skin. Consistent with protein levels, *K5.Smad4-/-* skin, but not *K5.Smad2-/-* skin, has increased VEGF transcript by qRT-PCR (Figure 28B). Furthermore, previous studies have demonstrated *K5.Smad4-/-* pre-neoplastic epithelium has increased TGFβ1 ligand (Figure 24). Similar to what was seen in SCCs, we found Alk1 to be upregulated in *K5.Smad4-/-* skin which correlated with endothelial phospho-Smad1/5/8 (Figure 28C). *K5.Smad2-/-* skin did not display increased endothelial TGFβ-signaling (Figure 28C).

As was seen in SCCs, *K5.Smad2-/-* neonatal skin had markedly increased HGF compared to WT skin (Figure 29A and 29B), not seen in *K5.Smad4-/-* skin. This correlated with increased activation of the HGF receptor, cMET (Figure 29A). Unlike *K5.Smad4-/-* SCCs, *K5.Smad4-/-* skin did not demonstrate increased cMET transcript (Figure 29C), and there was only a modest level of activated receptor (Figure

29A). Therefore, the increased cMET in *K5.Smad4-/-* tumors is likely due to secondary changes of carcinogenesis.

Furthermore, *K5.Smad2-/-* and *K5.Smad4-/-* neonatal skins displayed increased downstream effectors of VEGF and HGF, as demonstrated by increased endothelial pAKT (Figure 29A). However, unlike in *K5.Smad2-/-* and *K5.Smad4-/-* SCCs which both exhibited increased eNOS, only *K5.Smad2-/-* neonatal skin had increased eNOS (Figure 29A and 29D) suggesting the increased eNOS seen in *K5.Smad4-/-* SCCs is secondary to other carcinogenic and angiogenic changes.

Smad knockdown in cultured keratinocytes altered VEGF and HGF expression

To determine if increased VEGF in *K5.Smad4-/-* keratinocytes and increased HGF in *K5.Smad2-/-* keratinoctyes are the direct effect of epithelial loss of these two proteins, we knocked down each Smad in the human keratinocytes, HaCaT cells, and assayed for expression levels of VEGF and HGF. siRNA knockdown of Smad4 lead to transcriptional upregulation of VEGF (Figure 30A) and Smad3 (Figure 30B). Previous studies have shown Smad3 can strongly induce VEGF (66, 119, 120). To assess if Smad4-knockdown induction of VEGF is mediated by increased TGFβ-induced Smad3 activation, we concomitantly knocked down Smad3 with Smad4, which resulted in the reduction of VEGF compared to Smad4 siRNA treatment alone. Additionally, knockdown of all three Smads reduced VEGF expression below that of mock treated controls (Figure 30A). These results suggest that increased VEGF expression was a result of an enhanced Smad2/3 effect. siRNA knockdown of Smad2 lead to induction of HGF (Figure 31A). Concomitant knockdown of Smad3 or Smad4 along with Smad2 abrogated the increased HGF mRNA levels upon Smad2 knockdown (Figure 31A). Furthermore, knockdown of Smad3 and Smad4 together resulted in reduced HGF transcript compared to mock treatment (Figure 31A). These results suggest Smad2 repressed HGF while Smad3/4 promoted HGF expression (121, 122).

Differential binding of Smad2, Smad3, and Smad4 to the HGF promoter

Increased HGF protein and transcript in *K5.Smad2-/-* neonatal skin, and previous reports of HGF regulation by TGFβ (67, 121, 122) prompted us to evaluate the promoter occupancy of HGF by Smad-2, -3, and -4. WT, *K5.Smad2-/-*, and *K5.Smad4-/-* skin showed different Smad binding affinities for the Smad binding element (SBE) –466bp upstream of the HGF transcriptional start site (Figure 31B). In *K5.Smad2-/-* skin that expressed increased amounts of HGF, Smad3 and more dramatically, Smad4, showed increased binding at the SBE by comparative chromatin immunoprecipitation (ChIP) (Figure 31B). In *K5.Smad4-/-* skin that expressed reduced HGF, Smad2 binding is increased at the SBE while Smad3 binding is reduced (Figure 31B). This data implies Smad2 binding to the –466bp SBE had a primarily repressive role while Smad3 and Smad4 binding had a promoting role.

To further evaluate if Smad2 binding recruited transcriptional repressors while Smad3/4 binding recruited transcriptional activators, we performed comparative ChIP for RNA Polymerase II (RNA Pol II), transcriptional co-activator CBP/p300, and transcriptional repressors TGIF, CtBP, and HDAC-1, -2, and -3. In *K5.Smad2-/-* skin with increased Smad3/4 binding to the HGF promoter, we found increased RNA Pol II and CBP/p300 also bound (Figure 31B). Additionally, in *K5.Smad4-/-* skin with increased Smad2 and reduced Smad3 bound, we found increased TGIF, CtBP, and HDAC3, while less RNA Pol II, bound to the HGF promoter (Figure 31B). These data indicate Smad2 may recruit transcriptional co-repressors to the HGF promoter, while Smad3/4 recruits transcriptional co-activators.

To confirm that Smad2 was directly bound in a complex with transcriptional repressors on the HGF promoter, while Smad4 was bound in a complex with transcriptional activators, we preformed a dual-IP ChIP. First, we immunoprecipitated Smad2 and Smad4, then we immunoprecipitated HDAC3 and CBP/p300, since they displayed the largest fold-change difference by ChIP. We found that HDAC3 bound to Smad2 10-fold more than to Smad4 on the HGF promoter (Figure 31C). Further, we found that CBP/p300 bound to Smad4 75-fold more than Smad2 on the HGF promoter (Figure 31C). Taken together

these data confirm that Smad2 recruits transcriptional co-repressors to the HGF promoter, while Smad3/4 recruits transcriptional activators.

Smad2-knockdown induces HGF promoter activity

Based on our findings, we created an HGF luciferase construct containing the –466bp SBE. HaCaT cells were transfected with the HGF luciferase construct, control renilla construct, and siRNAs. Knockdown of Smad2 alone dramatically upregulated HGF promoter activity (Figure 31D). Knockdown of Smad3 or Smad4 along with Smad2 knockdown abrogated the Smad2-knockdown induction of the HGF promoter (Figure 31D) indicating Smad3 and Smad4 are necessary for the Smad2-loss-mediated transcription of HGF.

Expression of HGF in Human Skin SCCs Correlated with Smad2 Loss

To determine the HGF expression pattern among human skin SCCs, we evaluated 74 human skin SCCs for HGF protein. We found 70% (52/74) of human skin SCCs expressed HGF. Additionally, we found that amongst skin SCCs that lacked Smad2 protein, HGF expression positively correlated with retained Smad4 expression (Figure 32). Indicating that Smad2-negative, Smad4-positive tumors are more likely to have increased HGF levels, consistent with our in vivo and in vitro data.

DISCUSSION

K5.Smad2-/- *and* K5.Smad4-/- *Tumors and Skin Have Increased Angiogenesis*

Tumor angiogenesis is amongst the six alterations needed in the tumor microenvironment for an epithelial tumor to become invasive and metastatic (4). Multiple genetic alterations occur in tumors that can contribute to the angiogenic switch (4), therefore we aimed to determine whether epithelial loss of TGFβ-signaling components alone is sufficient to promote an angiogenic microenvironment. When compared to wildtype mouse skin, *K5.Smad2-/-* skin and *K5.Smad4-/-* both contained increased vessel number and density, indicating loss of Smad2 or Smad4 alone is sufficient to induce a pro-angiogenic environment.

Smad4 loss leads to increased VEGF- and TGFβ-related angiogenesis

K5.Smad4-/- tumors and skin both harbored elevated levels of VEGF protein and transcript. As VEGF is a known target of TGFβ, this finding may be somewhat surprising (66, 119). However, studies have shown Smad3 is mainly responsible for this TGFβ responsiveness due to Smad3 and HIF1α binding to the VEGF promoter (66). *K5.Smad4-/-* epithelium has elevated levels of Smad3 (current study, and unpublished data from our lab). Consistently, keratinocytes with Smad4 knockdown had increased Smad3 expression as well as increased VEGF expression. Furthermore, we demonstrated that keratinocytes with Smad3 and Smad4 co-knockdown abrogated the Smad4-knockdown induction of VEGF. Thus, Smad4-loss elevation of Smad3 levels may be responsible for the increased VEGF-related angiogenesis.

In addition, increased endothelial TGFβ-signaling in *K5.Smad4-/-* tumors and preneoplastic skin contributed to the increased angiogenesis. *K5.Smad4-/-* epithelium had increased TGFβ1. TGFβ promotes angiogenesis through the TGFβR, Alk1, and subsequent signaling through pSmads1/5/8 (63). *K5.Smad4-/-* skin and tumors had increased Alk1 activation and pSmads1/5/8. Therefore, contributions from both VEGF- and TGFβ-mediated angiogenesis lead to increased vessel number and density in *K5.Smad4-/-* skin and SCCs.

HGF transcription is negatively regulated by Smad2

K5.Smad2-/- skin and tumors did not exhibit alterations in VEGF- and TGFβ-signaling seen in the *K5.Smad4-/-* skin and tumors. *K5.Smad2-/-* skin and tumors possessed increased HGF and increased activated receptor, p-cMET. Mesenchymal cells have been shown to promote VEGF-independent angiogenesis through the production of HGF (69, 70, 116, 123, 124). *K5.Smad2-/-* skin and tumors undergo early changes of epithelial-to-mesenchymal transition (EMT) (115), which may allow a mesenchymal transcriptional environment that promotes HGF transcription. Furthermore, TGFβ can stimulate HGF production (47, 67, 68), but can also repress HGF (69, 70). We hypothesized the differential response to TGFβ reflected the differential regulation of the HGF promoter by Smad2 and

Smad4. We found the SBE located at –466bp upstream of the mouse HGF transcriptional start site was negatively regulated by Smad2, such that in *K5.Smad2-/-* skin, Smad3, Smad4, CBP/p300, and RNA Polymerase II had increased binding to the SBE in the absence of transcriptional co-repressors recruited by Smad2. In contrast, in *K5.Smad4-/-* skin, which expressed reduced HGF, Smad2, TGIF, CtBP, and HDAC3 binding to the SBE was increased consistent with Smad2-regulated repression of HGF. Therefore, Smad3 and Smad4 mediate TGFβ induction of HGF in the absence of Smad2-mediated repression. Furthermore, keratinocytes with Smad2 knockdown had increased HGF transcript, which was abrogated by concomitant knockdown of Smad3 or Smad4 with Smad2. Consistently, luciferase activity of the HGF promoter was induced by Smad2 knockdown, but abrogated by Smad3 or Smad4 siRNAs. Thus, Smad2-loss induction of HGF is responsible for the increased angiogenesis in *K5.Smad2-/-* skin and tumors.

While the HGF receptor, cMET, was transcriptionally upregulated in *K5.Smad4-/-* tumors, this increase was not seen in *K5.Smad4-/-* skin, nor in levels of active phosphorylated-cMET in *K5.Smad4-/-* skin. Additionally, knockdown of Smad4 had no effect on keratinocyte production of cMET (Figure 33). Therefore, it is likely that upregulation of cMET is a secondary effect of carcinogenesis. Consistent with this finding, many cancer types have increased MET (125). In particular, head and neck SCCs (HNSCCs), a tumor type with a high prevalence of TGFβ-signaling defects including Smad4 loss (102, 126, 127), have shown gene amplification of cMET or activating mutations in cMET (128-131), leading to ligand-independent activation of HGF-signaling pathway. A common mechanism may be involved linking TGFβ-signaling and other carcinogenic hits in the activation of cMET, however this does not appear to be a direct effect of Smad4 loss.

Angiogenic pathways converge on common mediators

Despite the different diffusible angiogenic factors released from *K5.Smad2-/-* and *K5.Smad4-/-* keratinocytes, some downstream effectors are the same. Both *K5.Smad2-/-* and *K5.Smad4-/-* skin and tumors show increased endothelial pAKT and eNOS, which act downstream of HGF and VEGF (116-118). Therefore, TGFβ-signaling defects have some functional redundancy in contributing to the angiogenic

phenotype. However, VEGF and HGF can influence angiogenesis through unique mechanisms we did not explore making AKT an attractive, but possibly not entirely effective therapeutic target.

While most human skin SCCs are caught early and easily treated by surgical resection, metastatic skin SCCs carry a high morbidity and mortality. Angiogenesis is a critical regulator of tumor invasion and metastasis (4). TGFβ-signaling defects contribute not only to escape from TGFβ-mediated growth inhibition (31, 32) and epithelial-to-mesenchymal transition (115), but also promote an angiogenic microenvironment (current study). We have shown that TGFβ signaling defects are amongst the most frequent mutations in human skin SCCs (115). Therefore, tumor cells with TGFβ-signaling mutations are more fit to survive as they possess multiple alterations necessary to overcome the hurdles to metastatic carcinoma (4). Therapy restoring TGFβ-signaling in tumors is complicated by the pro-carcinogenic effects of TGFβ expression: inflammation, EMT and angiogenesis (13, 14, 29). Thus, therapy must be targeted to the procarcinogenic downstream effectors. More investigation is warranted to study the true angiogenic potential of cMET and VEGF in vivo using small molecule inhibitors to assess the necessity of cMET and VEGF in vessel formation and tumor progression. This will provide the groundwork for whether inhibition of p-cMET, VEGF, and potentially pAKT have clinical value. With continued research, it is possible that small molecule inhibitors directed to these targets may provide the possibility of preventing skin SCC angiogenesis and metastasis, without disrupting the tumor suppressive roles of TGFβ.

TABLES

	K5.Smad2-/- SCC Fold Change	*p-value*	*n*
TSP1	1.20	0.82	10
Flt	1.20	0.30	10
sFlt	0.60	0.10	10
VEGFb	1.40	0.35	10

Table 5. Angiogenic molecules statistically unaltered as determined by qRT-PCR.

FIGURES

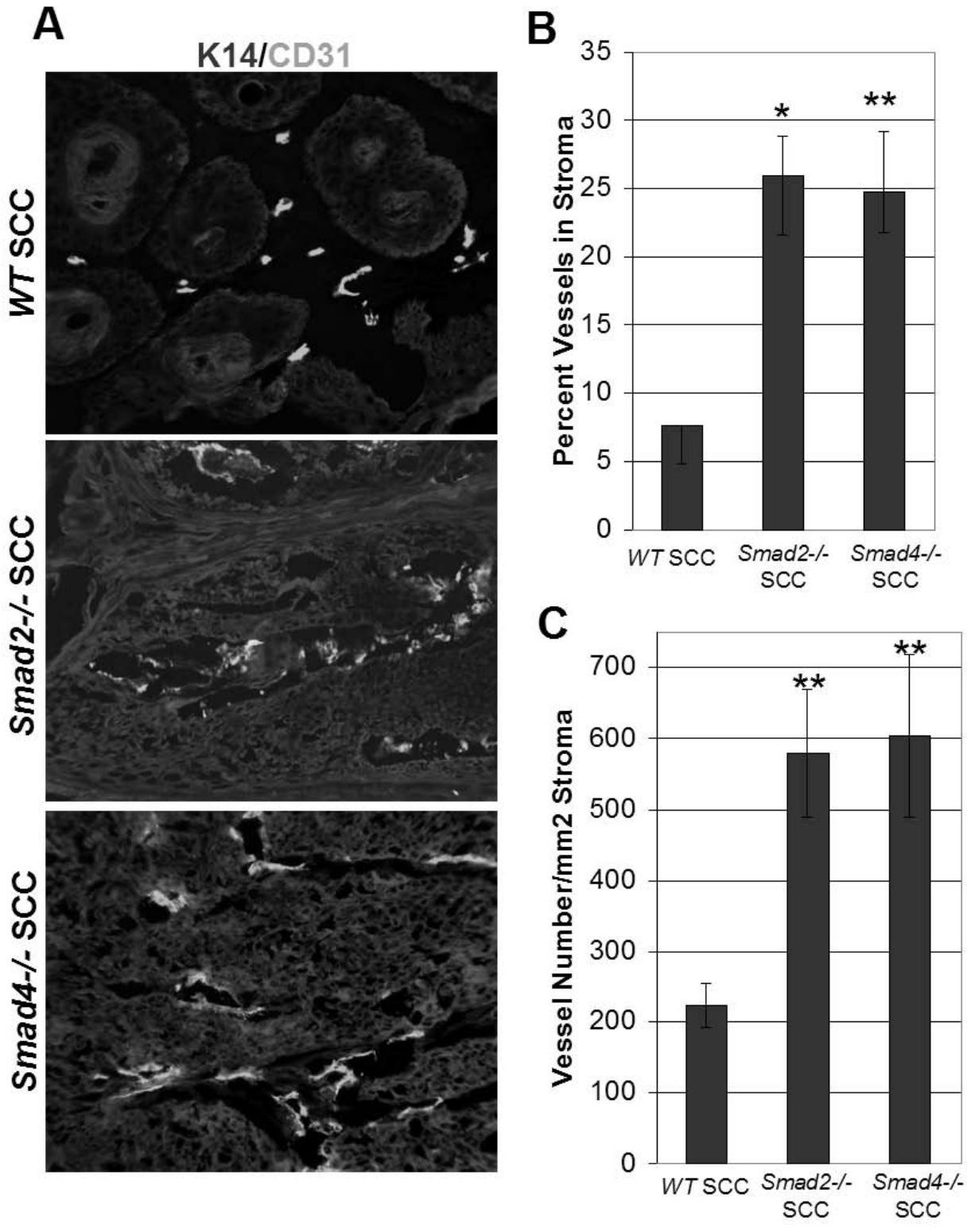
A
K14/CD31
WT SCC
Smad2-/- SCC
Smad4-/- SCC
B
Percent Vessels in Stroma
35
30
25
20
15
10
5
0
*
**
WT SCC
Smad2-/- SCC
Smad4-/- SCC
C
Vessel Number/mm2 Stroma
700
600
500
400
300
200
100
0
**
**
WT SCC
Smad2-/- SCC
Smad4-/- SCC

Figure 22. *K5.Smad2-/-* and *K5.Smad4-/-* SCCs had increased angiogenesis.

A: Immunoflourescence of *K5.Smad2-/-* and *K5.Smad4-/-* SCCs for CD31 (green) showed increased vessel number and vessel area compared to SCCs derived from wildtype mice. Keratin 14 (K14, Red) was used as a counterstain. B: Increased vessel area per stromal area in *K5.Smad2-/-* and *K5.Smad4-/-* SCCs as determined by quantitation of immunofluorescence images. n=5 samples per group. C: Increased vessel number per stromal area in *K5.Smad2-/-* and *K5.Smad4-/-* SCCs as determined by quantitation of immunofluorescence images. n=5 samples per group. *$p<0.05$ compared to WT SCC. **$p<0.001$ compared to WT SCC.

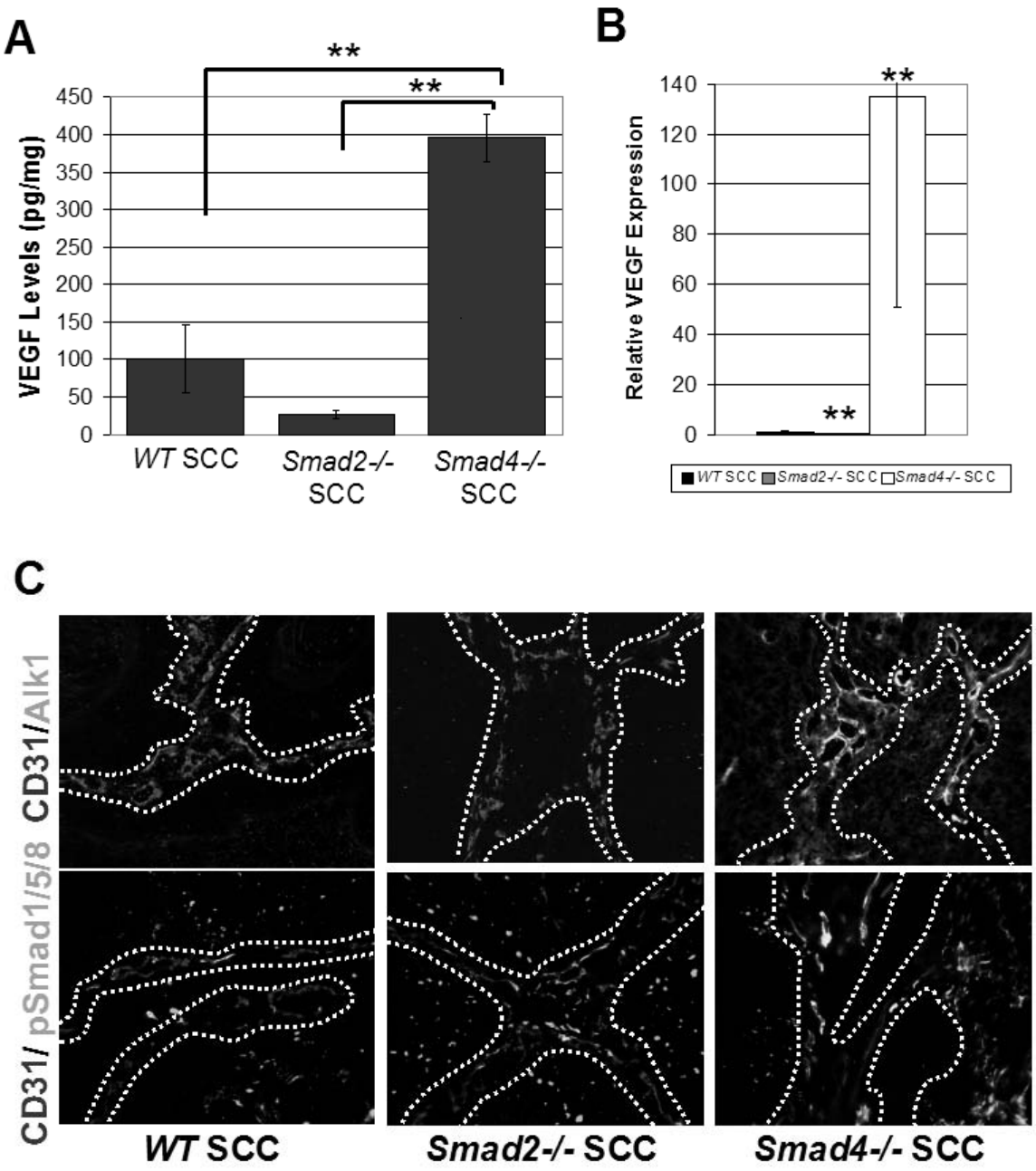

Figure 23. *K5.Smad4-/-* SCCs had increased VEGF- and TGFβ-mediated angiogenesis.

A: VEGF protein levels were increased in *K5.Smad4-/-*, but not *K5.Smad2-/-* SCCs, compared to wildtype SCCs as determined by ELISA. n=5 samples per group. B: *K5.Smad4-/-* SCCs had increased VEGFa transcript, while *K5.Smad2-/-* SCCs had reduced VEGFa transcript compared to wildtype SCCs. n=5

samples per group. C: *K5.Smad4-/-* SCCs had increased TGFβ-mediated angiogenesis. Immunofluorescence for pro-angiogenic endothelial TGFβ-receptor Alk1 (green, upper panel) was increased in *K5.Smad4-/-* SCCs. Downstream signaling mediators, phospho-Smad-1, -5, and –8 (green, lower panel) were also increased in *K5.Smad4-/-* SCCs, but not *K5.Smad2-/-* SCCs. Endothelium marker CD31 (red) was used as counterstain. Dashed lines indicate tumor-stoma border. **$p<0.001$ compared to WT SCC.

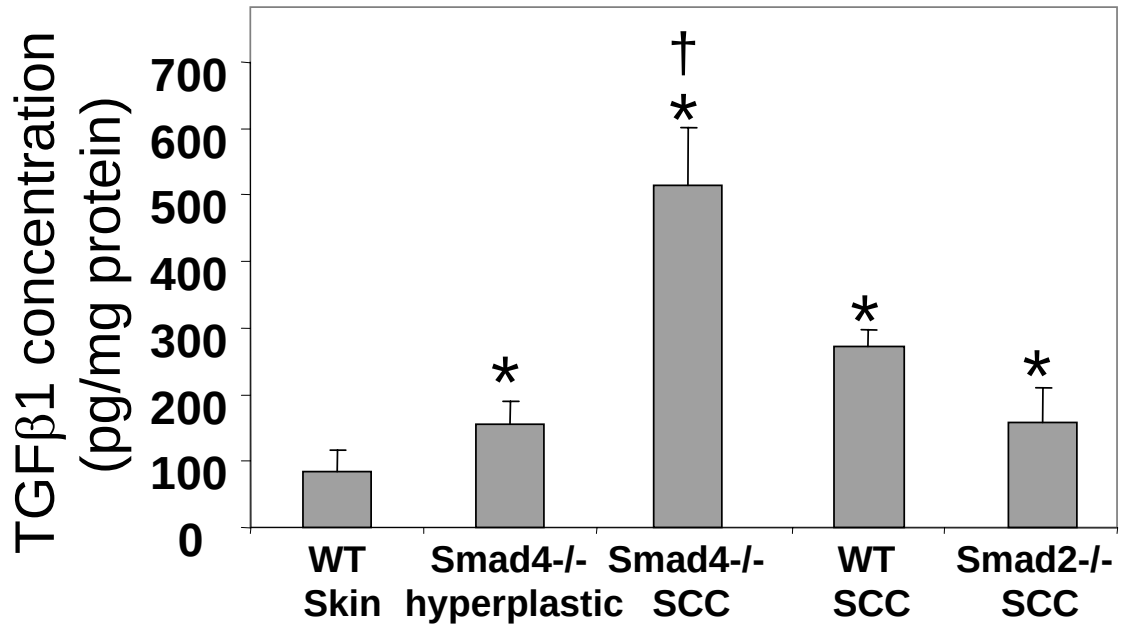

Figure 24. *Smad4-/-* hyperplastic tissue and *Smad4-/-* SCCs exhibit more TGFβ1 protein compared to WT tissue.

ELISA for TGFβ1 shows *Smad4-/-* hyperplastic skin has more TGFβ ligand than WT skin, and is approximately equivalent to the TGFβ in *Smad2-/-* SCCs. *Smad4-/-* SCCs have more TGFβ than WT skin, WT SCC, or *Smad2-/-* SCC. *Smad2-/-* SCCs do not exhibit increased TGFβ levels compared to WT SCCs. n=5 samples per group. * $p<0.05$ compared to WT Skin. † $p<0.05$ compared to WT SCC.

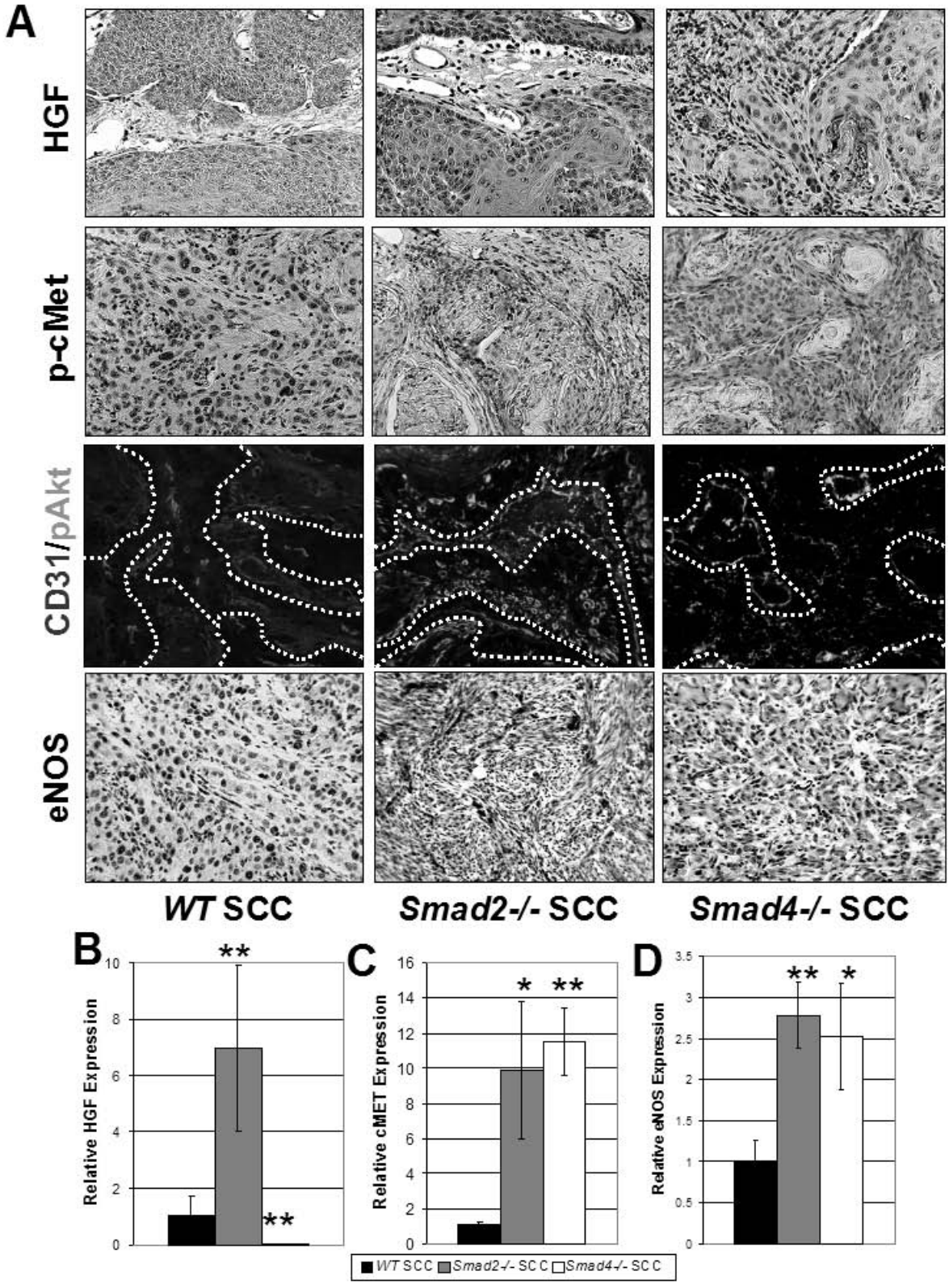
A
HGF
p-cMet
CD31/pAkt
eNOS
WT SCC
Smad2-/- SCC
Smad4-/- SCC
B
Relative HGF Expression
C
Relative cMET Expression
D
Relative eNOS Expression
WT SCC
Smad2-/- SCC
Smad4-/- SCC

Figure 25. *K5.Smad2-/-* SCCs had increased HGF leading to convergence of *K5.Smad2-/-* and *K5.Smad4-/-* angiogenesis on pAKT.

A: *K5.Smad2-/-* SCCs had increased HGF by immunohistochemistry (top panel). *K5.Smad2-/-* and to a lesser extent *K5.Smad4-/-* SCCs had increased activated endothelial HGF receptor, p-cMET (second panel). VEGF and HGF pathways converge downstream as seen by increased endothelial pAKT (green, third panel) in both *K5.Smad2-/-* and *K5.Smad4-/-* SCCs. eNOS, downstream of pAKT, was also increased in both *K5.Smad2-/-* and *K5.Smad4-/-* SCCs (bottom panel). Dashed lines indicate tumor-stoma border. B: *K5.Smad2-/-* SCCs had increased, while *K5.Smad4-/-* SCCs had reduced, HGF mRNA levels. n=5 samples per group. C: Both *K5.Smad2-/-* and *K5/Smad4-/-* SCCs had increased p-cMET mRNA. n=5 samples per group. D: *K5.Smad2-/-* and *K5.Smad4-/-* SCCs had increased eNOS mRNA expression. n=5 samples per group. *$p<0.05$ compared to WT SCC. **$p<0.001$ compared to WT SCC.

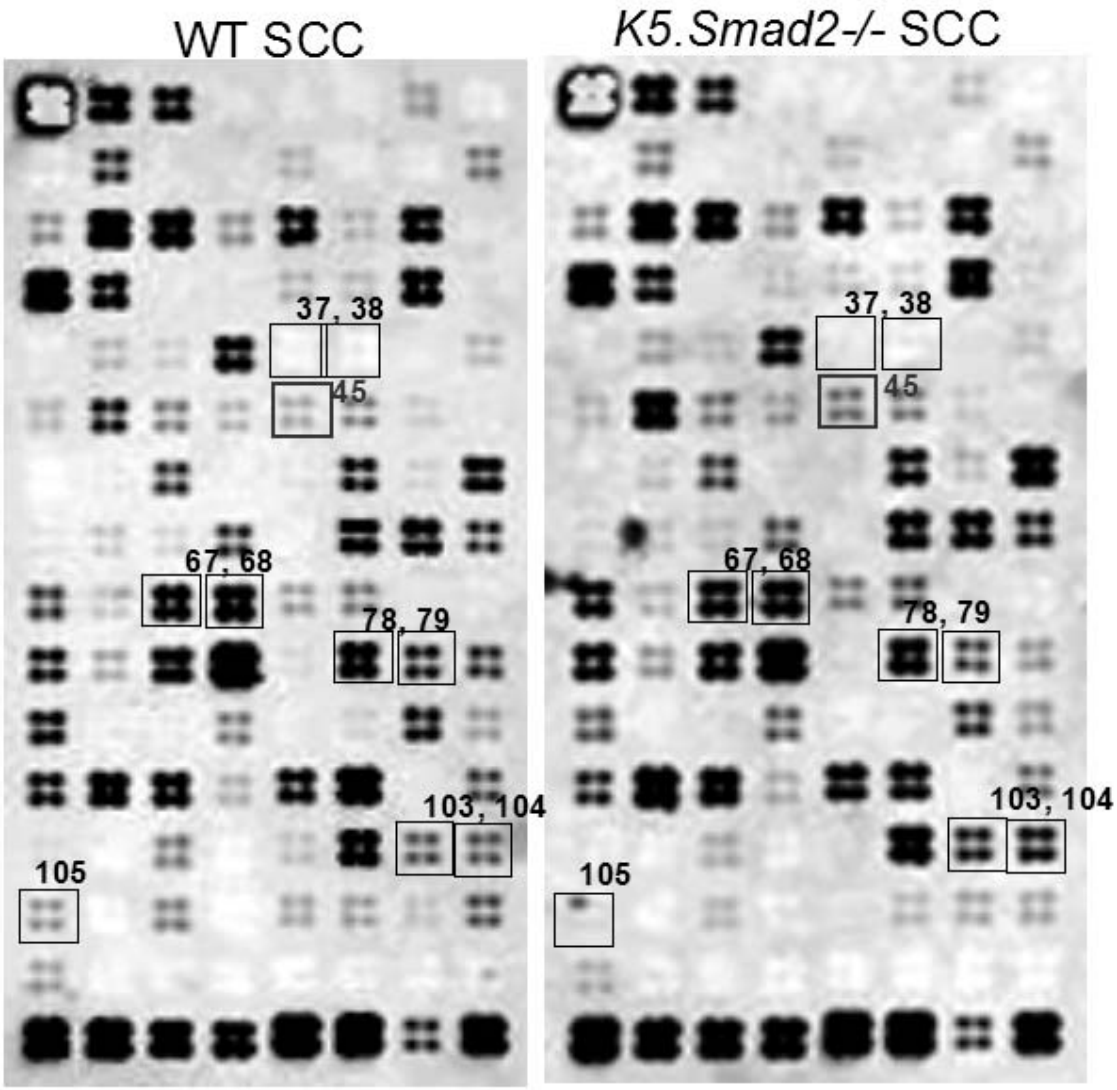

Figure 26. Representative cancer pathway superarray with angiogenic markers identified.

Markers boxed in black are angiogenesis-related molecules which do not contribute to *K5.Smad2-/-* SCCs when compared to WT SCCs. Upregulated HGF is boxed in red. 103, 104 – TIMPS (upregulated), 105 – TNFα (downregulated), 67 -- MMP2 (unchanged), 68 -- MMP9 (unchanged), 37 -- FGF1 (unchanged), 38 -- FGF2 (unchanged), 78 – PDGFa (unchanged), 79 – PDGFb (downregulated). n=3 samples per group.

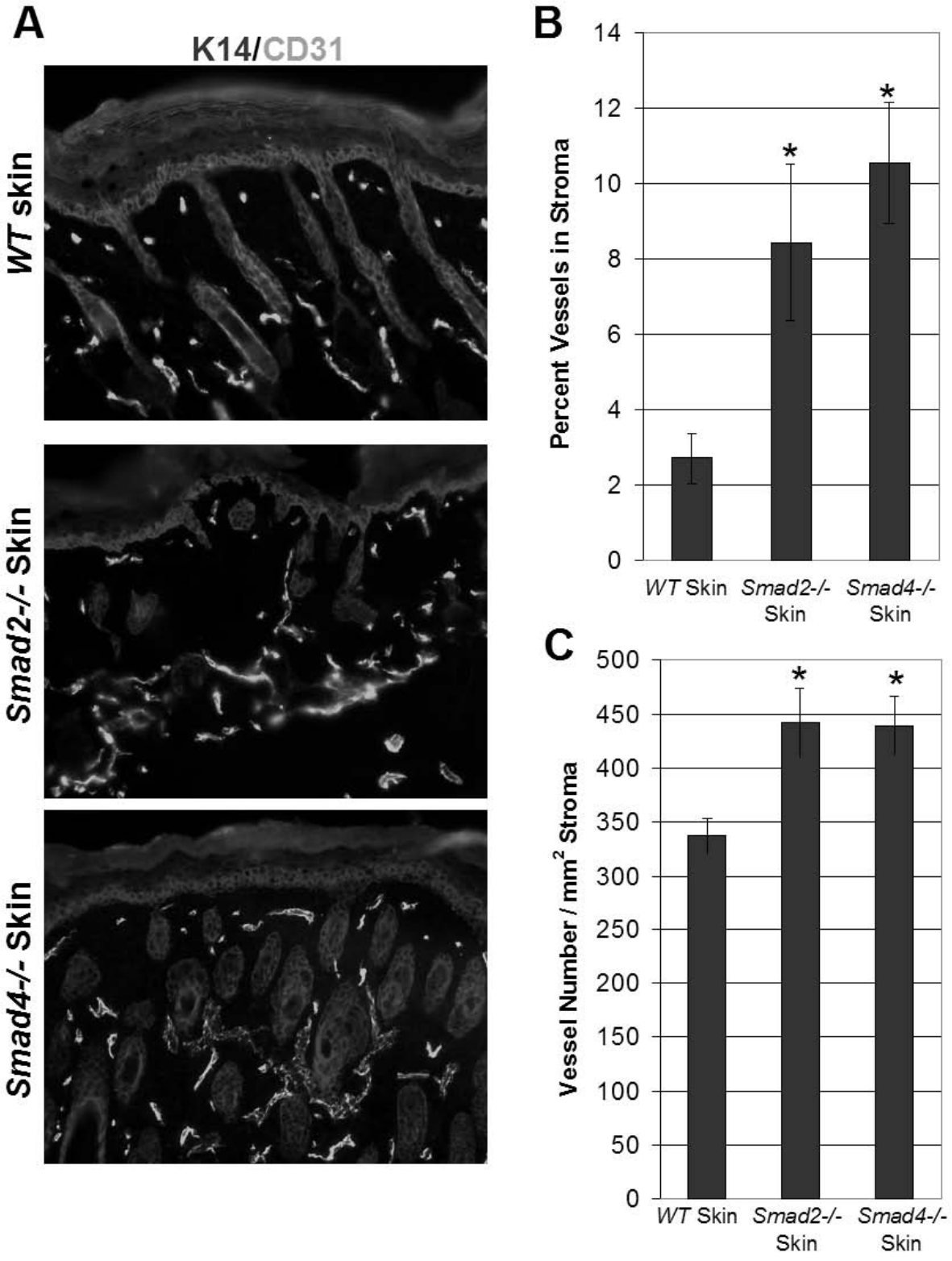

Figure 27. *K5.Smad2-/-* and *K5.Smad4-/-* pre-neoplastic skin had increased angiogenesis.

A: Immunoflourescence of *K5.Smad2-/-* and *K5.Smad4-/-* skin for CD31 (green) showed increased vessel number and vessel area compared to skin derived from wildtype mice. Keratin 14 (K14, Red) was used as a counterstain. B: Increased vessel area per stromal area in *K5.Smad2-/-* and *K5.Smad4-/-* skin as determined by quantitation of immunofluorescence images. n=6 samples per group for *WT* and *K5.Smad2-/-*. n=6 samples per group for *K5.Smad4-/-*. C: Increased vessel number per stromal area in *K5.Smad2-/-* and *K5.Smad4-/-* skin as determined by quantitation of immunofluorescence images. n=6 samples per group for *WT* and *K5.Smad2-/-*. n=6 samples per group for *K5.Smad4-/-*. *$p<0.05$ compared to WT skin.

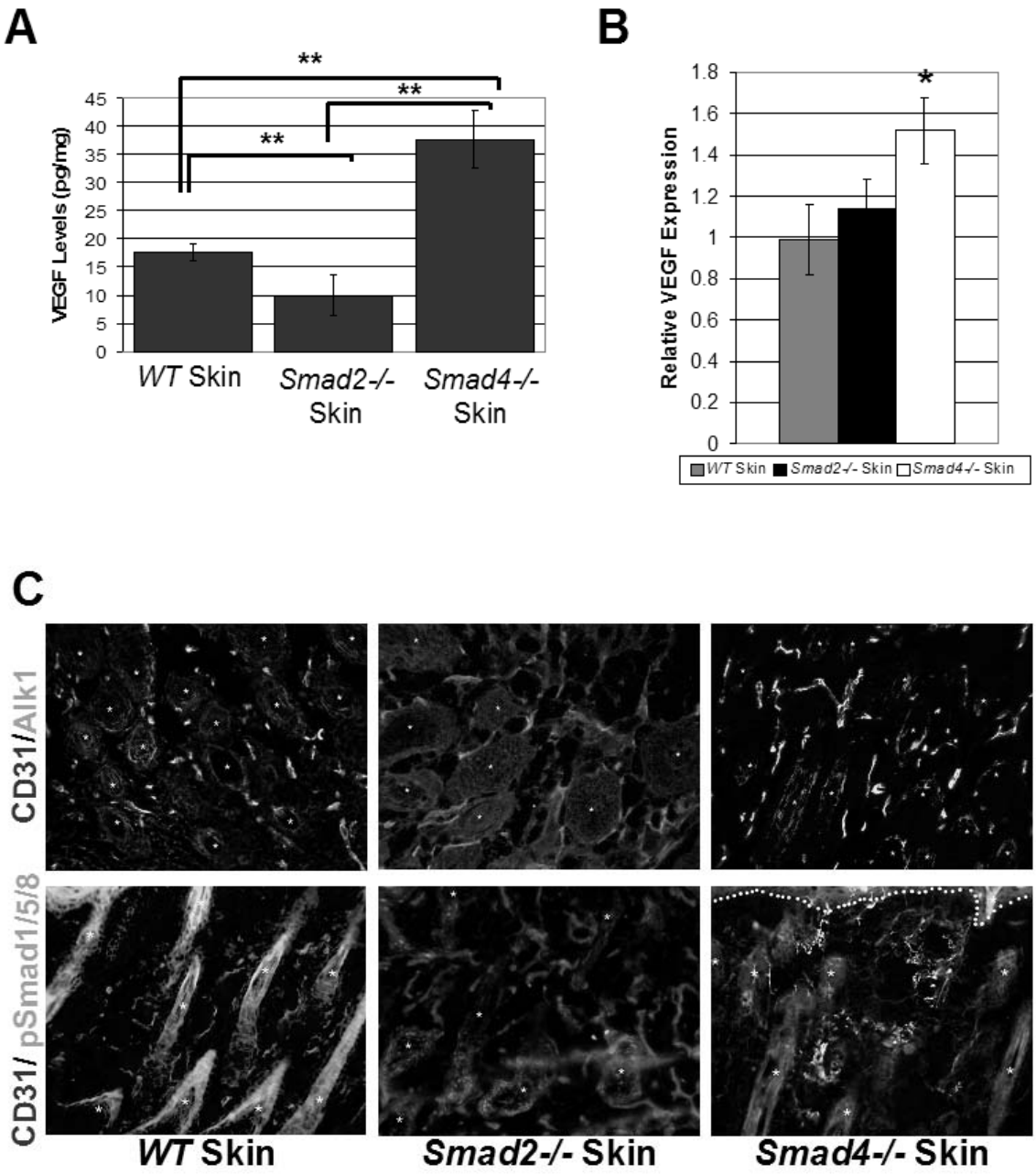

Figure 28. *K5.Smad4-/-* preneoplastic skin had increased VEGF- and TGFβ-mediated angiogenesis.

A: VEGF protein levels were increased in *K5.Smad4-/-*, but reduced in *K5.Smad2-/-*, skin compared to wildtype skin as determined by ELISA. n=6 samples per group for *WT* and *K5.Smad2-/-*. n=6 samples per group for *K5.Smad4-/-*. B: *K5.Smad4-/-* skin had increased VEGFa transcript, while *K5.Smad2-/-* did not when compared to wildtype skin. n=6 samples per group for *WT* and *K5.Smad2-/-*. n=6 samples per group for *K5.Smad4-/-*. C: *K5.Smad4-/-* skin had increased TGFβ-mediated angiogenesis. Immunofluorescence

for pro-angiogenic endothelial TGFβ-receptor Alk1 (green, upper panel) was increased in *K5.Smad4-/-* skin. Downstream signaling mediators, phospho-Smad-1, -5, and –8 (green, lower panel) were also increased in *K5.Smad4-/-* skin, but not *K5.Smad2-/-* SCCs. Endothelium marker CD31 (red) was used as counterstain. Asterisks images denote hair follicles. *$p<0.05$ compared to WT skin. **$p<0.001$ compared to WT skin.

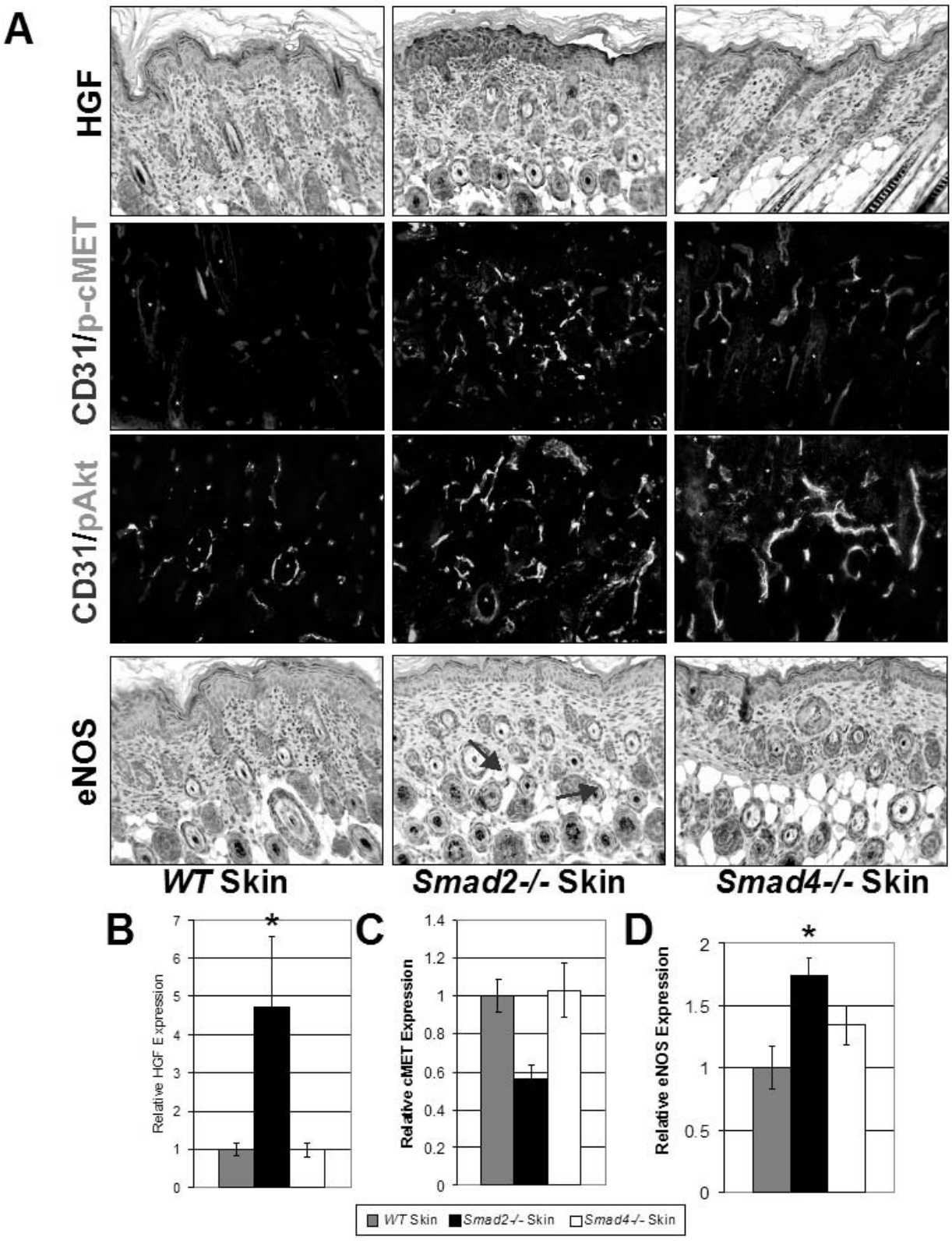
A
HGF
CD31/p-cMET
CD31/pAkt
eNOS
WT Skin
Smad2-/- Skin
Smad4-/- Skin
B
Relative HGF Expression
C
Relative cMET Expression
D
Relative eNOS Expression
WT Skin
Smad2-/- Skin
Smad4-/- Skin

Figure 29. *K5.Smad2-/-* skin had increased HGF leading to convergence of *K5.Smad2-/-* and *K5.Smad4-/-* angiogenesis on pAKT.

A: *K5.Smad2-/-* skin had increased HGF by immunohistochemistry (top panel). *K5.Smad2-/-*, but not *K5.Smad4-/-*, skin had increased activated endothelial HGF receptor, p-cMET (second panel). VEGF and HGF pathways converge downstream as seen by increased endothelial pAKT (green, third panel) in both *K5.Smad2-/-* and *K5.Smad4-/-* skin. eNOS was increased in *K5.Smad2-/-*, but not *K5.Smad4-/-* skin (bottom panel). Red arrows highlight eNOS-positive vessels. -/-. Asterisks in images denote hair follicles. B: *K5.Smad2-/-*, but not *K5.Smad4-/-*, skin had increased HGF mRNA levels. C: Neither *K5.Smad2-/-* nor *K5/Smad4-/-* skin had increased p-cMET mRNA. D: *K5.Smad2-/-*, but not *K5.Smad4-/-*, skin had increased eNOS mRNA levels. n=6 samples per group for *WT* and *K5.Smad2-/-*. n=6 samples per group for *K5.Smad4* *$p<0.05$ compared to WT skin.

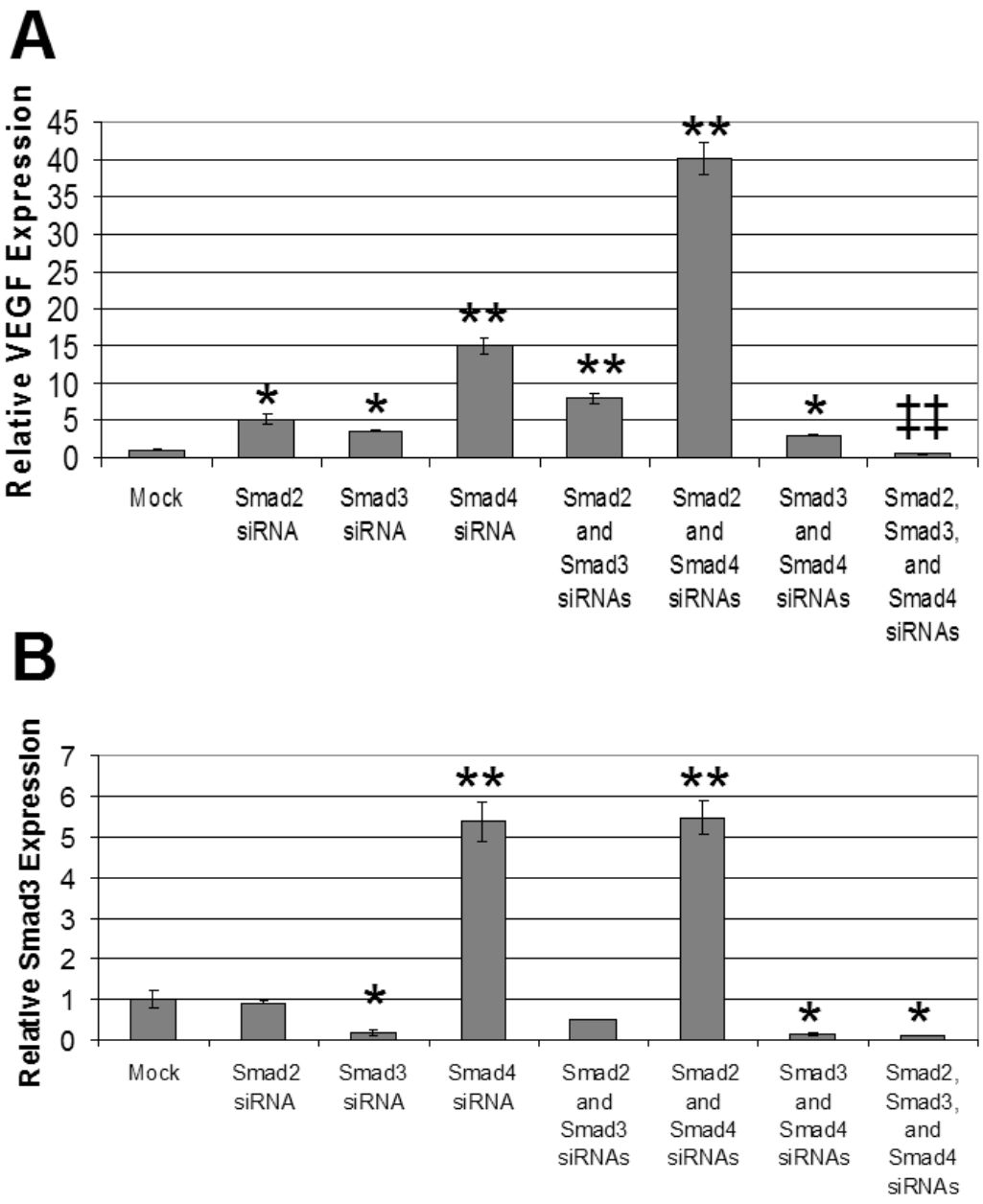

Figure 30. Smad4 knockdown increased VEGF and Smad3 expression.

A: Knockdown of Smad4 in human keratinocytes dramatically upregulated VEGF expression, which was abrogated by concomitant knockdown of Smad3 and Smad2. B: Smad3 mRNA levels increased when Smad4 was reduced. This increase was abrogated by concomitant knockdown of Smad3. *$p<0.05$

compared to mock treatment. **p<0.001 compared to mock treatment. ‡‡ p<0.001 compared Smad4 siRNA

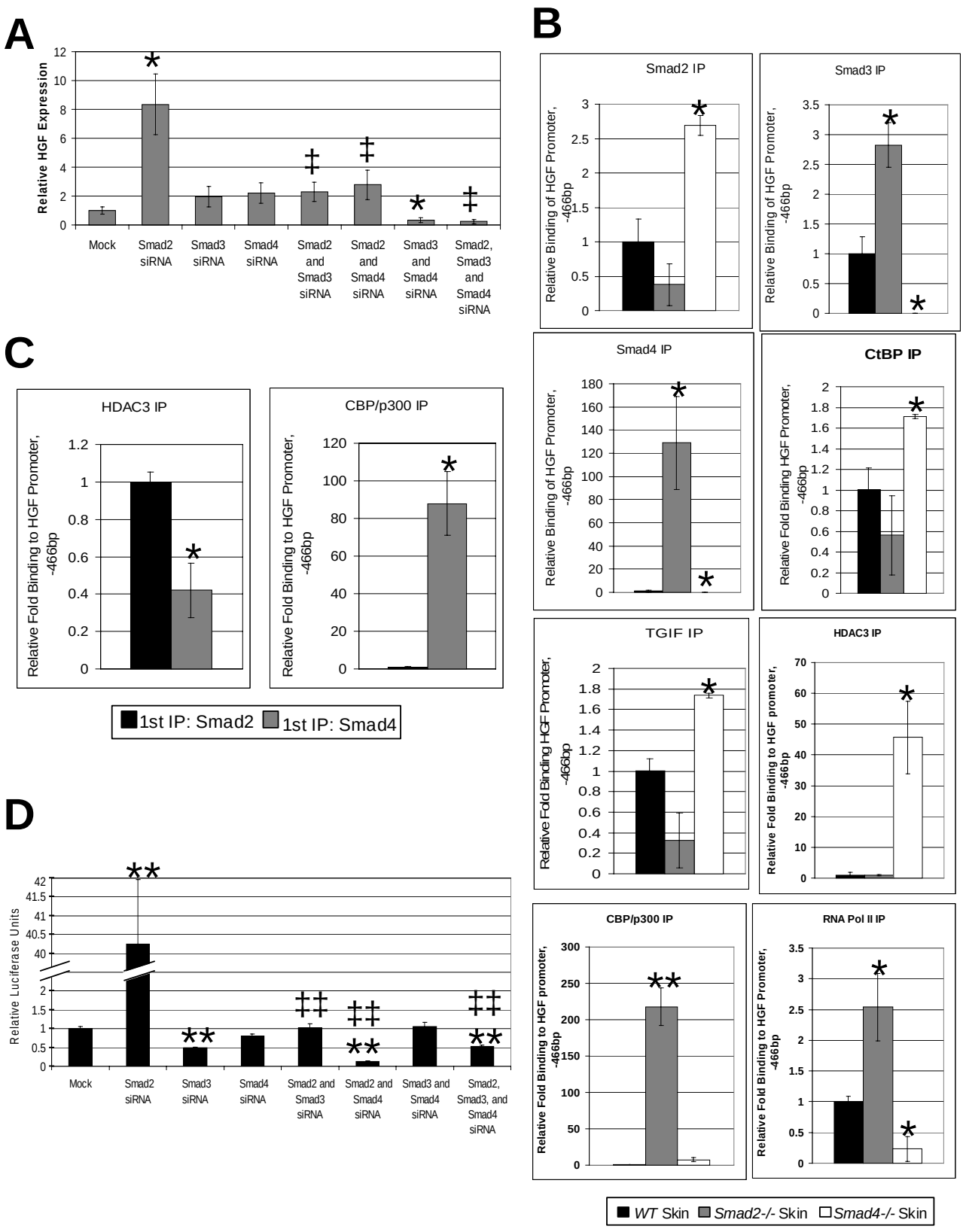
A
Relative HGF Expression
Mock
Smad2 siRNA
Smad3 siRNA
Smad4 siRNA
Smad2 and Smad3 siRNA
Smad2 and Smad4 siRNA
Smad3 and Smad4 siRNA
Smad2, Smad3 and Smad4 siRNA
B
Smad2 IP
Smad3 IP
Smad4 IP
CtBP IP
TGIF IP
HDAC3 IP
CBP/p300 IP
RNA Pol II IP
Relative Binding of HGF Promoter, -466bp
Relative Fold Binding HGF Promoter, -466bp
Relative Fold Binding to HGF promoter, -466bp
C
HDAC3 IP
CBP/p300 IP
Relative Fold Binding to HGF Promoter, -466bp
1st IP: Smad2
1st IP: Smad4
D
Relative Luciferase Units
Mock
Smad2 siRNA
Smad3 siRNA
Smad4 siRNA
Smad2 and Smad3 siRNA
Smad2 and Smad4 siRNA
Smad3 and Smad4 siRNA
Smad2, Smad3, and Smad4 siRNA
WT Skin
Smad2-/- Skin
Smad4-/- Skin

Figure 31. Smad2 and Smad4 regulated transcription of angiogenic mediators.

A: Knockdown of Smad2 dramatically increased HGF transcript, which was abrogated by concomitant knockdown of either Smad3 or Smad4. Knockdown of Smad3 and Smad4 led to reduced HGF transcript compared to mock treatment. *$p<0.05$ compared to mock treatment. ‡ $p<0.05$ compared Smad2 siRNA treatment. B: Different cofactors bound the HGF promoter under the presence and absence of Smad2. Smad3, Smad4, and transcriptional repressors TGIF, CtBP, and HDAC3 had increased binding to the HGF promoter in *K5.Smad4-/-*, and reduced binding in *K5.Smad2-/-*, skin compared to wildtype skin by comparative ChIP. Consistently, transcriptional activators CBP/p300 and RNA Polymerase II were bound increasingly in *K5.Smad2-/-* skin, correlating with Smad2-loss associated HGF upregulation. *$p<0.05$ compared to WT skin. **$p<0.001$ compared to WT skin. C: Dual-IP ChIP revealed HDAC3 had nearly 3-fold more binding to Smad2 on the HGF promoter, while CBP/p300 preferentially bound Smad4 on the HGF promoter. *$p<0.05$ compared to WT skin. D: Smad2 knockdown increased HGF promoter activity, which was abrogated by concomitant knockdown of Smad3 or Smad4. n=3 per group. **$p<0.001$ compared to mock treatment. ‡‡ $p<0.001$ compared Smad2 siRNA

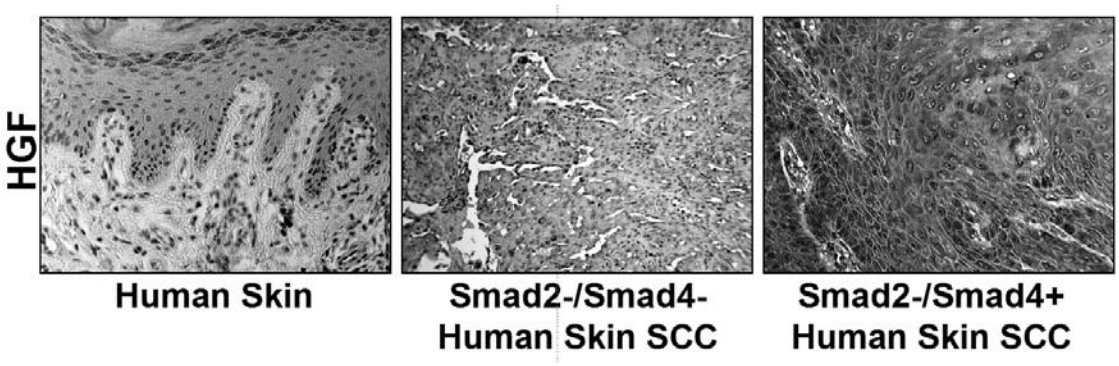

Figure 32. HGF expression in human skin squamous cell carcinomas lacking Smad2 correlated with Smad4-positive tumors.

70% (52/74) of human skin SCCs expressed HGF. Additionally, amongst skin SCCs that lacked Smad2 protein, HGF expression positively correlated with retained Smad4 expression indicating that Smad2-negative, Smad4-positive tumors are more likely to have increased HGF levels.

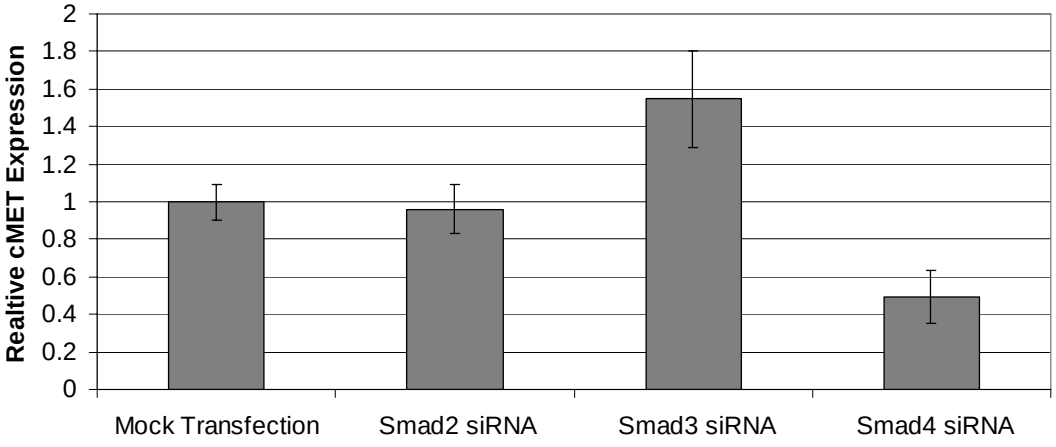

Figure 33. cMET expression unchanged with Smad siRNA treatment.

HaCaT cells treated with siRNA to Smad2, Smad3, or Smad4 resulted in no change in cMET transcript levels as assayed by qRT-PCR.

IV. SUMMARY AND CONCLUSIONS

Skin cancer is the most frequently occurring form of cancer (1). While most cases are well controlled if caught early, aggressive skin cancer, as seen in immunocompromised patients, is life threatening. Aggressive skin cancer grows rapidly, is highly invasive, and metastasizes. Based on Gatenby et al.'s model of squamous cell carcinogenesis, the epithelium must undergo somatic evolution to overcome six physiologic barriers to metastasis. In this study, we elucidated how loss of TGFβ-signaling components can contribute to overcoming multiple barriers, leading to more aggressive tumorigenesis.

SMAD2-LOSS CONTRIBUTED TO EPITHELIAL-TO-MESENCHYMAL TRANSITION

In the current study, we found Smad2 and Smad4, but not Smad3 were commonly lost in human skin SCCs. To further evaluate the tumor suppressive role of Smad2 in the epidermis, we developed mice with keratinocyte-specific *Smad2* deletion. *K5.Smad2-/-* mice did not develop spontaneous skin cancer, nor did they develop tumors after DMBA treatment alone or TPA treatment alone. The inability of *K5.Smad2-/-* mice to spontaneously form tumors indicates that it is insufficient to act as a tumor initiator. Therefore, it is likely that *Smad2* loss alone cannot increase cellular proliferation or inhibit apoptosis, as is common amongst tumor initiators. However, we observed that TPA treated *K5.Smad2-/-* skin did exhibit increased proliferation, indicating additional mutagenesis is needed to reveal Smad2-loss abrogation of TGFβ-mediated growth inhibition. Further, TGFβ-mediated growth inhibition may be more a function of Smad3, than Smad2 (14). DMBA treatment, which induces *H-Ras* mutation, of *K5.Smad2-/-* skin did not progress to tumor formation indicating that *Smad2* loss cannot act independently as a tumor promoting agent. Additionally, DMBA treatment alone did not lead to increased proliferation compared to controls perhaps due to the ability of oncogenic *Ras* to bypass TGFβ-mediated growth inhibition by phosphorylation and subsequent cytoplasmic sequestration of *Smad-2* and *-3* in both wildtype and *K5.Smad2-/-* skin (132).

However, *K5.Smad2-/-* mice exhibited accelerated tumor formation and malignant conversion during a two-stage chemical carcinogenesis protocol. *K5.Smad2-/-* tumors were poorly differentiated at the papilloma stage and had increased numbers of poorly differentiated carcinomas compared to *K5.Smad2+/+* tumors, including spindle-cell carcinomas (SPCCs). Loss of epithelial Smad2 led to epithelial-to-mesenchymal transition beginning in untreated neonatal skin and progressing through the papilloma stage, predominantly through upregulation of Snail and subsequent loss of E-cadherin. As Snail is a well-established TGFβ-target gene, Smad2-loss induction of Snail was a surprising result. However, we determined Smad2 primarily recruited co-repressors, like TGIF, to the Snail promoter, silencing Snail transcription (Figure 33). Loss of Smad2 allowed TGFβ-signaling components Smad3 and Smad4 to induce and bind HMGA2 on the Snail promoter and recruit transcriptional activators (Figure 33).

Interestingly, while oncogenic *Ras* has been shown to inhibit TGFβ-signaling at early stages, at later stages Ras-signaling no longer sequesters Smads, but instead causes a broad protection from various apoptotic stimuli, while allowing TGFβ-responsiveness with increased invasiveness while avoiding cell death. The Raf-MAP kinase pathway thus synergizes with TGFβ in promoting malignancy but does not directly impair TGFβ-induced Smad signaling (133). TGFβ-induced EMT is dependent on Ras signaling, which is provided by DMBA treatment in the two-stage carcinogenesis model, however Smad2-loss EMT appears to be free of this *H-Ras* dependency as EMT occurs in non-DMBA treated neonatal skin and in vitro without *Ras* activation. Additionally, activation of MAPK pathways were unaltered between wildtype and *K5.Smad2-/-* tumors indicating Smad2-loss EMT occurred through a unique pathway.

SMAD-LOSS CONTRIBUTED TO ANGIOGENESIS

Smad2-loss induction of HGF

K5.Smad2-/- skin and tumors possessed increased angiogenesis due to Smad2-loss induction of HGF. In the presence of Smad2, Smad-2, and -3 bound to the HGF promoter, while Smad2 recruited transcriptional co-repressors TGIF, CtBP, and HDAC3 to the promoter, inhibiting HGF expression (Figure 34). When Smad2 was lost, Smad3 and Smad4 displayed increasing binding to the HGF promoter and

recruited transcriptional activators RNA Polymerase II and CBP/p300, inducing HGF expression (Figure 34). Therefore, when Smad2 was lost, HGF expression increased (Figure 34 and 35).

Interestingly, recent evidence suggests TGFβ-induction and Ras stabilization of Snail acts to inhibit a RAB5 guanine nucleotide exchange factor, Rin1(134). Rin1 normally acts to inhibit receptor tyrosine kinases, such as Met, by increasing their endocytosis. Therefore, when Snail is activated, it acts through inhibition of Rin1 to stabilize c-Met leading to increased sensitivity to HGF(134). This provides an interesting connection between Ras activation, Snail activation, and HGF sensitivity seen in our K5.Smad2-/- tumors leading to increased EMT and angiogenesis through cooperative mechanisms.

Smad4-loss induction of TGFβ- and VEGF-mediated angiogenesis

Keratinocyte-specific deletion of *Smad4* lead to spontaneous malignant tumor formation. Smad4 loss in the epithelium relieves TGFβ-mediated growth inhibition leading to hyperproliferation (77, 78). However, the invasive nature of the tumors prompted us to investigate the role of epidermal Smad4 loss on the underlying stroma. We found *Smad4*-null neonatal skin and tumors had increased TGFβ ligand, inflammation, and angiogenesis (our unpublished data and the current study). Increased TGFβ acted directly and indirectly to stimulate Smad4-loss mediated angiogenesis by acting on the endothelial TGFβRI, Alk1, stimulating growth and migration of the vessels, while simultaneously acting on the keratinocytes to stimulate Smad3-dependent VEGF production (Figure 35). Interestingly, while Smad2- and Smad4-loss made different contributions to angiogenesis, the downstream effectors appeared to be the same. Keratinocyte-specific loss of either Smad2 or Smad4 lead to angiogenesis driven by pAKT, making AKT an appealing therapeutic target.

ROLE OF SMADS IN SKIN SCC PROGRESSION

TGFβ has an early tumor-suppressing role through growth inhibition, maintenance of differentiation, and apoptosis, while in late stages, TGFβ promotes tumorigenesis through angiogenesis, inflammation, and EMT. Evidence suggests different Smads mediate the different roles of TGFβ. Based

on the current study, we can modify our view of Smads in carcinogenesis. When normal epithelia loses Smad2, it undergoes EMT and angiogenesis, promoting tumorigenesis. However, Smad2 loss alone is insufficient to cause spontaneous tumorigenesis, and once a tumor has formed, *Smad2*-null tumors do not metastasize with increased frequency (Figure 36). In contrast, Smad4 loss alone is sufficient to induce spontaneous, metastatic tumors partially due to increased TGFβ ligand acting on the stroma inducing inflammation, angiogenesis, and matrix degradation (77, 78). Additionally, germline *Smad3* loss protects against carcinogenesis (38, 61) due in part to abrogation of TGFβ-induced inflammation (61). We found Smad3 and Smad4 were necessary for Smad2-loss induction of Snail and HGF, while Smad4-loss increased TGFβ, Smad3, and Smad3-mediated expression of VEGF. Therefore, we conclude that Smad2-loss EMT and angiogenesis require functional Smad3 and Smad4 (Figures 33 and 36). Smad4 loss leads to spontaneous tumor formation, and progression to metastasis without undergoing EMT, as it is indispensable for EMT (current study and (14)) (Figure 36). Thus, we conclude that Smad4 is not required for invasion and metastasis, but rather that the enhanced Smad3 effect in *Smad4*-null tissue may promote invasion. Furthermore, *Smad2*-null tumors may progress to invasive, metastatic tumors, however they require further somatic mutations, to do so (Figure 36).

FUTURE PERSPECTIVES

Although the roles of each Smad in cancer have been rigorously investigated in both in vitro and in vivo models, many questions still remained to be answered. Given the multiple functions of TGFβ signaling, it is not surprising that contradictory results for the roles of Smads in carcinogenesis have been reported. Indeed, according to the results summarized in the introduction, and in light of the current study, Smad-2, and -3 have characteristics of both tumor suppressors and promoters. Future studies on the expression patterns of individual Smads in clinical specimens and determination of the clinical outcomes of the corresponding patients will help to elucidate whether the role of Smad -2 and -3 are primarily tumor suppressing or promoting in vivo. With respect to Smad4, although it is clear that its major role is tumor suppression, the underlying mechanisms remain largely unknown. Further characterization of tumors derived from genetically modified mouse models will help to determine which cancer-related pathways

such as proliferation, differentiation, apoptosis, inflammation, angiogenesis, and/or genomic instability are predominantly affected by alteration of each Smad. Also, further identification of target genes for each Smad involved in each cancer-related pathway will indicate the mechanisms by which Smads exert their distinct functions.

To this end, several experiments remain that will clarify the roles of Smad2 and Smad4 in skin squamous cell carcinomas. First, we should evaluate the necessity of Snail in epithelial-to-mesenchymal transition in vivo by crossing the existing *Snail-flox* mouse (135) with our *Smad2-flox* mouse and *K5.Cre*PR1* mouse creating a triple-genic knockout mouse. This mouse can then be subjected to chemical carcinogenesis and assayed for resistance to EMT and tumor formation. This will help assess whether Snail is necessary for Smad2-loss associated EMT and tumor malignancy. Second, we should assess whether small molecules targeting cMET (EXEL-7592, Exelixis) or VEGF (bevacizumab, Genentech) are sufficient to inhibit Smad-loss associated angiogenesis in vivo. Using EXEL-7592 to inhibit cMET in *Smad2* knockout mice both prior to and after tumor formation will determine whether the tumor promoting microenvironment contributed to the increased number of tumors and increased malignant conversion of the tumors. Further, application of the inhibitor after tumor formation will determine whether cMET inhibition is a potential therapeutic option in subjects whose SCC is Smad2-negative. Likewise, VEGF inhibition in *Smad4*-null mice will determine whether Smad4-loss angiogenesis requires VEGF, and if it is necessary for tumor formation, growth, and metastasis. Bevacizumab application after tumor formation will determine the efficacy of VEGF inhibition as a therapeutic for *Smad4*-null skin SCCs. Finally, we need to assess whether Smad2 and Smad4 combined loss, as is seen in 83% of human skin SCCs (the current study), creates a more invasive, angiogenic, and metastatic tumor in vivo. However, since *Smad2* and *Smad4* are located on the same chromosome, a double knockout mouse is not possible. Therefore, we have created a Cre-inducible Smad2 siRNA mouse, the *pSicoSmad2* mouse. This mouse, can be crossed with our *Smad4-floxed* mouse and *K5.Cre*PR1* mouse creating a triple-genic mouse with Smad4 loss and Smad2 knockdown in the keratinoctyes. We can follow these mice to determine whether they get spontaneous tumor formation, whether the tumors are invasive and metastatic. We can also compare the

angiogenesis between these tumors and the *Smad2*-null and *Smad4*-null tumors to determine if the effects of Smad2- and Smad4-loss are additive, despite their apparent conversion on a single mediator, Akt. This information will ultimately help us to understand the complex role of TGFβ in carcinogenesis, and thus allow the development of more specific therapeutic strategies to block the tumor promoting roles, while still preserving the tumor suppressing roles of TGFβ signaling.

FIGURES

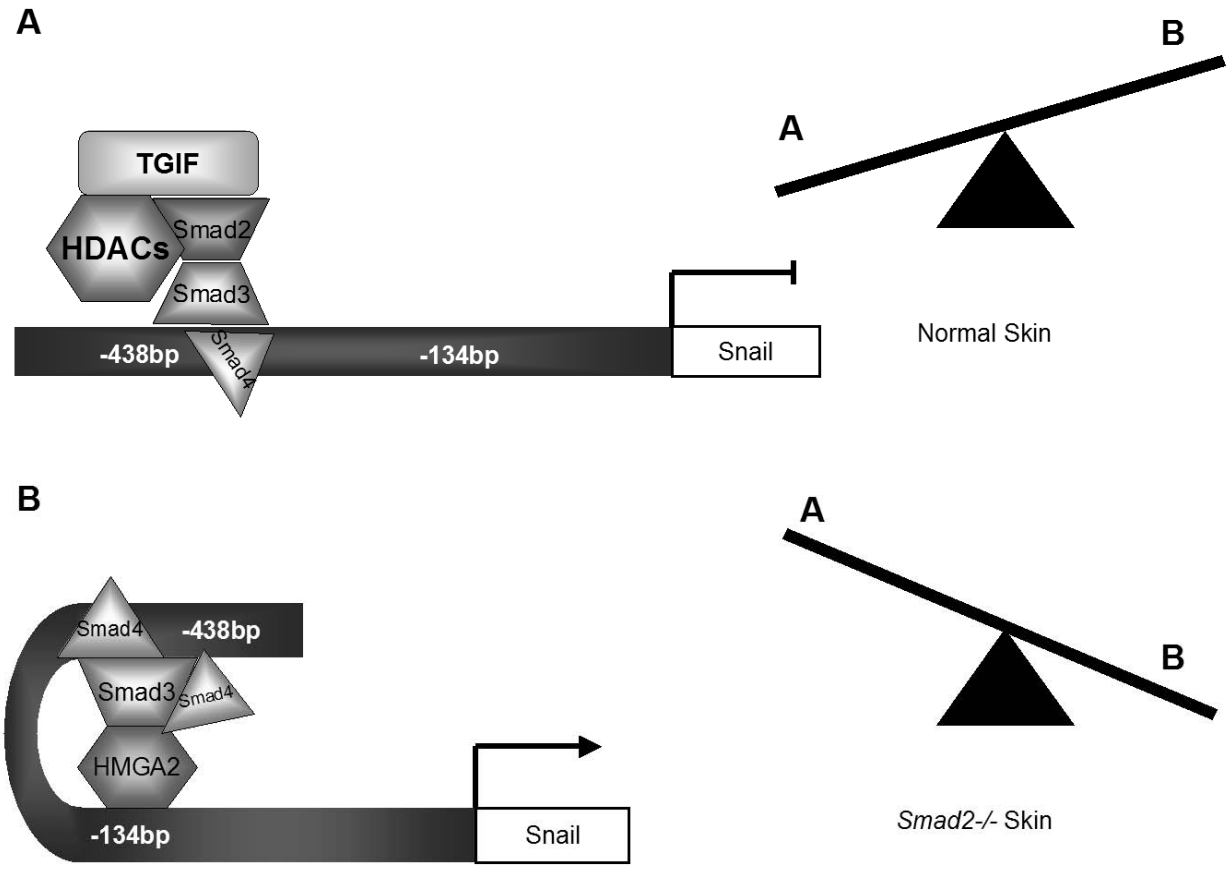

Figure 34. Schematic representation of Smad2-loss induction of Snail expression.

A: In the presence of Smad2, Smad-2, -3, and -4 bind to the promoter region of Snail. Smad2 recruits co-repressor TGIF to the promoter and prevents transcriptional activation of Snail. B: In the absence of Smad2, Smad4 and HMGA2 have increased binding to the Snail promoter, which recruits transcriptional co-activators and increases Snail transcription. The balance of these two transcriptional complexes is skewed towards Snail repression in normal epidermis, but in *Smad2-/-* skin, schematic B outweighs schematic A leading to transcriptional activation of Snail.

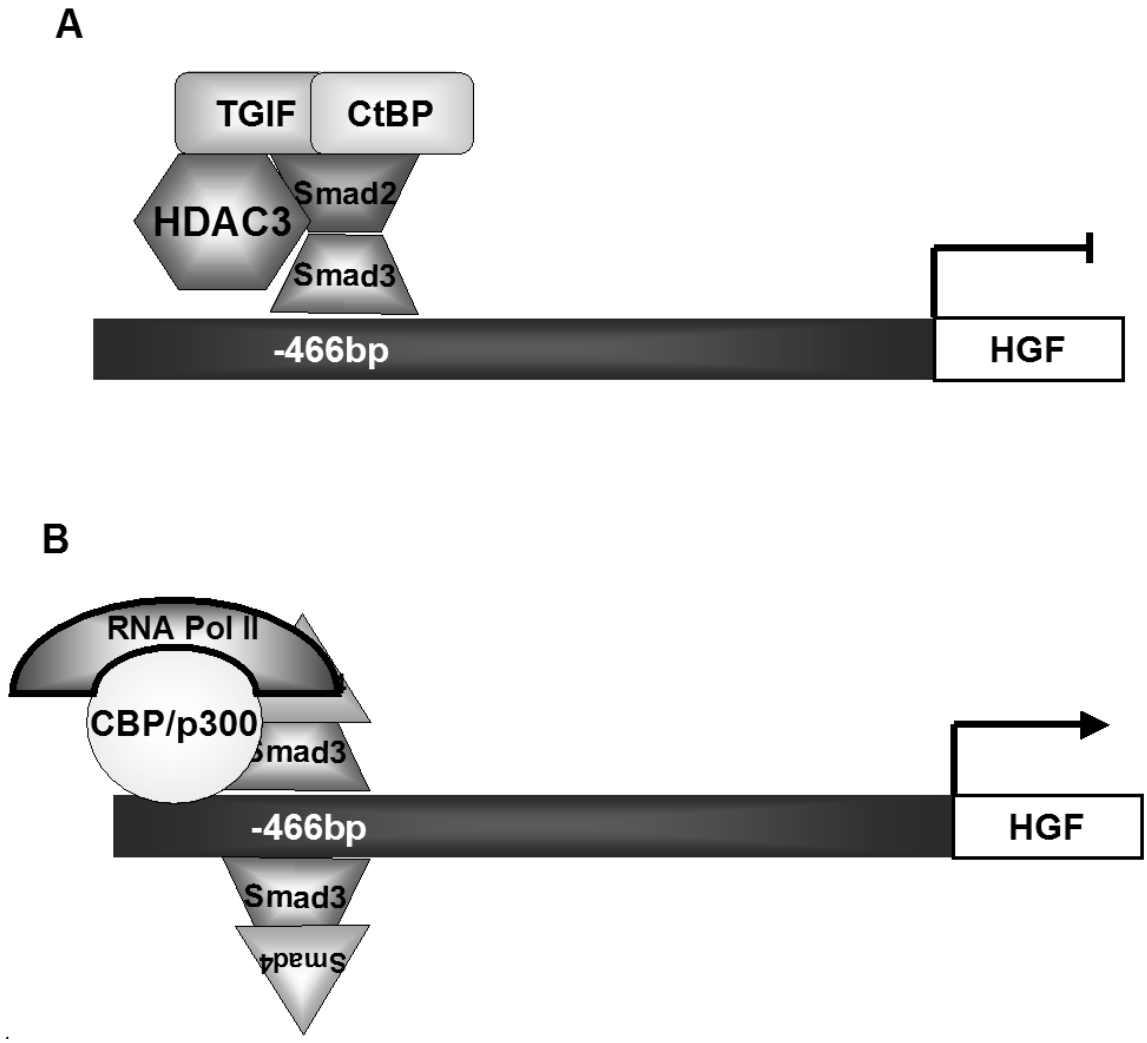

Figure 35. Schematic representation of Smad2-loss induction of HGF.

A: In the presence of Smad2, Smad-2, and -3 bind to the HGF promoter. Smad2 recruits transcriptional co-repressors TGIF, CtBP, and HDAC3 to the promoter, inhibiting HGF expression. B: When Smad2 is lost, Smad3 and Smad4 have increased binding to the HGF promoter and recruit transcriptional activators RNA Polymerase II and CBP/p300, inducing HGF expression. Therefore, when Smad2 is lost in skin SCCs, HGF expression increases.

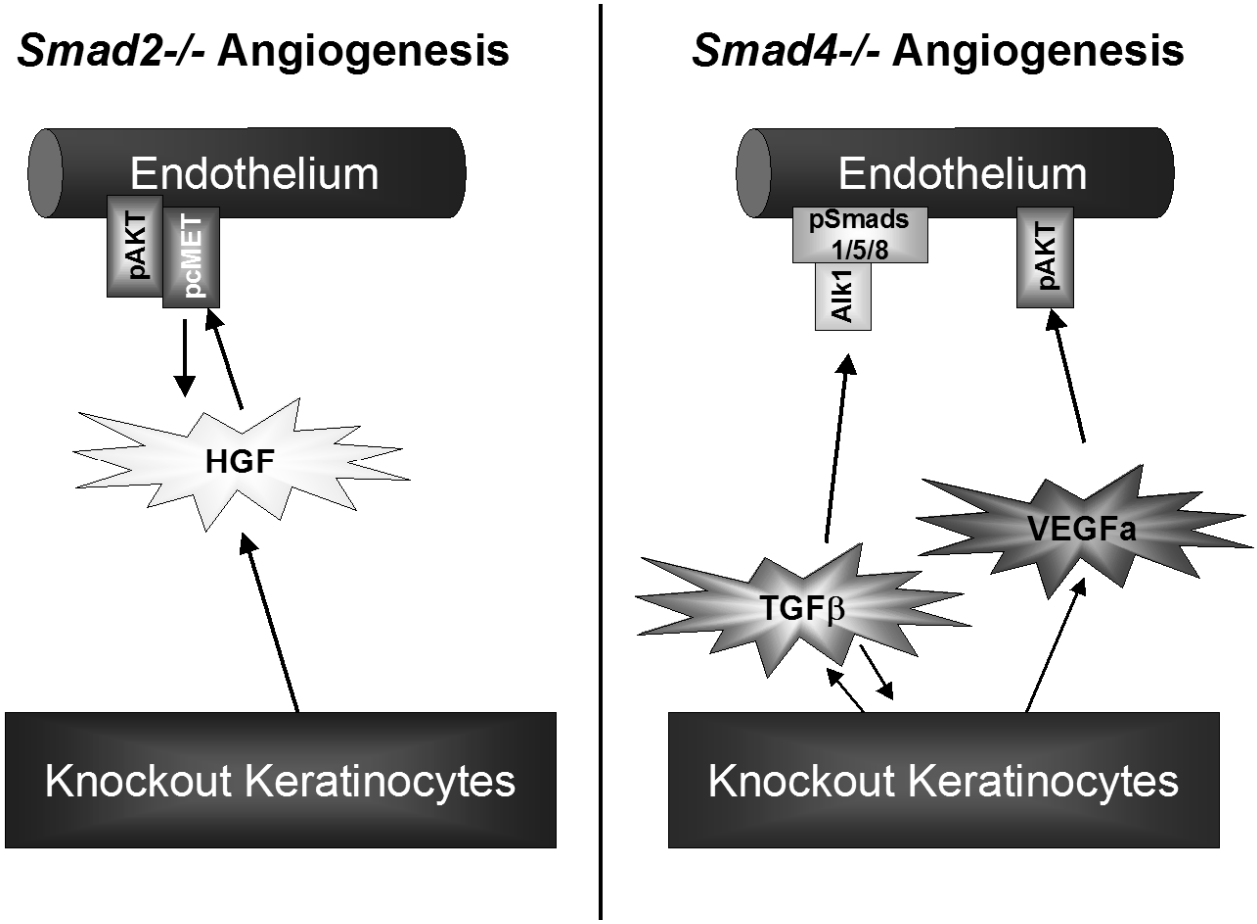

Figure 36. Schematic of Smad2- and Smad4-loss mediated angiogenesis.

Left: *Smad2-/-* keratinocytes produce HGF, which acts on its receptor, cMET on the underlying endothelia. Active, phosphorylated cMET then activates a downstream mediator of angiogenesis, Akt. Right: *Smad4-/-* keratinocytes produce TGFβ which acts on its pro-angiogenic endothelial receptor, Alk1, to activate receptor Smads, Smad-1, -5, and –8. In addition, *Smad4-/-* keratinocytes produce VEGFa, which activates a downstream mediator of angiogenesis, Akt.

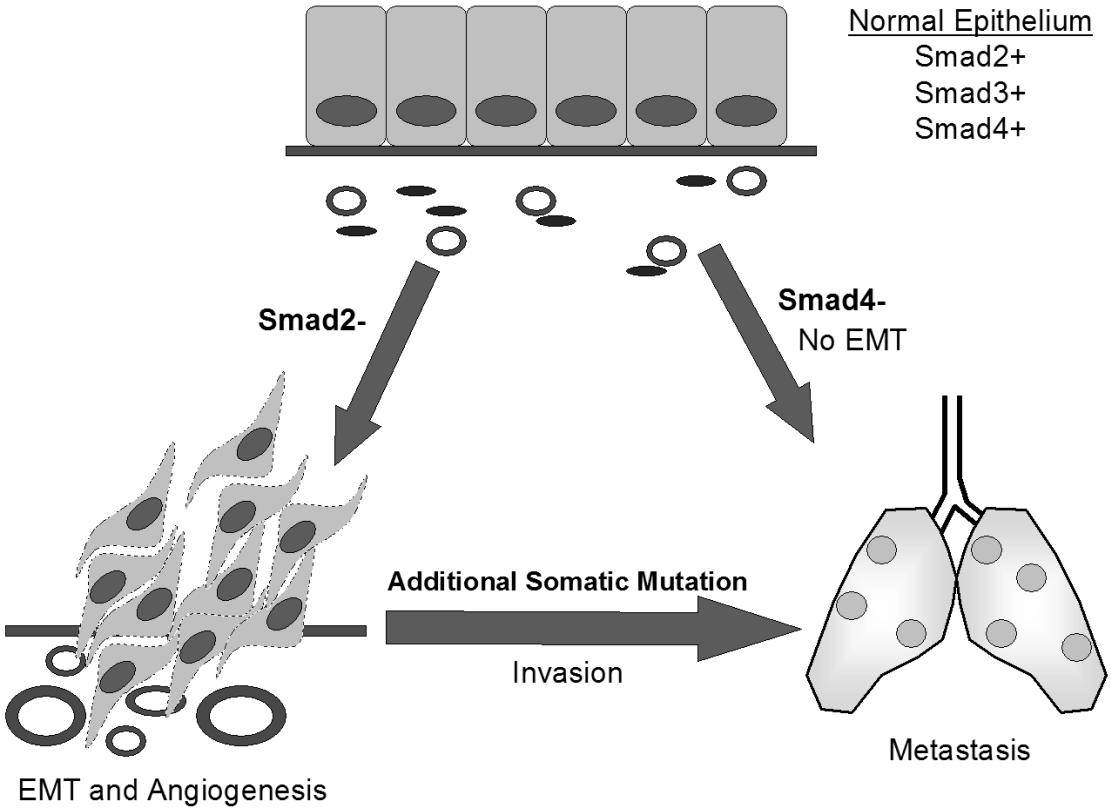

Figure 37. Role of Smads in skin squamous cell carcinoma progression.

Normal skin expresses Smad-2, -3, and –4 with E-cadherin (solid lines) maintaining apical-basal polarity. Underlying the basement membrane are sufficient vessels (red) and immune cells (purple) to support normal growth and differentiation of the epithelia. Loss of Smad2 (left) leads to loss of E-cadherin (dashed lines) and subsequent epithelial-to-mesenchymal transition (EMT). In addition, loss of Smad2 leads to increased angiogenesis in the underlying stroma (red). However, loss of Smad2 is insufficient to cause widespread invasion and metastasis. Subsequent somatic mutation allows matrix degradation and metastasis. Epithelial Smad4 loss (right) can progress directly to invasive, metastatic carcinoma, however the metastatic tumor will still maintain E-cadherin, having not undergone EMT.

REFERENCES

1. http://www.skincancer.org/squamous/index.php. 2008. Squamous Cell Carcinoma. Skin Cancer Foundation.
2. Tsai KY, Tsao H. 2004. The genetics of skin cancer. *Am J Med Genet C Semin Med Genet* 131C:82-92.
3. Hanahan D, Weinberg RA. 2000. The hallmarks of cancer. *Cell* 100:57-70.
4. Gatenby RA, Gillies RJ. 2008. A microenvironmental model of carcinogenesis. *Nat Rev Cancer* 8:56-61.
5. Athar M, Lloyd JR, Bickers DR, Mukhtar H. 1989. Malignant conversion of UV radiation and chemically induced mouse skin benign tumors by free-radical-generating compounds. *Carcinogenesis* 10:1841-1845.
6. Glick A, Ryscavvage A, Perez-Lorenzo R, Hennings H, Yuspa S, Darwiche N. 2007. The high-risk benign tumor: evidence from the two-stage skin cancer model and relevance for human cancer. *Mol Carcinog* 46:605-610.
7. Khavari TA, Rinn J. 2007. Ras/Erk MAPK signaling in epidermal homeostasis and neoplasia. *Cell Cycle* 6:2928-2931.
8. COSMIC. www.sanger.ac.uk/genetics/CGP/cosmic/.
9. Scholl FA, Dumesic PA, Barragan DI, Harada K, Bissonauth V, Charron J, Khavari PA. 2007. Mek1/2 MAPK kinases are essential for Mammalian development, homeostasis, and Raf-induced hyperplasia. *Dev Cell* 12:615-629.
10. Lazarov M, Green CL, Zhang JY, Kubo Y, Dajee M, Khavari PA. 2003. Escaping G1 restraints on neoplasia -- Cdk4 regulation by Ras and NF-kappa B. *Cell Cycle* 2:79-80.
11. Lazarov M, Kubo Y, Cai T, Dajee M, Tarutani M, Lin Q, Fang M, Tao S, Green CL, Khavari PA. 2002. CDK4 coexpression with Ras generates malignant human epidermal tumorigenesis. *Nat Med* 8:1105-1114.

12. Massagué J, Seoane J, Wotton D. 2005. Smad transcription factors. *Genes Dev* 19:2783-2810.

13. Massague J, Gomis RR. 2006. The Logic of TGFbeta Signaling. *FEBS Letters* 580:2811-2820.

14. Bierie B, Moses HL. 2006. TGF-beta and cancer. *Cytokine Growth Factor Rev* 17:29-40.

15. Izzi L, Attisano L. 2004. Regulation of the TGFbeta signalling pathway by ubiquitin-mediated degradation. *Oncogene* 23:2071-2078.

16. Goumans MJ, Lebrin F, Valdimarsdottir G. 2003. Controlling the angiogenic switch: a balance between two distinct TGF-b receptor signaling pathways. *Trends Cardiovasc Med* 13:301-307.

17. Wrana JL, Attisano L, Wieser R, Ventura F, Massague J. 1994. Mechanism of activation of the TGF-beta receptor. *Nature* 370:341-347.

18. Goumans MJ, Valdimarsdottir G, Itoh S, Rosendahl A, Sideras P, ten Dijke P. 2002. Balancing the activation state of the endothelium via two distinct TGF-beta type I receptors. *Embo J* 21:1743-1753.

19. Massague, J. 2000. How cells read TGF-beta signals. *Nat Rev Mol Cell Biol* 1:169-178.

20. Massague J, Blain SW, Lo RS. 2000. TGFbeta signaling in growth control, cancer, and heritable disorders. *Cell* 103:295-309.

21. Wahl, SM. 1994. Transforming growth factor beta: the good, the bad, and the ugly. *J Exp Med* 180:1587-1590.

22. Wahl, SM. 1992. Transforming growth factor beta (TGF-beta) in inflammation: a cause and a cure. *J Clin Immunol* 12:61-74.

23. Brown KA, Pietenpol JA, Moses HL. 2007. A Tale of Two Proteins: Differential Roles and Regulation of Smad2 and Smad3 in TGFβ Signaling. *J Cell Biochem* 101:9-33.

24. Nomura M, Li E. 1998. Smad2 role in mesoderm formation, left-right patterning and craniofacial development. *Nature* 393:786-790.

25. Yang X, Li C, Xu X, Deng C. 1998. The tumor suppressor SMAD4/DPC4 is essential for epiblast proliferation and mesoderm induction in mice. *Proc Natl Acad Sci U S A* 95:3667-3672.

26. Yang X, Letterio JJ, Lechleider RJ, Chen L, Hayman R, Gu H, Roberts AB, Deng C. 1999. Targeted disruption of SMAD3 results in impaired mucosal immunity and diminished T cell responsiveness to TGF-beta. *EMBO* 18:1280-1291.

27. Wotton D, Lo RS, Lee S, Massague J. 1999. A Smad transcriptional corepressor. *Cell* 97:29-39.

28. Yu J, Zhang L, Chen A, Xiang G, Wang Y, Wu J, Mitchelson K, Cheng J, Zhou Y. 2008. Identification of the Gene Transcription and Apoptosis Mediated by TGF-β-Smad2/3-Smad4 Signaling. *J Cell Physiol* 215:422-433.

29. Bierie B, Moses HL. 2006. TGFbeta: the molecular Jekyll and Hyde of cancer. *Nat Rev Cancer* 6:506-520.

30. Li AG, Lu SL, Han G, Kulesz-Martin M, Wang XJ. 2005. Current view of the role of transforming growth factor beta 1 in skin carcinogenesis. *J Investig Dermatol Symp Proc* 10:110-117.

31. Oft M, Akhurst RJ, Balmain A. 2002. Metastasis is driven by sequential elevation of H-ras and Smad2 levels. *Nat Cell Biol* 4:487-494.

32. Cho HJ, Baek KE, Saika S, Jeong MJ, Yoo J. 2007. Snail is require for transforming growth factor-beta-induced epithelial-mesenchymal transition by activating PI3 kinase/Akt signal pathway. *Biochem Biophys Res Commun* 353:337-343.

33. Ten Dijke P, Goumans MJ, Itoh F, Itoh S. 2002. Regulation of Cell Proliferation by Smad Proteins. *J Cell Physiol* 191:1-16.

34. Quan T, He T, Voorhees JJ, Fisher GJ. 2005. Ultraviolet irradiation induces Smad7 via induction of transcription factor AP-1 in human skin fibroblasts. *J Biol Chem* 280:8079-8085.

35. Han KH, Choi HR, Won CH, Chung JH, Cho KH, Eun HC, Kim KH. 2005. Alteration of the TGF-beta/SMAD pathway in intrinsically and UV-induced skin aging. *Mech Ageing Dev* 126:560-567.

36. He W, Cao T, Smith DA, Myers TE, Wang XJ. 2001. Smads mediate signaling of the TGFbeta superfamily in normal keratinocytes but are lost during skin chemical carcinogenesis. *Oncogene* 20:471-483.

37. Wan M, Cao X, Wu Y, Bai S, Wu L, Shi X, Wang N. 2002. Jab1 antagonizes TGF-beta signaling by inducing Smad4 degradation. *EMBO Rep* 3:171-176.

38. Tannehill-Gregg SH, Kusewitt DF, Rosol TJ, Weinstein M. 2004. The roles of Smad2 and Smad3 in the development of chemically induced skin tumors in mice. *Vet Pathol* 41:278-282.

39. Pittelkow MR, Coffey RJ Jr., Moses HJ. 1988. Keratinocytes produce and are regulated by transforming growth factors. *Ann N Y Acad Sci* 548:211-224.

40. Sellheyer K, Bickenbach JR, Rothnagel JA, Bundman D, Longley MA, Krieg T, Roche NS, Roberts AB, Roop DR. 1993. Inhibition of skin development by overexpression of transforming growth factor beta 1 in the epidermis of transgenic mice. *Proc Natl Acad Sci U S A* 90:5237-5241.

41. Wang XJ, Liefer KM, Tsai S, O'Malley BW, Roop DR. 1999. Development of gene-switch transgenic mice that inducibly express transforming growth factor beta1 in the epidermis. *Proc Natl Acad Sci U S A* 96:8483-8488.

42. Li AG, Wang D, Feng XH, Wang XJ. 2004. Latent TGFbeta1 overexpression in keratinocytes results in a severe psoriasis-like skin disorder. *EMBO* 23:1770-1781.

43. Liu X, Alexander V, Vijayachandra K, Bhogte E, Diamond I, Glick A. 2001. Conditional epidermal expression of TGFbeta 1 blocks neonatal lethality but causes a reversible hyperplasia and alopecia. *Proc Natl Acad Sci U S A* 98:9139-9144.

44. Cui W, Fowlis DJ, Cousins FM, Duffie E, Bryson S, Balmain A, Akhurst RJ. 1995. Concerted action of TGF-beta 1 and its type II receptor in control of epidermal homeostasis in transgenic mice. *Genes Dev* 9:945-955.

45. Fowlis DJ, Cui W, Johnson SA, Balmain A, Akhurst RJ. 1996. Altered epidermal cell growth control in vivo by inducible expression of transforming growth factor beta 1 in the skin of transgenic mice. *Cell Growth Differ* 7:679-687.

46. Cui W, Fowlis DJ, Bryson S, Duffie E, Ireland H, Balmain A, Akhurst RJ. 1996. TGFbeta1 inhibits the formation of benign skin tumors, but enhances progression to invasive spindle carcinomas in transgenic mice. *Cell* 86:531-546.

47. Weeks BH, He W, Olson KL, Wang XJ. 2001. Inducible expression of transforming growth factor beta1 in papillomas causes rapid metastasis. *Cancer Res* 61:7435-7443.

48. Zavadil J, Cermak L, Soto-Nieves N, Bottinger EP. 2004. Integration of TGF-beta/Smad and Jagged1/Notch signalling in epithelial-to-mesenchymal transition. *EMBO* 23:1155-1165.

49. Medici D, Hay ED, Goodenough DA. 2006. Cooperation between Snail and LEF-1 Transcription Factors Is Essential for TGF-beta1-induced Epithelial-Mesenchymal Transition. *Mol Biol Cell* 17:1871-1879.

50. Jungert K, Buck A, von Wichert G, Alder G, Konig A, Buchholz M, Gress TM, Ellenrieder V. 2007. Sp1 is Required for Transforming Growth Factor-beta-Induced Mesenchymal Transition and Migration in Pancreatic Cancer Cells. *Cancer Res* 67:1563-1570.

51. Jinnin M, Hironobu I, Yoshihide A, Kenichi Y, Trojanowska M, Tamaki K. 2004. Tenascin-C upregulation by transforming growth factor-beta in human dermal fibroblasts involves Smad3, Sp1, and Ets1. *Oncogene* 23:1656-1667.

52. Peinado H, Quintanilla M, Cano A. 2003. Transforming Growth Factor Beta-1 Induces Snail Transcription Factor in Epithelial Cell Lines. *J Biol Chem* 278:21113-21123.

53. Phanish MK, Wahab NA, Colville-Nash P, Hendry BM, Dockrell MEC. 2006. The differenital role of Smad2 and Smad3 in the regulation of profibrotic TFGbeta1 responses in human proximal-tubule epithelial cells. *Biochem J* 393:601-607.

54. Valcourt U, Kowanetz M, Niimi H, Heldin CH, Moustakas A. 2005. TGF-beta and the Smad Signaling Pathway Support Transcriptomic Reprogramming during Epithelial-Mesenchymal Cell Transition. *Mol Biol Cell* 16:1987-2002.

55. Thuault S, Valcourt U, Petersen M, Manfioletti G, Heldin CH, Moustakas A. 2006. Transforming growth factor-beta employs HMGA2 to elicit epithelial-mesenchymal transition. *J Cell Biol* 174:175-183.

56. Han G, Lu SL, Li AG, He W, Corless CL, Kulesz-Martin M, Wang XJ. 2005. Distinct mechanisms of TGF-beta1-mediated epithelial-to-mesenchymal transition and metastasis during skin carcinogenesis. *J Clin Invest* 115:1714-1723.

57. Vicari AP, Caux C. 2002. Chemokines in cancer. *Cytokine Growth Factor Rev* 13:143-154.

58. Coussens LM, Werb Z. 2002. Inflammation and cancer. *Nature* 420:860-867.

59. Nickoloff, BJ. 2004. The skin cancer paradox of psoriasis: a matter of life and death decisions in the epidermis. *Arch Dermatol* 140:873-875.

60. Daniel D, Meyer-Morse N, Bergsland EK, Dehne K, Coussens LM, Hanahan D. 2003. Immune enhancement of skin carcinogenesis by CD4+ T cells. *J Exp Med* 197:1017-1028.

61. Li AG, Lu SL, Zhang MX, Deng C, Wang XJ. 2004. Smad3 knockout mice exhibit a resistance to skin chemical carcinogenesis. *Cancer Res* 64:7836-7845.

62. Ferrera, N. 2002. VEGF and the quest for tumour angiogenesis factors. *Nat Rev Cancer* 2:795-803.

63. Lebrin F, Deckers M, Bertolino P, Ten Dijke P. 2005. TGF-beta receptor function in the endothelium. *Cardiovasc Res* 65:599-608.

64. Bussolino F, DiRenzo MF, Ziche M, Bocchietto E, Olivero M, Naldini L, Gaudino G, Tamagnone L, Coffer A, Comoglio PM. 1992. Hepatocyte Growth Factor Is a Potent Angiogenic Factor Which Stimulates Endothelial Cell Motility and Growth. *J Cell Biol* 119:629-641.

65. Takahashi H, Shibuya M. 2005. The vascular endothelial growth factor (VEGF)/VEGF receptor system and its role under physiological and pathological conditions. *Clin Sci (Lond)* 109:227-241.

66. Sánchez-Elsner T, Botella LM, Velasco B, Corbí A, Attisano L, Bernabéu C. 2001. Synergistic cooperation between hypoxia and transforming growth factor-beta pathways on human vascular endothelial growth factor gene expression. *J Biol Chem* 276:38527-38535.

67. Chu SH, Ma YB, Zhang H, Feng DF, Zhu ZA, Li ZQ, Yuan XH. 2007. Hepatocyte growth factor production is stimulated by gangliosides and TGF-beta isoforms in human glioma cells. *J Neurooncol* 85:33-38.

68. Lewis MP, Lygoe KA, Nystrom ML, Anderson WP, Speight PM, Marshall JF, Thomas GJ. 2004. Tumour-derived TGF-beta1 modulates myofibroblast differentiation and promotes HGF/SF-dependent invasion of squamous carcinoma cells. *Br J Cancer* 90:822-832.

69. Bhowmick NA, Chytil A, Plieth D, Gorska AE, Dumont N, Shappell S, Washington MK, Neilson EG, Moses HL. 2004. TGF-beta signaling in fibroblasts modulates the oncogenic potential of adjacent epithelia. *Science* 303:848-851.

70. Sakurai H, Nigam SK. 1997. Transforming growth factor-beta selectively inhibits branching morphogenesis but not tubulogenesis. *Am J Physiol* 272:F139-146.

71. Sjoblom T, Jones S, Wood LD, Parsons DW, Lin J, Barber TD, Mandelker D, Leary RJ, Ptak J, Silliman N, Szabo S, Buckhaults P, Farrell C, Meeh P, Markowitz SD, Willis J, Dawson D, Willson JK, Gazdar AF, Hartigan J, Wu L, Liu C, Parmigiani G, Park BH, Bachman KE, Papadopoulos N, Vogelstein B, Kinzler KW, Velculescu VE. 2006. The consensus coding sequences of human breast and colorectal cancers. *Science* 314:268-274.

72. Zhu Y, Richardson JA, Parada LF, Graff JM. 1998. Smad3 mutant mice develop metastatic colorectal cancer. *Cell* 94:703-714.

73. Datto MB, Frederick JP, Pan L, Corton AJ, Zhuang Y, Wang XF. 1999. Targeted disruption of Smad3 reveals an essential role in transforming growth factor-beta mediated signal transduction. *Mol Cell Biol* 19:2495-2504.

74. Yang X, Chen L, Xu X, Li C, Huang C, Deng CX. 2001. TGF-beta/Smad3 signals repress chondrocyte hypertrophic differentiation and are required for maintaining articular cartilage. *J Cell Biol* 153:35-46.

75. Vijayachandra K, Lee J, Glick AB. 2003. Smad3 Regulates Senescence and Malignant Conversion in a Mouse Multistage Skin Carcinogenesis Model. *Cancer Res* 63:3447-3452.

76. Bierie, B., and Moses, H. L. 2006. TGF-beta and cancer. *Cytokine Growth Factor Rev* 17:29-40.

77. Qiao W, Li AG, Owens P, Xu X, Wang XJ, Deng CX. 2006. Hair follicle defects and squamous cell carcinoma formation in Smad4 conditional knockout mouse skin. *Oncogene* 25:207-217.

78. Yang L, Mao C, Teng Y, Li W, Zhang J, Cheng X, Li X, Han X, Xia Z, Deng H, Yang X. 2005. Targeted Disruption of Smad4 in Mouse Epidermis Results in Failure of Hair Follicle Cycling and Formation of Skin Tumors. *Cancer Res* 65:8671-8678.

79. He W, Li AG, Wang D, Han S, Zheng B, Goumans MJ, ten Dijke P, Wang XJ. 2002. Overexpression of Smad7 results in severe pathological alterations in multiple epithelial tissues. *EMBO* 21:2580-2590.

80. Liu X, Lee J, Cooley M, Bhogte E, Hartley S, Glick A. 2003. Smad7 but not Smad6 cooperates with oncogenic ras to cause malignant conversion in a mouse model for squamous cell carcinoma. *Cancer Res* 63:7760-7768.

81. Han G, Li AG, Liang, YY, Owens P, He W, Lu S, Yoshimatsu Y, Wang D, Ten Dijke P, Lin X, Wang XJ. 2006. Smad7-induced beta-catenin degradation alters epidermal appendage development. *Dev Cell* 11:301-312.

82. Niemann C, Owens DM, Hulsken J, Birchmeier W, Watt FM. 2002. Expression of DeltaNLef1 in mouse epidermis results in differentiation of hair follicles into squamous epidermal cysts and formation of skin tumours. *Development* 129:95-109.

83. Gat U, DasGupta R, Degenstein L, Fuchs E. 1998. De Novo hair follicle morphogenesis and hair tumors in mice expressing a truncated beta-catenin in skin. *Cell* 95:605-614.

84. Aldaz CM, Conti CJ, Klein-Szanto AJ, Slaga TJ. 1987. Progressive dysplasia and aneuploidy are hallmarks of mouse skin papillomas: relevance to malignancy. *Proc Natl Acad Sci U S A* 84:2029-2032.

85. Zhou Z, Wang D, Wang XJ, Roop DR. 2002. In utero activation of K5.CrePR1 induces gene deletion. *Genesis* 32:191-192.

86. Yang X, Li C, Herrera PL, Deng CX. 2002. Generation of Smad4/Dpc4 conditional knockout mice. *Genesis* 32:80-81.

87. Ju W, Ogawa A, Heyer J, Nierhof D, Yu L, Kucherlapati K, Shafritz DA, Bottinger EP. 2006. Deletion of Smad2 in Mouse Liver Reveals Novel Functions in Hepatocyte Growth and Differentiation. *Mol Cell Biol* 26:654-667.

88. Caulin C, Nguyen T, Longley MA, Zhou Z, Wang XJ, Roop DR. 2004. Inducible activation of oncogenic K-ras results in tumor formation in the oral cavity. *Cancer Res* 64:5054-5058.

89. Rugg EL, Leigh IM. 2004. The keratins and their disorders. *Am J Med Genet C Semin Med Genet* 131C:4-11.

90. Huber MA, Kraut N, Beug H. 2005. Molecular requirements for epithelial-mesenchymal transition during tumor progression. *Curr Opin Cell Biol* 17:548-558.

91. Hendrix MJ, Seftor EA, Seftor RE, Trevor KT. 1997. Experimental co-expression of vimentin and keratin intermediate filaments in human breast cancer cells results in phenotypic interconversion and increased invasive behavior. *Am J Pathol* 150:483-495.

92. Masszi A, Di Ciano C, Sirokmány G, Arthur WT, Rotstein OD, Wang J, McCulloch CA, Rosivall L, Mucsi I, Kapus A. 2003. Central role for Rho in TGF-beta1-induced alpha-smooth muscle actin expression during epithelial-mesenchymal transition. *Am J Physiol Renal Physiol* 248:F911-924.

93. Zavadil J, Bottinger EP. 2005. TGFbeta and epithelial-to-mesenchymal transitions. *Oncogene* 24:5764-6774.

94. Lüttges J, Galehdari H, Bröcker V, Schwarte-Waldhoff I, Henne-Bruns D, Klöppel G, Schmiegel W, Hahn SA. 2001. Allelic loss is often the first hit in the biallelic inactivation of the p53 and DPC4 genes during pancreatic carcinogenesis. *Am J Pathol* 158:1677-1683.

95. Kavsak P, Rasmussen RK, Causing CG, Bonni S, Zhu H, Thomsen GH, Wrana JL. 2000. Smad7 binds to Smurf2 to form an E3 ubiquitin ligase that targets the TGF beta receptor for degradation. *Mol Cell* 6:1365-1375.

96. Lin X, Liang M, Feng XH. 2000. Smurf2 is a ubiquitin E3 ligase mediating proteasome-dependent degradation of Smad2 in transforming growth factor-beta signaling. *J Biol Chem* 275:36818-36822.

97. Wan M, Tang Y, Tytler EM, Lu C, Jin B, Vickers SM, Yang L, Shi X, Cao X. 2004. Smad4 protein stability is regulated by ubiquitin ligase SCF beta-TrCP1. *J Biol Chem* 279:14484-14487.

98. Liang M, Liang YY, Wrighton K, Ungermannova D, Wang XP, Brunicardi FC, Liu X, Feng XH, Lin X. 2004. Ubiquitination and proteolysis of cancer-derived Smad4 mutants by SCFSkp2. *Mol Cell Biol* 24:7524-7537.

99. Dlugosz A, Merlino G, Yuspa SH. 2002. Progress in cutaneous cancer research. *J Investig Dermatol Symp Proc* 7:17-26.

100. Xie W, Bharathy S, Kim D, Haffty BG, Rimm DL, Reiss M. 2003. Frequent alterations of Smad signaling in human head and neck squamous cell carcinomas: a tissue microarray analysis. *Oncol Res* 14:61-73.

101. Corominas M, Sloan SR, Leon J, Kamino H, Newcomb EW, Pellicer A. 1991. ras activation in human tumors and in animal model systems. *Environ Health Perspect* 93:19-25.

102. Lu SL, Herrington H, Reh D, Weber S, Bornstein S, Wang D, Li AG, Tang CF, Siddiqui Y, Nord J, Andersen P, Corless CL, Wang XJ. 2006. Loss of transforming growth factor b type II receptor promotes metastatic head-and-neck squamous cell carcinoma. *Genes Dev* 20:1331-1342.

103. Bardeesy N., Cheng K.H., Berger J.H., Chu G.C., Pahler J., Olson P., Hezel A.F., Horner J., Lauwers G.Y., Hanahan D., DePinho R.A. 2006. Smad4 is dispensable for normal pancreas development yet critical in progression and tumor biology of pancreas cancer. *Genes Dev* 20:3130-3146.

104. Dong R, Wang Q, He XL, Chu YK, Lu JG, Ma QJ. 2007. Role of nuclear factor kappa B and reactive oxygen species in the tumor necrosis factor-alpha-induced epithelial-mesenchymal transition of MCF-7 cells. *Braz J Med Biol Res* 40:1071-1078.

105. Lester RD, Jo M, Montel V, Takimoto S, Gonias SL. 2007. uPAR induces epithelial-mesenchymal transition in hypoxic breast cancer cells. *J Cell Biol* 178:425-436.

106. Zha Y, He J, Mei Y, Yin T, Mao L. 2007. Zinc-finger transcription factor Snail accelerates survival, migration, and expression of matrix metalloproteinase-2 in human bone mesenchymal stem cells. *Cell Biol Int* 31:1089-1096.

107. Peinado H, Olmeda D, Cano A. 2007. Snail, ZEB, and bHLH factors in tumor progression: an alliance against the epithelial phenotype? *Nat Rev Cancer* 7:415-428.

108. Papadavid E, Pignatelli M, Zakynthinos S, Krausz T, Chu AC. 2002. Abnormal immunoreactivity of the E-cadherin/catenin (a-, b-, and g-) complex in premalignant and malignant non-melanocytic skin tumours. *J Pathol* 196:154-162.

109. Wu WS, Heinrichs S, Xu D, Garrison SP, Zambetti GP, Adams JM, Look AT. 2005. Slug antagonizes p53-mediated apoptosis of hematopoietic progenitors by repressing *puma*. *Cell* 123:641-653.

110. Craene BD, vanRoy F, Berx G. 2005. Unraveling signalling cascades for the Snail family of transcription factors. *Cell Signal* 17:535-547.

111. Jamora C, Lee P, Kocieniewski P, Azhar M, Hosokawa R, Chai Y, Fuchs E. 2005. A signaling pathway involving TGF-beta2 and snail in hair follicle morphogenesis. *PLoS Biol* 3:e11.

112. Ballard VL, Sharma A, Duignan I, Holm JM, Chin A, Choi R, Hajjar KA, Wong SC, Edelberg JM. 2006. Vascular tenascin-C regulates cardiac endothelial phenotype and neovascularization. *FASEB J* 20:717-719.

113. Teng Y, Sun AN, Pan XC, Yang G, Yang LL, Wang MR, Yang X. 2006. Synergistic function of Smad4 and PTEN in suppressing forestomach squamous cell carcinoma in the mouse. *Cancer Res* 66:6972-6981.

114. Wang XJ, Greenhalgh DA, Lu XR, Bickenbach JR, Roop DR. 1995. TGF alpha and v-fos cooperation in transgenic mouse epidermis induces aberrant keratinocyte differentiation and stable, autonomous papillomas. *Oncogene* 10:279-289.

115. Hoot KE, Lighthall J, Han G, Lu SL, Li AG, Ju W, Kulesz-Martin M, Bottinger E, Wang XJ. 2008. Keratinocyte-Specific Smad2 ablation results in increased epithelial-mesenchymal transition during skin cancer formation and progression. *J Clin Invest* In Press.

116. Sengupta S, Gherardi E, Sellers LA, Wood JM, Sasisekharan R, Fan TD. 2003. Hepatocyte Growth Factor/Scatter Factor Can Induce Angiogenesis Independently of Vascular Endothelial Growth Factor. *Arterioscler Thromb Vasc Biol* 23:69-75.

117. Ahmad S, Hewett PW, Wang P, Al-Ani B, Cudmore M, Fujisawa T, Haigh JJ, le Noble F, Wang L, Mukhopadhyay D, Ahmed A. 2006. Direct evidence for endothelial vascular endothelial growth factor receptor-1 function in nitric oxide-mediated angiogenesis. *Circ Res* 99:715-722.

118. Sengupta S, Sellers LA, Gherardi E, Sasisekharan R, Fan TP. 2004. Nitric oxide modulates hepatocyte growth factor/scatter factor-induced angiogenesis. *Angiogenesis* 7:285-294.

119. Jeon SH, Chae BC, Kim HA, Seo GY, Seo DW, Chun GT, Kim NS, Yie SW, Byeon WH, Eom SH, Ha KS, Kim YM, Kim PH. 2007. Mechanisms underlying TGF-beta1-induced expression of VEGF and Flk-1 in mouse macrophages and their implications for angiogenesis. *J Leukoc Biol* 81:557-566.

120. Nakagawa T, Lan HY, Zhu HJ, Kang DH, Schreiner GF, Johnson RJ. 2004. Differential regulation of VEGF by TGF-beta and hypoxia in rat proximal tubular cells. *Am J Physiol Renal Physiol* 287:F658-664.

121. Plaschke-Schlütter A, Behrens J, Gherardi E, Birchmeier W. 1995. Characterization of the scatter factor/hepatocyte growth factor gene promoter. Positive and negative regulatory elements direct gene expression to mesenchymal cells. *J Biol Chem* 270:830-836.

122. Liu Y, Michalopoulos GK, Zarnegar R. 1994. Structural and functional characterization of the mouse hepatocyte growth factor gene promoter. *J Biol Chem* 269:4152-4160.

123. Gherardi E, Gray J, Stoker M, Perryman M, Furlong R. 1989. Purification of scatter factor, a fibroblast-derived basic protein that modulates epithelial interactions and movement. *Proc Natl Acad Sci U S A* 86:5844-5848.

124. Nakamura T, Teramoto H, Ichihara A. 1986. Purification and characterization of a growth factor from rat platelets for mature parenchymal hepatocytes in primary cultures. *Proc Natl Acad Sci U S A* 83:6489-6493.

125. Benvenuti S, Comoglio PM. 2007. The MET receptor tyrosine kinase in invasion and metastasis. *J Cell Physiol* 213:316-325.

126. Qiu W, Schönleben F, Li X, Su GH. 2007. Disruption of transforming growth factor beta-Smad signaling pathway in head and neck squamous cell carcinoma as evidenced by mutations of SMAD2 and SMAD4. *Cancer Lett* 245:163-170.

127. Lu SL, Reh D, Li AG, Woods J, Corless CL, Kulesz-Martin M, Wang XJ. 2004. Overexpression of transforming growth factor beta1 in head and neck epithelia results in inflammation, angiogenesis, and epithelial hyperproliferation. *Cancer Res* 64:4405-4410.

128. Di Renzo MF, Olivero M, Martone T, Maffe A, Maggiora P, Stefani AD, Valente G, Giordano S, Cortesina G, Comoglio PM. 2000. Somatic mutations of the MET oncogene are selected during metastatic spread of human HNSC carcinomas. *Oncogene* 19:1547-1555.

129. Galeazzi E, Olivero M, Gervasio FC, De Stefani A, Valente G, Comoglio PM, Di Renzo MF, Cortesina G. 1997. Detection of MET oncogene/hepatocyte growth factor receptor in lymph node metastases from head and neck squamous cell carcinomas. *Eur Arch Otorhinolaryngol* 254:S138-143.

130. Sawatsubashi M, Sasatomi E, Mizokami H, Tokunaga O, Shin T. 1998. Expression of c-Met in laryngeal carcinoma. *Virchows Arch* 432:331-335.

131. Morello S, Olivero M, Aimetti M, Bernardi M, Berrone S, Di Renzo MF, Giordano S. 2001. MET receptor is overexpressed but not mutated in oral squamous cell carcinomas. *J Cell Physiol* 189:285-290.

132. Kretzschmar M, Doody J, Timokhina I, Massagué J. 1999. A mechanism of repression of TGFbeta/Smad signaling by oncogenic Ras. *Genes Dev* 13:804-816.

133. Lehmann K, Janda E, Pierreux CE, Rytömaa M, Schulze A, McMahon M, Hill CS, Beug H, Downward J. 2000. Raf induces TGFbeta production while blocking its apoptotic but not invasive responses: a mechanism leading to increased malignancy in epithelial cells. *Genes Dev* 14:2610-2622.

134. Hu H, Milstein M, Bliss JM, Thai M, Malhotra G, Huynh LC, Colicelli J. 2008. Integration of transforming growth factor beta and RAS signaling silences a RAB5 guanine nucleotide exchange factor and enhances growth factor-directed cell migration. *Mol Cell Biol* 28:1573-1583.

135. Murray SA, Carver EA, Gridley T. 2006. Generation of a Snail1 (Snai1) conditional null allele. *Genesis* 44:7-11.

APPENDIX I:

Reagent Information

Table 6. Immunohistochemistry and Immunofluorescence antibody information.

*Concentration refers to paraffin IHC, unless otherwise noted

Antibody	Host	Vendor	Catalog #	Primary Concentration*
Alk1	Goat	R&D Systems	AF770	1:100
aSMA	Mouse	Sigma	A2547	1:400
B220	Rat	eBioscience	14-0452	1:320 (IF), 1:160 (IHC)
CD11c	Hamster	BD Pharmingen	550283	1:20
CD19	Mouse	eBioscience	14-0191	1:80
CD3	Hamster	BD Pharmingen	550275	1:160; 1:20 (Frozen)
CD31	Rat	BD Biosciences	553370	1:100 (Frozen)
CD4	Rat	eBioscience	14-0041	1:160; 1:20 (Frozen)
CD45	Rat	BD Pharmingen	550539	1:160
CD8a	Rat	eBioscience	14-0081	1:160
COX2	Rabbit	Cell Signaling	4842	1:100
ECadherin	Mouse	BD Bioscience	610182	1:100
Endoglin / CD105	Rat	BD Pharmingen	550546	1:50
eNOS	Mouse	Abcam	ab49533-100	1:50
F4/80	Rat	Invitrogen (Caltag)	MF48000	1:40; 1:160 (Frozen)
Foxp3	Mouse	eBioscience	14-7979-82	1:400; 1:100(Frozen IF); 1:200 (Frozen IHC)
Gamma delta T cell	Hamster	eBioscience	14-5811	1:100
Gr-1 or Ly6G	Rat	eBioscience	14-5931	1:40, 1:20 (Frozen)
HGF		R&D Systems	AF2207	1:10
HMGA2	Rabbit	Santa Cruz Biotechnologies	sc-30223X	1:2000
IL-17 (biotinylated)	Rat	BD Pharmingen	555067	1:200
Keratin 13	Mouse	Chemicon	CBL176	1:100
Keratin 14	Giunea Pig	Fitzgerald	20R-CP002	1:400
Keratin 8/18	Giunea Pig	Fitzgerald	20R-CP004	1:100
Loricrin	Rabbit	Covance	PRB-145P	1:400
LYVE-1	Rabbit	BD Bioscience	no longer carried	1:800 (Frozen)
MHCII-Iad	Rat	Fitzgerald	PDI-MMHC2-2G9	1:40
pAkt	Rabbit	Cell Signaling	4051S	1:100

p-cMET	Rabbit	Cell Signaling	3121	1:50
Pericentrin	Rabbit	Covance	PRB-432C	1:150
phospho Smad2	Rabbit	Cell Signaling	3104	1:100
phospho Smad2/Smad3	Goat	Santa Cruz Biotechnologies	sc-11769	1:100
pSmad1/5/8	Rabbit	Cell Signaling	9511S	1:50
Smad2	Rabbit	Invitrogen (Zymed)	51-1300	1:200
Smad4	Mouse	Santa Cruz Biotechnologies	sc-7966	1:200
Snail	Rabbit	Abcam	17732	1:200
Tenascin C	Mouse	Sigma	MTn-12	1:200
TGFB1	Chicken	R&D Systems	AB-101-NA	1:500
TGFB1 LAP	Goat	Santa Cruz Biotechnologies	sc-34830	1:200
TGFBRI	Rabbit	Santa Cruz Biotechnologies	sc-398	1:100
TGFbRII	Rabbit	Santa Cruz Biotechnologies	sc-400	1:100
total Smad3	Rabbit	Santa Cruz Biotechnologies	sc-8332	1:100
TSP1	Mouse	Lab Vision/Neomarkers	MS-418	1:200
Twist	Rabbit	Santa Cruz Biotechnologies	sc-15393	1:100
VEGF	Mouse	Zymed	18-7328	1:100
Vimentin	Chicken	Sigma	V2258	1:500

Table 7. ChIP Antibody Information.

Antibody	Host	Vendor	Catalog #
CBP/p300	Mouse	Upstate	05-257
CtBP	Rabbit	Gift from Qinghong Zhang	
HDAC1	Mouse	Upstate	05-614
HDAC2	Mouse	Abcam	ab51832-100
HDAC3	Rabbit	Abcam	ab7030-50
HMGA2	Rabbit	Santa Cruz Biotechnologies	sc-30223X
IgG	Rabbit	Santa Cruz Biotechnologies	sc-2027
IgG	Mouse	Santa Cruz Biotechnologies	sc-2025
RNA Pol II	Mouse	Upstate	05-623B
Smad1	Rabbit	Upstate	06-702
Smad2	Rabbit	Zymed	51-1300
Smad3	Rabbit	Upstate	06-920
Smad4	Rabbit	Upstate	06-693
Smad5	Rabbit	Zymed	51-3700
TGIF	Mouse	Santa Cruz Biotechnologies	sc-17800X

Table 8. Western Blot Antibody Information.

Antibody	Host	Vendor	Catalog #	Primary Concentration
Actin	Mouse	Santa Cruz Biotechnologies	sc-8432	1:2500
Akt	Rabbit	Cell Signaling	9272	1:500
Erk1/2	Rabbit	Cell Signaling	9102	1:500
GAPDH	Rabbit	Santa Cruz Biotechnologies	sc-25778	1:5000
JNK	Rabbit	Cell Signaling	9252	1:250
p38	Rabbit	Cell Signaling	9212	1:500
p-Akt	Rabbit	Cell Signaling	4051S	1:500
pERK1/2	Rabbit	Cell Signaling	9101S	1:250
p-JNK	Rabbit	Sigma	9251S	1:100
p-p38	Rabbit	Cell Signaling	9211S	1:250
Smad2	Rabbit	Invitrogen (Zymed)	51-1300	1:1000
Smad3	Rabbit	Santa Cruz Biotechnologies	FL-425	1:1000
Smad4	Mouse	Santa Cruz Biotechnologies	B8	1:1000
Snail	Rabbit	Abcam	ab17732-100	1:1000
Tubulin	Mouse	Sigma	T5168	1:3000

Table 9. qRT-PCR Probe Information.

Probe Target	Species	Filter	Vendor	Catalog # or Sequence
aSMA	Mouse	FAM	Applied Biosystems	Mm00725412_s1
B2M	Mouse	FAM	Applied Biosystems	Mm00437762_m1
Cdk4	Mouse	FAM	Applied Biosystems	Mm00726334_s1
cMet	Mouse	FAM	Applied Biosystems	Mm00434924_m1
cMet	Human	FAM	Applied Biosystems	Hs00179845_m1
Col1a1	Mouse	FAM	Applied Biosystems	Mm00801666_g1
Cox2	Mouse	FAM	Applied Biosystems	Mm00478374_m1
cyclinA1	Mouse	FAM	Applied Biosystems	Mm00432337_m1
cyclinB3	Mouse	FAM	Applied Biosystems	Mm00805476_m1
Dab1	Mouse	FAM	Applied Biosystems	Mm00438366_m1
Ecad	Mouse	FAM	Applied Biosystems	Mm00486906_m1
Ecad	Human	FAM	Applied Biosystems	Hs00170423_m1
Endoglin	Mouse	FAM	Applied Biosystems	Mm00468256_m1
eNOS	Mouse	FAM	Applied Biosystems	Mm00435204_m1
Flk1	Mouse	FAM	Applied Biosystems	Mm00440099_m1
Flt1	Mouse	FAM	Applied Biosystems	Mm00438980_m1
Flt3	Mouse	FAM	Applied Biosystems	Mm00438996_m1
Flt4	Mouse	FAM	Applied Biosystems	Mm00433337_m1
GAPDH	Mouse	VIC	Applied Biosystems	4352339E
GAPDH	Human	VIC	Applied Biosystems	4326317E
Hey1	Mouse	FAM	Applied Biosystems	Mm00468865_m1
HGF	Mouse	FAM	Applied Biosystems	Mm01135185_m1
HGF	Mouse	None	Custom	1F-GAACTGCAAGCATGATGTGG 1R-GATGCTGGAAATAGGGCAGA
HGF	Mouse	None	Custom	2F- AGGAACAGGGGCTTTACGTT 2R- TCCGAGCCTTCCATACTCAC
HGF	Mouse	None	Custom	3F- CACACACCACCCTTCACTGT 3R-GTCAAATTCATGGCCAAACC
HGF	Human	FAM	Applied Biosystems	Hs00300159_m1
HGF	Human	None	Custom	1F- AAAGGACTTCCATTCACTTGC 1R-CGCTCTCCCTTACTCAAGCTA
HGF	Human	None	Custom	2F- CTGGTTCCCCTTCAATAGCA 2R- AAAGACCACTCTGGCAGGAA
Hif1a	Mouse	FAM	Applied Biosystems	Mm00468869_m1
Id2	Mouse	FAM	Applied Biosystems	Mm00711781_m1
Jag1	Mouse	FAM	Applied Biosystems	Mm00496902_m1
K14	Mouse	FAM	Applied Biosystems	Mm00516876_m1
KGF	Mouse	FAM	Applied Biosystems	Mm00433291_m1
Krt2-8	Mouse	FAM	Applied Biosystems	Mm00835759_m1
Krt2-8	Human	FAM	Applied Biosystems	Hs02339474_g1
Mapk1	Mouse	FAM	Applied Biosystems	Mm00442479_m1
p63	Mouse	FAM	Applied Biosystems	Mm00495788_m1

Rad51	Mouse	FAM	Applied Biosystems	Mm00485509_m1
sFlt1	Mouse	FAM	Custom through Applied biosystems	F-GAATTCCGCGCTCACCATGGTCAGC R-CAACAAACACAGAGAAGG
Slug	Mouse	FAM	Applied Biosystems	Mm00441531_m1
Slug	Human	FAM	Applied Biosystems	Hs00161904_m1
Slug	Human	FAM	Applied Biosystems	Hs00950344_m1
Smad2	Mouse	FAM	Applied Biosystems	Mm00487530_m1
Smad2	Human	FAM	Applied Biosystems	Hs00183425_m1
Smad3	Human	FAM	Applied Biosystems	Hs00232219_m1
Smad4	Mouse	FAM	Applied Biosystems	Mm00484724_m1
Smad4	Human	FAM	Applied Biosystems	Hs00232068_m1
Snail	Mouse	FAM	Applied Biosystems	Mm01249564_g1
Snail	Mouse		Custom	1F- AGCCCAACTATAGCGAGCTG 1R- GCCTTCGAGTCTTCAACTCC
Snail	Human	FAM	Applied Biosystems	Hs00195591_m1
Snail3	Mouse	FAM	Applied Biosystems	Mm00502016_m1
Snail3	Human	FAM	Applied Biosystems	Hs01018996_m1
TAp63	Mouse	FAM	Applied Biosystems	Mm00570095_m1
TenC	Mouse	FAM	Applied Biosystems	Mm00495681_m1
TenC	Human	FAM	Applied Biosystems	Hs00233648_m1
Thbs1	Mouse	FAM	Applied Biosystems	Mm00449022_m1
Thbs2	Mouse	FAM	Applied Biosystems	Mm00449041_m1
Twist	Mouse	FAM	Applied Biosystems	Mm00442036_m1
Twist	Human	FAM	Applied Biosystems	Hs00361186_m1
VEGF	Human	FAM	Applied Biosystems	Hs00900054_m1
VEGFa	Mouse	FAM	Applied Biosystems	Mm01281449_m1
VEGFb	Mouse	FAM	Applied Biosystems	Mm00442102_m1
VEGFc	Mouse	FAM	Applied Biosystems	Mm00437313_m1
Vimentin	Mouse	FAM	Applied Biosystems	Mm00449201_m1
Vimentin	Human	FAM	Applied Biosystems	Hs00185584_m1

Table 10. Genotyping primer sequence information.

Gene	Primer Sequences
K14CrePR1	CGGTCGATGCAACGAGTGAT
	CCACCGTCAGTACGTGAGAT
K5Cre*PR1	TACAGCTCCTGGGCAACGTG
	CACAGCATTGGAGTCAGAAG
K15CrePR1	CGGTCGATGCAACGAGTGAT
	CCACCGTCAGTACGTGAGAT
Smad4 floxed	GGGCAGCGTAGCATATAAGA
	GACCCAAACGTCACCTTCA
Kras	CCTTTACAAGCGCACGCAGACTGTAGA
	AGCTAGCCACCATGGCTTGAGTAAGTCTGC
TGFbRII floxed	GCAGGCATCAGGACCTCAGTTTGATCC
	AGAGTGAAGCCGTGGTAGGTGAGCTTG
Smad4 Deletion	AAGAGCCACAGGTCAAGCAG
	GACCCAAACGTCACCTTCA
Smad2 floxed	TTCCATCATCCTTCATGCAAT
	CTTGTGGCAAATGCCCTTAT

Table 11. Loss of heterozygosity primer information.

Marker	Primer Sequences
D18S460	FAM-CTGAAGGGTCCTTGCC
	GCCAGCCTTGGCAGTC
D18S1137	GAM-TGACTATTTGCACATCTGGC
	GGACTTGCACGCTAATGAC
D18S555	FAM-GTGCGATGGCAAAATAGATG
	ATTTTCTAGGAAAGAGCTAGC
D18S46	FAM-GAATAGCAGGACCTATCAAAGAGC
	CAGATTAAGTGAAAACAGCATATGTG
D18S474	FAM-TGGGGTGTTTACCAGCATC
	TGGCTTTCAATGTCAGAAGG
D18S1110	FAM- TGACCTTGGCTACCTTGC
	TCGAAAGCCTTAAACTCTGA

Forward primers are all FAM-labeled for AFLP analysis. Markers located as designated below.

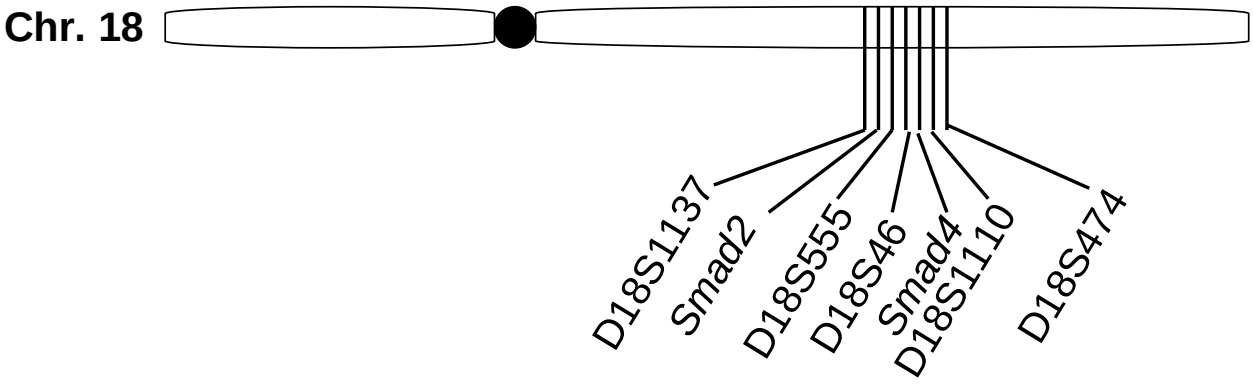

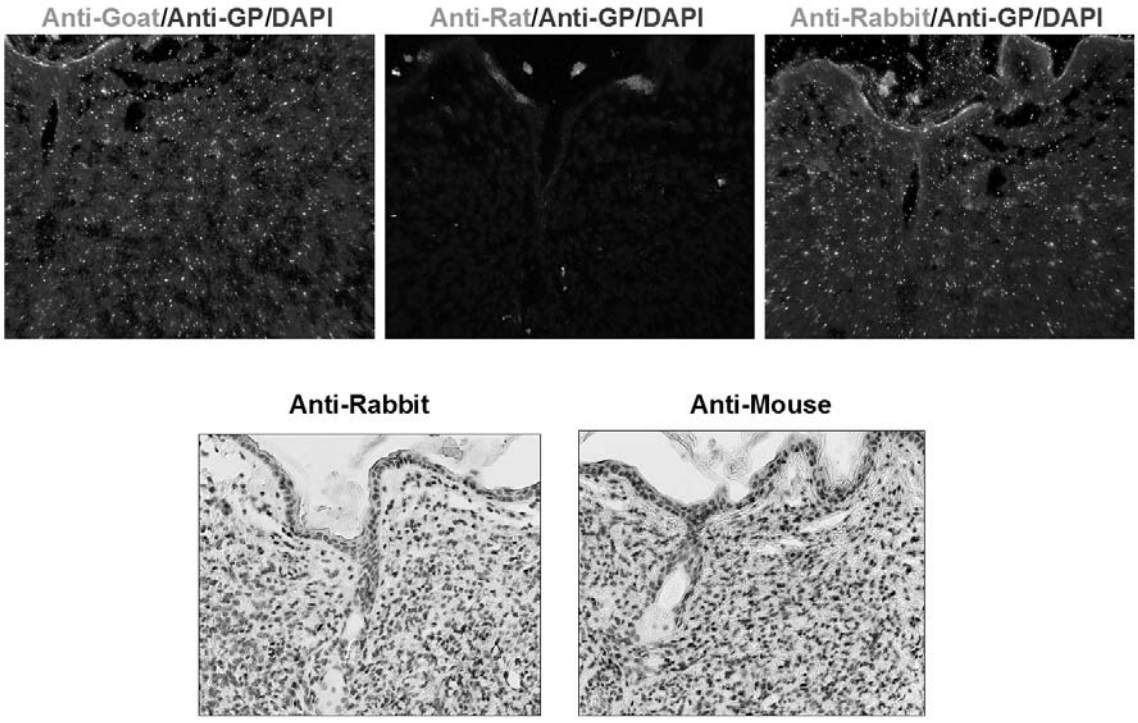

Figure 38. No primary antibody negative control images for IHC and IF.

Immunohistochemistry and immunofluorescence images for mouse tissue without use of primary antibody.